

2D-Crystal-Based Functional Inks

Francesco Bonaccorso,* Antonino Bartolotta, Jonathan N. Coleman, and Claudia Backes

The possibility to produce and process graphene, related 2D crystals, and heterostructures in the liquid phase makes them promising materials for an ever-growing class of applications as composite materials, sensors, in flexible optoelectronics, and energy storage and conversion. In particular, the ability to formulate functional inks with on-demand rheological and morphological properties, i.e., lateral size and thickness of the dispersed 2D crystals, is a step forward toward the development of industrial-scale, reliable, inexpensive printing/coating processes, a boost for the full exploitation of such nanomaterials. Here, the exfoliation strategies of graphite and other layered crystals are reviewed, along with the advances in the sorting of lateral size and thickness of the exfoliated sheets together with the formulation of functional inks and the current development of printing/coating processes of interest for the realization of 2D-crystal-based devices.

1. Introduction

Since the first demonstration that liquid-phase exfoliation (LPE) can be used to transform graphite into large numbers of graphene nanosheets,^[1] this process has become a widely used method for the production of a range of 2D sheets from their parent bulk crystals.^[2] Layered crystals such as graphite consist of individual monolayers, which are stacked into a crystal by interlayer interactions that are much weaker than the mostly covalent intralayer bonding.^[3] Hence, it is possible to peel off individual layers from the parent crystal by supplying sufficient energy in the order of 25 meV per atom in the case of graphite.^[4] While graphite is the most well-known layered crystal, numerous others exist such as boron nitride (BN),^[5] transition metal dichalcogenides (TMDs),^[5–7]

Dr. F. Bonaccorso
Istituto Italiano di Tecnologia
Graphene Labs
Via Morego 30, Genova 16163, Italy
E-mail: francesco.bonaccorso@iit.it

Dr. A. Bartolotta
CNR-IPCF, Istituto per i Processi Chimico-Fisici
Via F. Stagno D'Alcontres 37, Messina 98158, Italy

Prof. J. N. Coleman
School of Physics and CRANN
Trinity College Dublin
Pearse St, Dublin 2, Ireland

Dr. C. Backes
Applied Physical Chemistry
University of Heidelberg
Im Neuenheimer Feld 253, Heidelberg 69120, Germany

DOI: 10.1002/adma.201506410



oxides,^[8,9] III–VI semiconductors,^[8] MXenes,^[10] layered silicate minerals,^[11] or layered double hydroxides (LDHs),^[12] just to name a few. Crucially important is that different types of layered crystals possess different intrinsic properties. For example, while BN is an insulator, graphene is a conductor and TMDs are mostly semiconductors with bandgaps ranging from <1 eV to ≈2 eV.

Layered crystals are interesting in their own right and have been studied for over a century. By the 1960s, researchers were asking if they could be thinned to the point where they would become 2D crystals.^[13] Pioneered by Robert Frindt, this research has clearly shown that 2D crystals, just a few monolayers thick, could be produced by mechanical cleavage.^[13] Most

exciting was the realization that as the crystal thickness was reduced, quantum confinement effects resulted in significant changes of the electronic structure,^[14] resulting in the emergence of interesting properties.^[15] However, this research was always hampered by the lack of high-resolution characterization tools^[8] and eventually petered out in the 1990s.

However, the excitement about 2D crystals was rekindled in 2004 by Geim and Novoselov with their demonstration that few-layer graphene could be produced by mechanical cleavage of bulk graphite^[2] using methods very similar to those used by Frindt in 1963.^[13] Critically, by this time characterization tools such as atomic force microscopy (AFM) were widely available, allowing Geim and Novoselov to publish a string of papers demonstrating the unique properties of graphene.^[2] These advances prompted a flood of research, which thoroughly documented not only the basic physics of graphene^[16] but the possibility of using graphene in a wide range of applications from composites^[17,18] to optoelectronics.^[19,20] In parallel, realization began to grow that other layered crystals could be exfoliated^[21] and that these too had a host of application areas.^[8,22,23]

Once it became clear that 2D crystals were useful, many researchers began to develop methods to produce them in large quantities.^[24] In general, 2D nanosheets can be obtained by bottom up or top down production techniques.^[24] In terms of bottom up techniques, it should be noted that significant progress has been achieved in chemical vapor deposition (CVD)^[25–27] or the growth on silicon carbide^[28–30] in the case of graphene making high quality, large-area 2D crystals accessible.^[6,7,31] While such materials are perfect for applications in areas such as electronics,^[23,32] for many other applications, e.g., composites^[33] and energy,^[34] it would be beneficial if nanosheets were dispersed in liquids to facilitate solution processing.^[8,24] Once nanosheets

are obtained in a liquid dispersion, it becomes simple to sort or modify them in many ways. Liquid-dispersed nanosheets represent an ideal platform for sorting by size^[35,36] and thickness,^[37–39] for chemical modification,^[22] for composite formation by solution mixing^[40] as well as the production of films or coatings by methods such as inkjet printing^[41–52] and screen printing,^[53,54] drop casting^[36] and dip casting,^[55] and spin coating^[56–58] and spray coating,^[59,60] just to cite a few.

This makes the ability to exfoliate layered crystals directly into liquid-dispersed nanosheets very important. Exfoliation in liquids can be classified in the two main categories of intercalation-based exfoliation and LPE, even though a number of sub-categories exist. Intercalation-based methods have long been used to widen the interlayer gap of layered crystals leading to the creation of intercalation compounds (see refs. [22,61] and references therein). It was shown by both Frindt^[62] and Walker^[63] that such intercalation compounds could be exfoliated in liquids to give few-layer nanosheets. As a consequence, this still remains an important production technique. However, reductive chemical intercalation often requires the use of inert gas conditions and harsh chemical treatments, which can result in the introduction of defects.^[62,63] In addition, the intercalation process typically produces negatively charged nanosheets with properties distinct from the neutral counterparts. In the case of graphene, these negatively charged nanosheets readily react with various electrophiles (including water) leading to functionalized material with modified properties.^[61,64] In contrast to negatively charged graphene (i.e., graphenide) which is only stable in aprotic solvents under inert conditions and will react otherwise with any electrophile,^[61,64] negatively charged nanosheets of transition metal dichalcogenides can be stably dispersed in water without reacting with the solvent.^[22] However, antibonding d-orbitals of the transition metals are filled leading to different electronic properties such as transition from semiconducting nanosheets to metallic ones in the case of group VI transition metal dichalcogenides.^[22] Intercalation and subsequent exfoliation can also be achieved electrochemically, with recent demonstrations of almost defect-free, predominantly monolayer graphene produced by using this strategy.^[65] It is expected that a similar product quality can be realized in the case of other layered crystals after careful process optimization. In addition, ion exchange reactions or organic molecule intercalation can result in high quality nanosheets of layered double hydroxides^[12] or MXenes,^[10] respectively. However, such approaches are restricted to only a limited number of layered crystals.

In the case of graphene, the intercalation of graphite with acids to ultimately yield graphene oxide (GO) has been widely studied over the past decade.^[64,66–70] Oxygenation of such acid intercalation compounds occurs to form graphite oxide, which can be delaminated by mild agitation to yield individual layers of exfoliated GO in polar solvents such as water and alcohols.^[64,66–70] While this results in the production of predominantly monolayer nanosheets of lateral sizes in the 50–100 μm range, the nanosheets are not pristine bearing a number of functional groups depending on the synthesis conditions.^[24,71] These can widely be removed by wet chemical reduction or reductive annealing to yield reduced graphene oxide (RGO).^[64,66–70] However, in addition, the carbon skeleton also becomes disrupted and holes are introduced and cannot easily be healed.^[24,71] Hence, the resultant material is not pristine and should be considered graphene-like with application



Francesco Bonaccorso gained his Ph.D. from the University of Messina in Italy after working at the Italian National Research Council, the University of Cambridge (UK) and the University of Vanderbilt (USA). In 2009 he was awarded a Royal Society Newton International Fellowship at Cambridge University, and elected to

a Research Fellowship at Hughes Hall, Cambridge. He was responsible for defining the 10 year scientific and technological roadmap for the European Graphene Flagship. Currently, he is leading the processing and prototyping group at the Istituto Italiano di Tecnologia, Graphene Labs, where his research interests encompass solution processing of nanomaterials, their spectroscopic characterization, incorporation into polymer composites and application in solar cells, light-emitting devices, lithium-ion batteries, and ultrafast lasers.



Jonathan Coleman is Professor of Chemical Physics at Trinity College Dublin. The focus of his research is liquid exfoliation of layered compounds yielding 2D nanosheets, which can easily be processed into thin films or composites for applications ranging from energy to mechanics.



Claudia Backes received her Ph.D. with honors in 2011 from the University of Erlangen, Germany, with Andreas Hirsch. After having supported the Erlangen Cluster of Excellence as Deputy Executive Director in 2011–2012, she joined Trinity College Dublin, Ireland as independent research fellow in Jonathan Coleman's group. In 2015, she moved to Heidelberg University, Germany, as Junior Research Group Leader funded within the Emmy Noether Program. Her research interests are optical properties and functionalization of liquid-exfoliated nanostructures.

areas distinct from the ones of graphene and will not be covered in this review. However, many processing strategies of other layered crystals build on the research into GO.

Compared to intercalation, a more versatile and simpler method for producing 2D nanosheets in liquids is the LPE, which is the process focus of this review. In this method, the intersheet forces are broken by the input of either shear or ultrasonic energy in the presence of a stabilizing liquid.^[1,8,41,72] The resultant nanosheets are generally defect-free and unfunctionalized.^[1,41,72–74] Most importantly, this technique is scalable and applicable to a wide range of layered materials and ideal for fabricating inks,^[41–46] pastes,^[53] composites,^[17,18,40] and coatings^[60,75] so that nanosheets can be integrated for example into printed devices.^[41–46] The key aspects of this review are summarized in Figure 1. We will first discuss recent advances and remaining challenges in nanosheet production by LPE. A major obstacle is that nanosheets in the resultant dispersions are highly polydisperse. However, in particular for electronic applications, it will be necessary to obtain nanosheets with predefined properties and hence uniform size^[35,36] and thickness.^[37–39] Hence, it will be important to devise strategies to sort nanosheets according to length and thickness as also summarized. We then address the formulation of 2D-crystal inks for their exploitation in printed and flexible electronics, which is emerging as the next ubiquitous platform in the electronics industry.^[76] We will discuss the formulation of 2D-crystal-based inks for different printing and coating technologies, such as drop,^[36,77,78] spin^[56] and spray^[59,60] coating, inkjet,^[41–46] gravure,^[79] and flexographic^[80] printing, analyzing the key issues to be addressed before these novel inks can be fully exploited in the aforementioned printing/coating techniques. We will also discuss the first attempts in the realization of pastes based on 2D crystals enabling the direct deposition by screen printing.^[53,54,81]

We will then provide the perspective of constructing hybrid heterostructures of different 2D crystals by printing one layer of exfoliated nanosheets on top of another one. This approach, although still at its infancy, could potentially have a game-changing impact on a variety of devices. We will also briefly summarize the role of printing technologies for the realization of novel devices having lightweight, foldable, and flexible designs with the potential to achieve performances similar to that of rigid platforms based on conventional materials. The possibility to directly fabricate such devices on flexible substrates, by using novel mass manufacturing approaches unavailable from more traditional platforms,^[82] would enable entirely new applications in the optoelectronic^[23,32,83] and energy^[34] fields, with the added value of reduced cost.

2. Dispersion of Layered Crystals

In the following, we will summarize basic principles of liquid exfoliation of layered crystals with an emphasis on recent progress to give a comprehensive, rather than exhaustive, overview of the field. For additional information, the reader is referred to a number of recent review papers.^[6,8,24,72,84–86] In general, LPE can be considered as a three-step process starting from the actual exfoliation of the layered crystals, which provides the energy to overcome the interlayer attraction between the

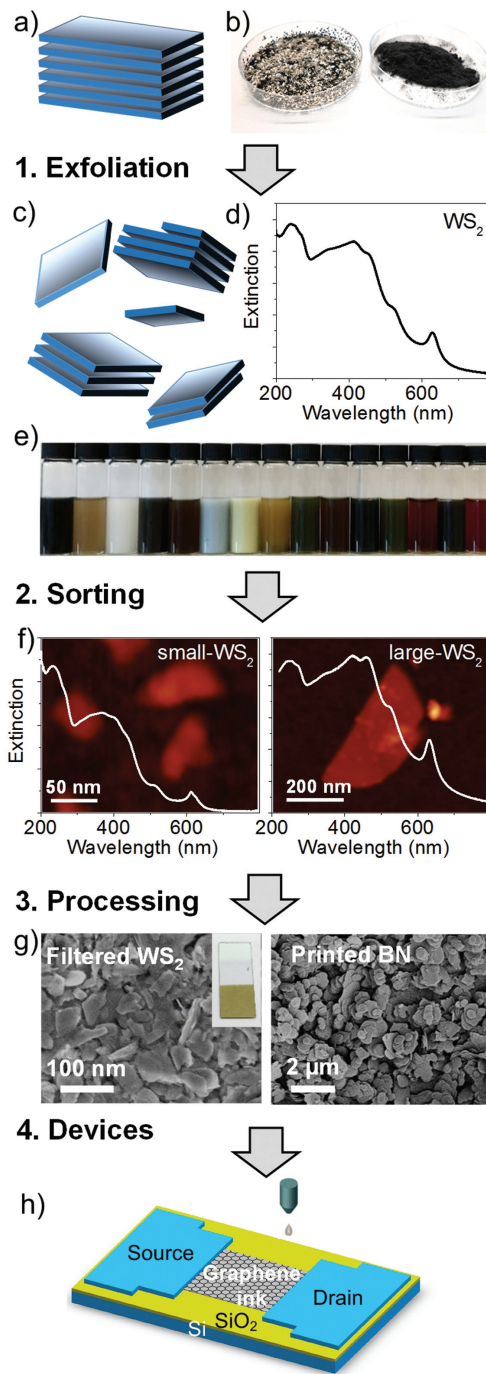


Figure 1. Process chain from exfoliation of layered crystals to devices. 1-a) Layered bulk crystals such as b) graphite are exfoliated in liquid to yield c) nanosheets of various sizes and thicknesses. d) An example of an extinction spectrum of liquid exfoliated WS_2 . e) Photograph of dispersions of different exfoliated layered crystals. 2) After the initial exfoliation, the nanosheets need to be size-selected to reduce their polydispersity. f) Atomic force micrograph and extinction spectrum of a WS_2 dispersion enriched in small and thin nanosheets (left) and enriched in large nanosheets (right). The size selection is evident from both the microscopy and spectroscopy data. 3) Such nanosheets can be further processed by various techniques. g) Scanning electron microscopy image of a filtered film of WS_2 nanosheets (left) and of inkjet-printed BN nanosheets (right). 4) By exploiting liquids processability, h) printed devices can be designed and fabricated.

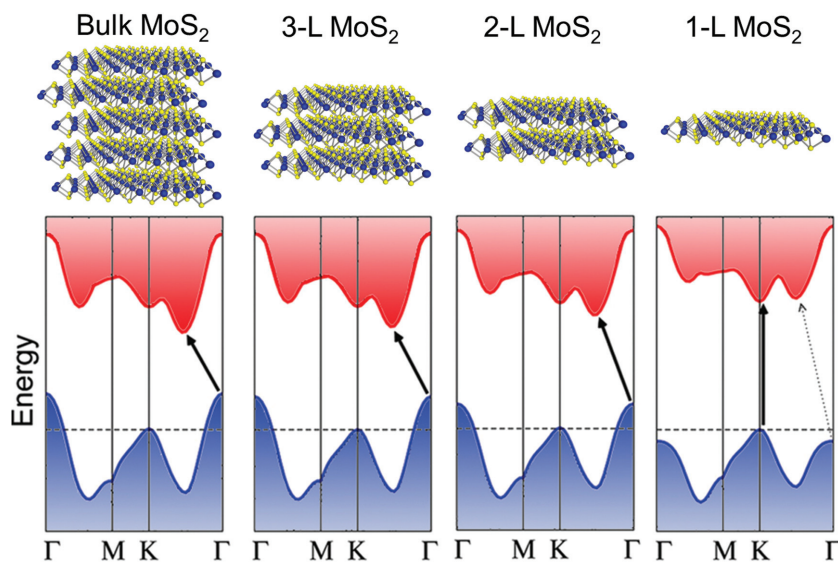


Figure 2. Thickness-dependent bandgap properties of molybdenum disulfide (MoS_2) sheets. In bulk, MoS_2 shows an indirect bandgap (1.29 eV), whereas in its monolayer form it has a direct bandgap (1.8 eV).^[31,120]

individual layers, to stabilization of the exfoliated nanosheets in liquid and, finally, size selection.

Traditionally, the exfoliation is achieved by ultrasonication of bulk crystals in appropriate media.^[1,8,24,72,73] While ultrasonication using sonic probes is efficient to achieve high concentrations (g L^{-1}),^[87,88] it is not easily scalable, as the ultrasonic intensity decreases rapidly both axially and radially from the probe, strongly restricting volumes that can be processed.^[89] Therefore, the past few years have seen tremendous research efforts^[74,90–101] in finding suitable techniques that can be scaled to produce industrially relevant quantities. Both ball milling^[90–95] and shear exfoliation^[74,96–100] have been identified as suitable candidates to replace ultrasonication in the future. After the exfoliation process, the re-aggregation of the nanosheets needs to be prevented by stabilizers.^[1,8,24,72,73] These can be suitable solvents^[1,46,73,74,93,98,99,102–110] or charged or neutral surfactants^[35,37,92,94,96,97,111–116] or polymers.^[38,39,100,117–119]

Specific applications require nanosheets of controlled size and thickness. For example, many 2D crystals have thickness-dependent bandgap^[31,120] (Figure 2). However, inherently the exfoliation process gives samples that are highly polydisperse with broad nanosheet size and thickness distributions and low monolayer contents.^[1,8,24,72,84]

While ideally, some initial control can likely be obtained by a careful optimization of both the exfoliation technique and stabilizers (e.g., solvents and surfactants/polymers), it is doubtful that this will be sufficient so that it is important to devise strategies for efficient nanosheets sorting.

2.1. Exfoliation of Bulk Crystals

2.1.1. Exfoliation Techniques

Any method of layered crystals exfoliation in liquid phase requires the input of energy to overcome the intersheet

interactions. A number of methods have been demonstrated to achieve this. Below we will give a brief description of the most common ones.

Ultrasonication: Partial exfoliation of graphite by sonication was first demonstrated by McEuen^[121] in 2005 with monolayer production achieved independently by Coleman and co-worker in 2008.^[1] Ultrasonication-induced exfoliation is largely due to cavitation.^[122] As a result of collapsing cavitation bubbles, tensile and shear stress acts on the nanomaterial leading to both exfoliation and fragmentation.^[85,89,123] Ultrasonication can be conducted using either sonic baths^[1,8,35,36,41] or tip ultrasonicators.^[37,124] In low-intensity bath sonication,^[1,8,35,36,41] the ultrasonic waves propagate through both tank and reaction container, setting up a standing wave.^[1,8,35,36,41] Intensities acting on the sample are lower than nominally expected and the nonuniform distribution of the sonic waves through the tank results in

poor reproducibility of the process.^[89] Alternatively, high-power sonic probes can be used,^[37,124] where the intense ultrasonication zone is located directly beneath the sonotrode. The exfoliation state achieved will therefore strongly depend not only on sonic power, amplitude, and frequency, but sonic probe and vessel shape. Either way, ultrasonication suffers from the drawbacks that it is poorly reproducible and results in significant material fragmentation.^[125] In addition, while equipment for continuous ultrasonication processing is available, the scale-up of the exfoliation to industrially relevant quantities has not yet been demonstrated.

Nonetheless, ultrasonication is still the most frequently used exfoliation technique to produce LPE nanomaterials on the lab-scale.^[72,84] This is mainly because the first publications on LPE of 2D crystals such as graphene^[1,111] or BN^[73,113] and various TMDs^[73,113] have shown that it can be reliably used to obtain mono- and few layer nanosheets. This has recently been further emphasized by the demonstration that other layered crystals can also be exfoliated in this way.^[104,106–108,110] One may imagine that the widespread use of ultrasonication has generated a deep understanding of the exfoliation process. However, this is not the case. While dispersed nanomaterial concentration is often analyzed as function of some process parameters, a comprehensive understanding of the process itself is still lacking. This is mostly due to the inherently poor reproducibility of ultrasonication and because many parameters (such as time, amplitude, power, frequency, vessel shape, etc.) have an impact on the exfoliation process. Accordingly, a systematic variation of process parameters can still lead to surprising results as recently shown in a study characterizing and optimizing the ultrasound acoustic cavitation for different immersion depths of the sonic probe in the liquid.^[105]

While it is widely believed that LPE generally results in defect-free nanosheets, a number of groups have recently considered defect formation during cavitation. The most comprehensive study thus far was probably carried out by Bracamonte et al.^[103]

An ultrasonication time study exfoliating graphite in *N*-methyl-2-pyrrolidone (NMP) was conducted and the resultant nanosheets were characterized by Raman spectroscopy. A separate analysis of G-linewidth (FWHM(G)) and the intensity ratio of the D and G peaks ($I(D)/I(G)$) was carried out^[103] to distinguish between basal plane and edge defects.^[36,41,46,103] The results suggested that the introduction of basal plane defects can occur at longer ultrasonication times.^[103] However, more work on other layered crystals using various ultrasonication techniques will be necessary to confirm this result.^[103] One complication is that, as the structural quality of the product will depend on the actual quality of the starting crystal, some researchers^[126–128] observe basal plane defects, while others^[36,41,72,84] do not.

Ball Milling: The ball milling technique is widely used industrially for grinding materials or dispersing nanoparticles and has been applied to graphite to yield liquid-exfoliated mono- and few-layer graphene in 2010.^[92] Unlike ultrasonication, ball milling is intrinsically scalable. The exfoliation is both driven by shear forces and collisions making careful process optimization as essential as in ultrasonication to minimize fragmentation of the exfoliated sheets. Both stirred media mills and planetary ball mills can be used to achieve exfoliation.^[85,90–95,129,130] In the case of planetary ball mills, longer process times at slower rotations are essential to avoid noticeable fragmentation and introduction of defects onto the exfoliated sheets.^[90,91] Compared to ultrasonication, exfoliation by ball milling is a rather young technique that will require further optimization of process parameters such as delamination tool, media size, and stirrer rotation. In the case of graphene, this has recently been addressed by a number of reports shining light on process parameters using stirred media mills for the production of graphene in solvent^[93] and surfactant media.^[114] In terms of layered crystals beyond graphene, very little research has been conducted so far. The first report on exfoliation of other layered crystals such as BN and molybdenum disulfide (MoS_2) used a combination of planetary ball milling and ultrasonication in 2012.^[94] Even though it has subsequently been shown that ball milling in stirred media mills can indeed be used to exfoliate TMDs without using additional production techniques,^[95] further studies will be required to demonstrate the broader applicability.

Shear Exfoliation: During the past 2 years, another scalable production technique to exfoliate layered crystals has emerged, which is based on fluid dynamics in rotor/stator^[74,98,110] or rotating blade mixers.^[96,97,99,100] The process is considered to be shear dominated with fragmentation limited to milling by the rotor. Widely used in industry and known to be scalable, it is therefore a highly promising production technique for LPE nanosheets in large quantities. Hence, it is not surprising that exfoliation of a number of layered crystals beyond graphene^[74,96,98,99,100] such as BN,^[73,74] TMDs^[73,74] or black phosphorous (BP)^[110] has already been demonstrated.

The first reports focused on using rotor/stator mixers.^[74,98] It was shown^[74] that exfoliation can occur even in laminar flow as long as shear rates $>10^4 \text{ s}^{-1}$ act on the layered crystals. For graphitic flakes, i.e., graphene and few layer graphene, the dispersed concentration and production rate was characterized as function of process parameters such as initial graphite concentration, rotor speed, rotor diameter, and liquid volume.^[74] This

lead to an understanding of the scaling laws of the process which has shown that production rates can indeed be enhanced by increasing the volume—an ideal case scenario for scale-up.^[74] One problem associated with rotor/stator mixers is that the exfoliation events are localized in the vicinity of the rotor/stator.^[74] Exfoliation using rotating blade mixers generates turbulent shear throughout the tank and would be expected to increase production rates as experimentally confirmed.^[96] The simplicity of this approach not requiring expensive equipment has already made this technique very popular.^[97,99,100]

From the brief overview above and the summary reported in **Table 1**, it is clear that the ultimate production technique still needs to be identified. In each case, process parameters are numerous and need to be carefully optimized. The major problem is that—if at all—only dispersed concentration is analyzed and little is known about the impact of the process parameters on nanosheet size and thickness distributions. This is because these quantities typically have to be determined by time-consuming and tedious statistical microscopy analysis. However, the groups of Peukert and Coleman have independently demonstrated a possible way forward recently by using high-throughput optical spectroscopy as a characterization technique.^[35,93,114,131] The Peukert group used statistical Raman spectroscopy to qualitatively gain insights in the impact of process parameters in ball milling of graphene on lateral size of the nanosheets as well as production of few-layer nanosheets.^[93,114] The Coleman group established quantitative metrics to relate spectral changes in the extinction spectra of liquid-exfoliated MoS_2 and WS_2 due to edge and confinement effects to mean nanosheet length and thickness.^[35,131] This has subsequently been used to analyze a number of process parameters in turbulent-assisted shear exfoliation of MoS_2 resulting in the first example of *in situ* size and thickness control by adjusting the exfoliation process.^[97] Similarly, the ratio of Raman and photoluminescence peaks intensity of liquid-exfoliated WS_2 can be qualitatively linked to the monolayer volume fraction.^[131] Similar metrics based on absorbance and Raman spectroscopy were established for liquid-exfoliated few-layer graphene.^[132] With such powerful high-throughput characterization techniques at hand, it is expected that optimization of various exfoliation processes will flourish in the near future.

2.1.2. Stabilization

Liquid-phase exfoliation requires the presence of a stabilizer for the process to occur efficiently (**Figure 3**). Stabilizers play a dual role: reducing the net energy cost of exfoliation via the stabilizer–nanosheet binding and preventing aggregation of the exfoliated nanosheets. As we outline below, there are three main classes of stabilizers which can achieve this target: solvents, surfactants, and polymers (**Table 2**).

Solvents: Layered crystals can be exfoliated and stabilized in suitable solvents without additional additives as demonstrated in 2008 for graphene,^[1] 2009 for BN,^[133] and 2011 for TMDs.^[73] Solution thermodynamics predicts that efficient stabilization occurs when the net energetic cost of mixing of a solute in a solvent is minimized. This is the case when the solubility parameters of solvent and solute match. While the classical

Table 1. Overview of the three main exfoliation methods and their advantages and disadvantages.

Exfoliation method	Materials	Advantages	Disadvantages
Ultrasonication	Graphene	Widely applicable	Scalability not demonstrated, low production rate
	BN	High concentration in relatively short times (tip ultrasonication)	Low concentrations in bath ultrasonication
	TMDs		Fragmentation, especially with tip ultrasonication
	MoO ₃	Widely used on labscale	Poor reproducibility
	MnO ₂		Introduction of defects not clear
	GaS		Impact of process parameters (amplitude, frequency, position of probe/sample, temperature, vessel) especially on length and thickness not understood
	BP		
Ball milling	Some LDH		
	Graphene	Scalable	Slow in planetary ball mills (otherwise it introduces defects)
	BN	When adjusted, shear not fragmentation dominates	Suitability for broad range of materials to be demonstrated
	MoS ₂		Process optimization needs further considerations, especially for new materials and in terms of sheet size
Shear exfoliation	Graphene	Scalable	Concentrations lower than for ultrasonication at equal process times
	BN	Highest production rates	Impact of process parameters only investigated in terms of concentration, not length and thickness of exfoliated sheets; direct comparison to ultrasonication lacking, but degree of exfoliation appears lower
	TMDs	Exfoliation not dominated by fragmentation	
	BP		

models strictly only apply to small molecules, they can be modified to account for the dimensionality of the nanomaterial.^[72,102] A number of solubility parameters such as solvent surface tension (γ ; mN m⁻¹), Hildebrandt or Hansen parameters describe exfoliation/stabilization of layered crystals very well,^[1,46,72,73] as experimentally shown by analyzing the dispersed nanomaterial concentration as function of solubility parameters. It should be noted that additional factors such as solvent degradation especially during ultrasonication-based exfoliation can play a role in nanomaterial stabilization. For example, it was recently shown that the controlled addition of water and subsequent sonochemical reactions with the widely used solvents such as NMP and dimethylformamide (DMF) can further increase the dispersed nanomaterial concentration in the case of MoS₂.^[134] However, more detailed studies will be required to exploit the potential of sonochemistry in this regard.

Recently, the palette of liquid-exfoliated crystals stabilized in solvents has been expanded beyond graphene, BN and TMDs to include MoO₃,^[106] as representative of a layered oxide, GaS^[108] as representative of a III-VI semiconductor and BP^[104,107,110] confirming the wide applicability of this approach. It is worth noting that one significant advantage of solvent stabilization has recently been demonstrated in this context. Unlike many of the well-studied layered crystals, BP degrades in the presence of water and oxygen making further processing challenging.^[135,136] However, when exfoliated in liquid, suitable solvents can protect the nanosheet surface significantly slowing down reaction rates.^[107]

The major problem associated with solvent stabilization is that identified good solvents are usually toxic, can be incompatible with other aspects of processing (especially

involving plastic substrates), have high boiling points, which makes their removal after the deposition process difficult, and can degrade, especially during ultrasonication (which also changes γ and solubility parameters).^[137] This is the case for the most popular solvent, i.e., NMP, which is, together with DMF for example, included in the candidate list of substances of very high concern^[138] and may have teratogenic effects.^[46,139–141] As a result, researchers have sought for alternatives, with the exploitation of environmentally benign and low-boiling-point solvents,^[106,108,142] such as acetone, isopropyl alcohol (IPA), etc. However, the γ of these solvents is too low (≈ 25 mN m⁻¹) for the exfoliation of layered crystals, making the concentration of the dispersed flakes as well as the percentage of single layers (SLs) in the solvent by far too low^[142] with respect to the ones achieved in NMP.^[1,41,143]

In this context, we would like to highlight two recent publications pointing toward alternatives. A major problem in the use of solubility parameters relies on the fact that

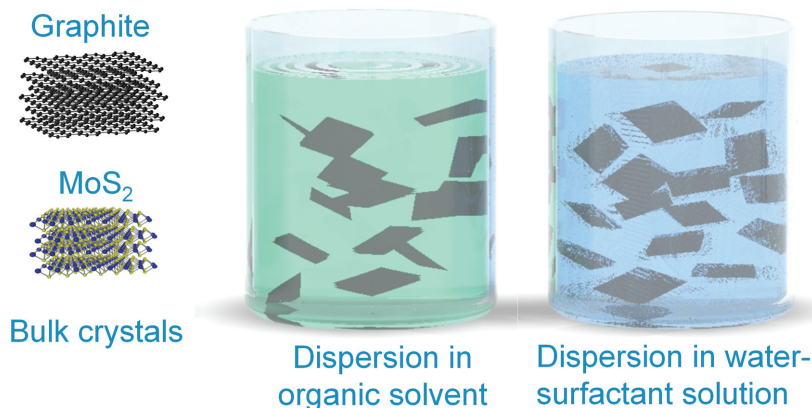


Figure 3. Exfoliation of bulk layered crystals and stabilization of exfoliated nanosheets in solvents and surfactant-assisted aqueous dispersion.

Table 2. Overview of 2D-crystal stabilization by solvents, surfactants, and polymers and their advantages and disadvantages.

Stabilizer	Materials	Advantages	Disadvantages
Solvent	Graphene	Processability of a broad range of materials	Often toxic
	BN	Solvent can protect chemically unstable materials from degradation	Typically high boiling points; therefore also residual solvent after processing
	TMDs		Solvent degradation during exfoliation, especially in ultrasonication
	MoO ₃	Nontoxic alternatives being exploited such as solvent/co-solvent systems also for tuning rheological properties	Solvent/co-solvent systems lower quality of exfoliation and problematic long-term stability
	MnO ₂		
	GaS		
	BP		
Surfactant	Some LDH		
	Graphene	Nontoxic	Some materials degrade in water
	BN	Negatively, positively or uncharged nanosheets available	Residual surfactant difficult to remove
	TMDs	Water based: easy processing and deposition	
	Some LDH		
Polymer	Graphene	Versatile: solvent or surfactant	Polymer difficult to remove; doping effects expected
	BN	Viscosity easily tunable	Least investigated, especially in terms of quality of exfoliation
	TMDs	Composite formation straight forward	Concentrations often lower than with surfactant or in good solvents
		Biocompatible when proteins are used	

solubilization/stabilization of solutes in liquids depends on a number of intermolecular forces such as London dispersive forces and polar forces (such as dipole–dipole interactions).^[144,145] Ideally, all contributions of solvent and solute need to be matched. This is experimentally difficult and has recently been addressed by Shen et al.^[109] The authors pointed out that the key to efficient stabilization is to match both the total γ as well as the ratio of polar and dispersive forces of nanomaterial and solvent, respectively.^[109] The latter can be obtained from fitting contact angle measurements of nanomaterials in various solvents.^[109] For example, Shen et al. observed^[109] that the dispersed concentration of both graphene and WS₂ is peaked at total solvent surface energies of 40 mN m⁻¹, in agreement with other reports.^[8,73] However, in addition, in the case of graphene, the ratio of polar to dispersive component should be close to 0.47, while for WS₂, it should be close to 0.56.^[109] In another recent publication, it was shown that graphene and other 2D crystals such as BN and TMDs can be exfoliated and stabilized even in the monolayer form in water at elevated temperatures.^[146] In the case of graphene sheets, this is attributed to the introduction of oxygen functionalities at the edges after ultrasonication at high temperatures.^[146] However, for BN and TMD sheets, this does not seem to be the case.^[146] The authors suggest that in the case of electrically less conductive materials, if compared with graphene, such as BN and TMDs, an electrical double layer is formed, increasing in thickness with the temperature, leading to efficient stabilization.^[146] However, the decreased γ of water at elevated temperatures^[147] may also have a role on the stabilization of the dispersion. In any case, these recent reports^[109,146] provide the foundation to identify new solvents, solvent blends and/or suggest that tuning γ by temperature or salts can result in improved stabilization in solvents alternative to the widely used teratogenic, high-boiling-point solvents such as NMP and DMF.^[1,8,24,73]

In the quest for the search of alternative solvents with appropriate rheological properties for safety and sustainability of the LPE process of 2D crystals, a promising approach involves the exploitation of co-solvents to increase the affinity between solvent and 2D crystals.^[46,148–151] Such co-solvent exfoliation and stabilization has recently been studied in depth in the case of BN nanotubes.^[152] First experimental attempts by using a mixture of solvents,^[148] e.g., water/ethanol,^[46,148,149] water/IPA,^[149] etc. have also been carried out in the case of 2D crystals. The rheological properties such as γ , viscosity (η ; mPa s) and density (ρ ; g cm⁻³)^[153] of the mixture can be tuned “on-demand” by adjusting the relative concentration of the co-solvents. However, there are several issues still to be faced. First, the quality of the as obtained dispersion (i.e., percentage of SL) as well as the concentration of the exfoliated and dispersed sheets is lower with respect to the ones achieved with NMP.^[150,151] Another critical point is the stability of the water and alcohols mixtures.^[46,86,148,149,153] In fact, γ changes exponentially after the addition of alcohols to water^[153] being also sensitive to solvent evaporation.^[149] Moreover, all the rheological properties of alcohol-based co-solvents are very sensitive to temperature variation.^[153] This is a critical problem both during the exfoliation process as well as for the long life stability of the dispersions.

Surfactants: Stabilization of exfoliated sheets by surfactant molecules in water^[111] offers a widely used alternative to stabilization in (mostly) toxic, high-boiling-point solvents.^[1] Surfactants can be either anionic, cationic, zwitterionic, or non-ionic.^[154,155] Exfoliation of layered crystals in a surfactant environment (e.g., sodium dodecylbenzenesulfonate (SDBS),^[111] sodium cholate (SC)^[37] and sodium deoxycholate (SDC)^[115,116]), results in the bare nanosheets being coated very rapidly by surfactant molecules.^[111] These adsorb by noncovalent interaction between the nanosheet plane and the surfactant tail group.^[156] The head group then interacts with the liquid and is responsible for the stabilization of the nanosheets in dispersion.^[156]

Re-aggregation of the exfoliated nanosheets in the liquid is prevented by electrostatic and/or steric repulsion.^[37,111,115,116] In the case of ionic surfactants,^[154,155] i.e., anionic, cationic, zwitterionic, the repulsion is due to the interaction of the charge distributions of surfactant coatings for adjacent nanosheets. As such, the dispersed concentration of exfoliated nanomaterial scales with the magnitude of the zeta potential as expected from DLVO theory.^[72] Alternatively, layered crystals can be exfoliated in non-ionic surfactants, where stabilization is mainly due to steric repulsion (see below).^[111] However, it should be noted that more exotic surfactants such as aromatic molecules,^[84] ionic liquids,^[157] or simply kitchen soap^[96] have also proven successful, although the stabilization mechanisms are not well understood.

Polymers: As an alternative to monomeric surfactants, polymers including proteins^[100,118] can be used as stabilizers for graphene and other 2D crystals in either organic or aqueous media.^[38,39,117,158] Here, the stabilization mechanism is mainly steric: the polymer adsorbs on the nanosheet surface at a number of sites with many loops and tails protruding into the solvent.^[38,39,117,155,158] When two nanosheets approach themselves and their protruding polymers begin to occupy the same region of space, the number of chain confirmations falls, resulting in an increase in the free energy of the system.^[159] This acts as a repulsive force and hence stabilization.^[159] Binding and protrusion of the polymer chains only occurs when the balance of energetics of adsorption and loop/tail entropy result in a favorable free energy.^[117] Analysis of this balance was used to develop a set of rules allowing the prediction of successful nanosheet polymer/solvent combinations.^[117]

An added value of using polymers is that η can potentially be tuned by the polymer concentration and that composites can easily be formed.^[17,18] Given that this probably offers the most flexible way to stabilize LPE nanosheets, it is very surprising that this is the least well-studied approach. This may be because quality of exfoliation (i.e., percentage of SL sheets) or dispersed concentration can be lower than in the case of surfactants-assisted exfoliation, as the bulky polymers do not easily slip between partially exfoliated nanosheets where the interlayer gap was widened during the exfoliation process. However, no direct comparison is provided in literature so that it is difficult to assess whether this is indeed the case. A definite downside is that polymers cannot be easily removed from the nanomaterial surface after exfoliation. This may change the intrinsic properties of 2D crystals due to doping effects.^[31] However, it should be pointed out that this can also be highly beneficial. For example, it has been shown that monolayer-enriched WS₂ nanosheets exfoliated in poly(vinyl alcohol) widely preserve their monolayer optoelectronic properties (such as photoluminescence) in the dried state due to efficient shielding of WS₂ nanosheet–WS₂ nanosheet interactions by the polymer matrix.^[119]

LPE – A Critical View: The main advantages of liquid exfoliation, with respect to other synthesis approaches,^[24] for the production of 2D crystals are clear: it is a scalable, versatile, and cheap production technique giving access to a host of materials in bulk quantities. At the same time, these can be solution-processed and different classes of materials can be

readily combined in composites to exploit synergistic effects between a broad range of materials. In addition, characterization in liquids is also beneficial, as thousands of nanosheets are probed in a single measurement so that the result will be representative of the sample. The resultant liquids are also readily processable into useful structures. However, a major problem of LPE is that the samples are always polydisperse in terms of nanosheet size and thickness. Despite significant progress in the past years (see Section 2.2), it will always remain a challenge to produce large and thin nanosheets. However, for many applications, this may not be necessary, especially when considering that many printing techniques require nanosheets with lateral sizes on the order of maximum few hundred of nanometers (see Section 3). Even though liquid exfoliation produces defect-free nanosheets, i.e., no additional defects are introduced during the exfoliation process, the quality of the exfoliated nanosheets will always depend on the grade of the starting bulk crystal. But due to the growing demand in high quality materials, significant efforts are devoted to developing novel synthesis techniques, which will in turn feed liquid exfoliation by a constant supply of new high quality starting materials in the future. It should be noted that some materials such as BP are not be stable under ambient conditions.^[160] However, these stability issues also arise in the case of vapor-grown^[24–27] or indeed mechanically cleaved 2D crystals^[2,13,21,161] and protection by a solvent shell can even be beneficial. Another potential disruptor of using liquid exfoliated nanosheets is that they may restack and re-aggregate upon deposition. But this hurdle can potentially be overcome by adding stabilizers such as polymers^[38,39,117,119,155,158] or in the future, potentially other nanosheets to shield the surface. Last but not least, it should be mentioned that nanosheets produced in liquids will always have residual solvent/surfactant adsorbed. This means, they are doped to a more or less greater extent (depending on the type and concentration of the stabilizer). While this appears to be a disadvantage, it can actually be used as potential tool to chemically dope the nanosheets in a controlled way by designing additives according to needs. Furthermore, similar problems arise when using 2D crystals grown by bottom-up approaches,^[24–30] as these are supported by a substrate, and/or residual polymers following the transfer process to the target substrate,^[24] which influence their properties.

2.2. Sorting of 2D Crystals

Whatever is the process used for the exfoliation of layered crystals, after this step, the as-produced dispersions have a heterogeneous composition of exfoliated sheets both in lateral size and thickness. However, in view of any application, ranging from mechanical to electronic and electrochemical, this is not the ideal condition to fully exploit the properties of the exfoliated 2D crystals. Thus, the full control of the morphological properties is a fundamental goal to be achieved in the short term. The most successful and investigated strategy for the sorting of 2D crystals is based on (ultra)centrifugation techniques,^[1,24,35–111] (Figure 4). In this context, exfoliated 2D crystals can be sorted both by lateral size and thickness by following different strategies based on ultracentrifugation in a uniform^[162] or density gradient

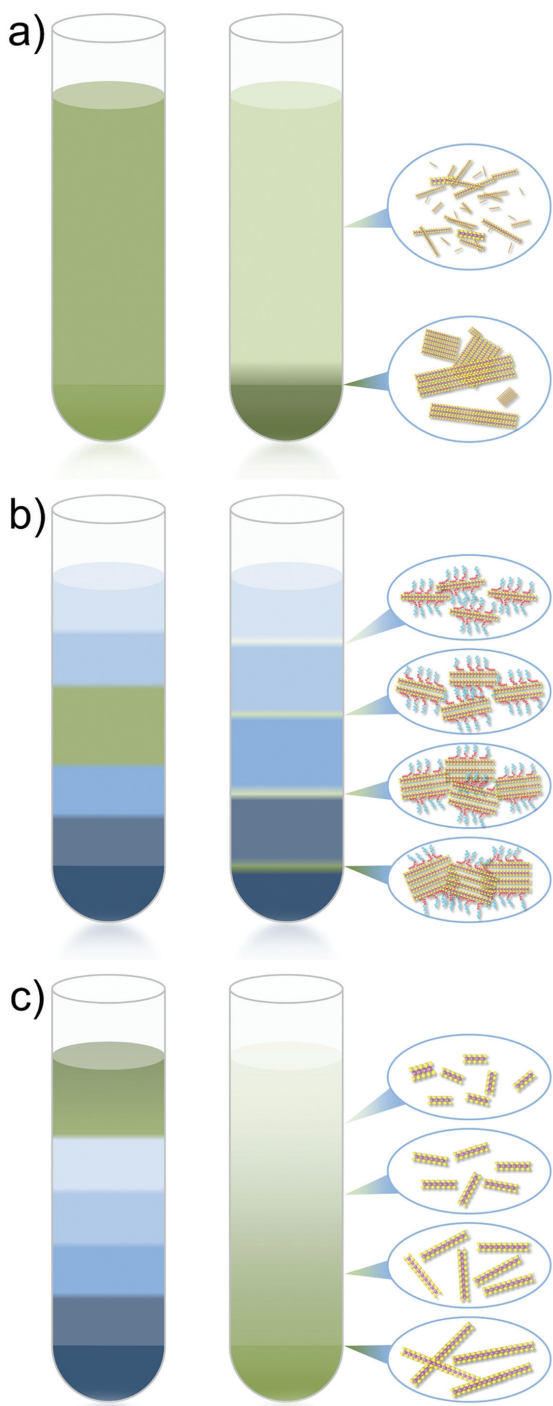


Figure 4. Sorting of 2D-crystal sheets (WS_2 as example) by ultracentrifugation. a) SBS permits the separation of thin and small lateral size sheets that are retained in dispersion (supernatant) from thicker and larger ones, which precipitate at the bottom of the ultracentrifuge tube. b) Isopycnic separation by DGU gives access to the sorting of sheets by their layer number. The buoyant density of the 2D-crystal–surfactant complexes increases with the number of layers, determining their spatial separation along the ultracentrifuge tube. c) RZS exploits differences in the sedimentation coefficient of 2D crystals under ultracentrifugation based on differences in their shapes. Larger and thicker flakes sediment faster than small and thinner ones.

medium (DGM).^[162] The first strategy, which is the most simple and common method, is the sedimentation-based separation (SBS),^[162] (Figure 4a) while the second, which is more precise but time consuming with respect to SBS, is named density gradient ultracentrifugation (DGU).^[162] The exploitation of SBS permits to separate nanomaterials (e.g., metallic nanoparticles (MNPs),^[163] carbon nanotubes (CNTs),^[155,164,165] and 2D-crystal sheets^[37–39,131,166]) on the basis of their sedimentation rate^[162] in response to a centrifugal force acting on them. In general, the sedimentation rate of dispersed materials subjected to a centrifugal field is described by the Svedberg equation:^[162]

$$s = m(1 - \rho v)/f \quad (1)$$

where s is the sedimentation coefficient, the time needed for the nanomaterial to sediment, commonly reported in Svedberg (S) unit (1S corresponds to 10^{-13} s),^[162] m is the mass, ρ is the density of the solvent, v is the volume that each gram of the nanoparticle, nanotube, or nanosheet occupies in solution, and f is the frictional coefficient. For 2D crystals, the latter depends on both the lateral size and thickness of the 2D sheets and the η of the solvent they are dispersed in. In general, large or elongated nano-objects experience more frictional drag than spherical ones,^[36,162] thus having higher f values. Overall, s depends on the morphological properties of the dispersed nanomaterial and it is proportional to its buoyant effective molar weight, while it is inversely proportional to f .^[162] As expressed by Equation (1), the sedimentation of 2D sheets depends on their mass and the frictional coefficient.^[24,36] Thick and large sheets, thus experiencing larger mass, sediment faster with respect to small and thin sheets (having smaller mass), which are thus retained in dispersion during a SBS process.^[36,116]

Exploiting SBS, to date, sheets ranging from few nanometers to a few micrometers have been produced, both for graphene^[1,36,41,74,111] and other 2D crystals.^[73,113,167] For example, dispersion with high content of SL graphene ($\approx 60\%$) was achieved in an aqueous dispersion with sodium deoxycholate as surfactant,^[116] while $\approx 33\%$ SL graphene was reported for NMP.^[41] By a centrifugation procedure using iterative SBS steps in cascades, monolayer volume fractions up to 75% were achieved in the case of WS_2 .^[131] The disadvantage of SBS is that it is very challenging to enrich thin and SL-nanosheets unless they are very small in lateral dimensions hence having low sedimentation coefficient values.

However, control on the number of layers can be achieved via DGU, where 2D crystals in dispersion are ultracentrifuged in a preformed DGM.^[168] During the DGU process, the 2D crystals move along the ultracentrifuge tube, until they reach the corresponding isopycnic point, i.e., the point where their buoyant density matches the one of the surrounding DGM.^[169] There are many parameters affecting the buoyant density such as the dispersed material,^[170] the type and concentration of surfactant/polymer,^[155] the DGM^[163] and also the pH.^[170] Isopycnic separation, see (Figure 4b), has been widely used to sort 1D nanomaterials such as CNTs by diameter^[164] owing to the intrinsic difference in the density between nanotubes of different diameters or by using the co-surfactant effect to exploit the affinity of metallic and semiconducting nanotubes towards a certain type of surfactant to obtain their separation.^[165] However, in

the case of 2D-crystal sheets, the sorting process shows notable differences and additional complications that need to be overcome. First, monolayers and bulk layered crystals have the same ρ , second, the large majority of 2D crystals have high density (e.g., MoS_2 , $\rho = 5.06 \text{ g cm}^{-3}$, WS_2 , $\rho = 7.5 \text{ g cm}^{-3}$, WSe_2 , $\rho = 9.32 \text{ g cm}^{-3}$), thus rendering their sorting in common DGM (e.g., Iodixanol $\rho = 1.32 \text{ g cm}^{-3}$)^[155] very challenging. Thus, in order to separate nanosheets by layer number, it is important to ensure a uniform and well controlled surfactant/polymer coverage^[155,171] as the stabilization layer also contributes to the buoyant density. This will result in slight variations of the buoyant densities of SL and few-layer nanosheets which can lead to isopycnic separation if the density gradient is well matched to these subtle differences.^[24,37] To date, up to $\sim 80\%$ SL graphene yield was reported by using isopycnic separation with bile salts surfactants such as SC,^[37] a rigid amphiphilic molecule, consisting of a steroid skeleton with a carboxylic acid side chain and one to three hydroxyl ($-\text{OH}$) groups on the steroid backbone.^[155,172,173] Isopycnic separation was also used to separate GO sheets with different thickness.^[166]

Recently, the Hersam group tackled the limitation of isopycnic separation for high density inorganic 2D crystals wrapped by small surfactant molecules, such as the anionic SC,^[154,155] that are unable to reduce the buoyant density of such 2D crystals. By using Pluronic F68, a nonionic difunctional triblock (PEO–PPO–PEO) copolymer, consisting of two-terminal hydroxyl groups PEO (poly(ethylene oxide)) and a central PPO (poly(propyleneoxide)) chain,^[155,174] they demonstrated the possibility to form a greater hydration shell compared with SC, thus reducing the buoyant density of the encapsulated 2D-crystal sheets.^[38,39] It was also shown that Pluronic F68 is able to reduce the buoyant density of BN^[39] as well as MoS_2 , MoSe_2 , WS_2 , and WSe_2 ^[38] within the limit of the used DGM, thus being able to get a spatial separation along the ultracentrifuge tube of sheets with different density.

Within the DGU process, another method to sort 2D crystals is the rate zonal separation (RZS),^[168,175] (Figure 4c). In general, in RZS, the ultracentrifugation is stopped during the transient centrifugal regime, before the nanoparticles under ultracentrifugation reach their own isopycnic points.^[175] Rate zonal separation exploits differences in the sedimentation coefficient of nanoparticles under ultracentrifugation.^[175] Thus, nanoparticles with different s values will travel along the ultracentrifuge tube at different sedimentation velocities.^[168,175] This will cause a spatial separation along the ultracentrifuge tube.^[163,175] In the context of 2D crystals, RZS was first used to separate GO sheets with different lateral size,^[176] exploiting the fact that the larger is the nanosheet lateral size, the larger is their sedimentation rate. More recently, a modification of the RZS was also exploited for the lateral size selection of MoS_2 sheets allowing the measurement of A-exciton- MoS_2 photoluminescence in liquid dispersions.^[35]

While DGU-based separation offers a unique opportunity to sort nanosheets by thickness rather than mass, it suffers from notable disadvantages. For example, yields are currently very low, not allowing for a mass production of separated nanosheets. This is partly linked to low contents of monolayers in stock dispersions after the LPE process and can potentially be improved by optimizing exfoliation procedures in the near

future. In addition, DGU is typically a time-consuming multi-step process involving multiple iterations to achieve efficient size selection and the DGM in the dispersion may interfere with further processing and ink formulation.

3. Ink Formulations and Coating/Printing Strategies

The dispersions of liquid-exfoliated nanosheets produced by the aforementioned methods can be further processed in a number of coating and printing strategies. However, in many cases, the dispersion itself cannot serve as an ink directly. The composition of functional inks strongly depends on the type of deposition/printing process. On the one hand, the deposition by spray and drop casting can be carried out directly with the obtained dispersion, where the critical parameter in view of the final application is the morphology control of the dispersed nanomaterials (e.g., 2D-crystal sheets). On the other hand, other printing processes, such as inkjet, flexographic and gravure printing processes, require the formulation of a much more complex (structured) ink or paste (e.g., for screen printing). For example, conductive inks are multi-component system containing functional (nano)materials (the active material) such as nanoparticles (e.g., zinc oxide,^[177] cadmium sulfide,^[178] silver^[179]) conducting polymers (e.g., polysilicon,^[180] poly(3,4-ethylenedioxy)-thiophene-poly(styrenesulfonate)(PEDOT-PSS),^[181] CNTs,^[182–184] as well as graphene,^[41–46] RGO,^[185–189] and TMD^[190–192] sheets dispersed in a liquid vehicle, consisting of resins (binders), solvents (aqueous or organic) and additives with varying contents from 20% up to 80% depending on the ink type. Rheology and γ modifiers are also added to prevent aggregation and/or precipitation in order to provide the best printability performances.^[193]

The rheology of the inks strongly determines whether printing results are consistent and reproducible,^[193] (i.e., study of flow and deformation of materials under external perturbation) and therefore must be controlled within a quite narrow window.^[80,194] Due to their intrinsic formulation, inks exhibit complex rheological properties with a non-Newtonian flow behavior^[195] (i.e., nonlinear relationship between shear stress (τ) and shear rate ($\dot{\gamma}$)) and an apparent η ($\eta_{app} = \sigma/\dot{\gamma}$) which depend on $\dot{\gamma}$ (or τ), different from liquid Newtonians where $\eta = \sigma/\dot{\gamma}$.^[196] As a general role, $\dot{\gamma}$ determines the η behavior of fluids, as well as that of inks, establishing the limits of their application range. Figure 5 shows the relationship between η and $\dot{\gamma}$ for Newtonian and non-Newtonian fluids. According to their flow behavior, there are different classifications for non-Newtonian inks:^[197] pseudoplastic or shear thinning, where η_{app} decreases with increasing $\dot{\gamma}$,^[197] dilatant or shear thickening where η_{app} increases with increasing $\dot{\gamma}$,^[197] and thixotropic, where η_{app} decreases with time under a constant deformation and will start to rebuild upon the removal of the shearing force η_{app} .^[197]

In addition, the rheology of the inks is strongly influenced by the nanoparticles volume fraction (or content) ϕ , as well as their shape and spatial arrangement.^[198] In general, nanoparticles dispersed in a flowing liquid affect its flow field resulting in an increase in energy dissipation due to fluid-particle and/

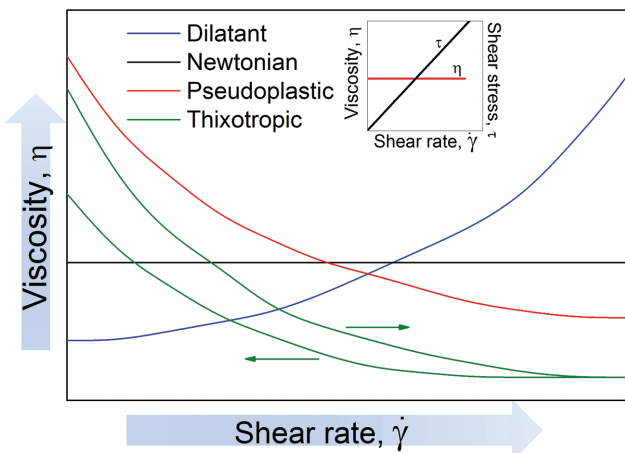


Figure 5. Newtonian and non-Newtonian flow behaviors of functional inks. Inset: Flow and viscosity curves for a Newtonian liquid.

or particle-particle interactions.^[198,199] The fluid-particle and/or particle-particle interactions increase with ϕ , restricting the particles diffusion into small “domains,” formed by the nearest neighbors and η diverges according to the generalized Stokes-Einstein relation:^[200] $D = (k_B T / 6\phi\eta r)$, which links the diffusion coefficient (D) of the particle to the η of the fluid where it is dispersed. Here k_B , T , and r are the Boltzmann constant ($k_B = 1.38 \times 10^{-23} \text{ J K}^{-1}$), the absolute temperature (K), and the particle radius (m), respectively.

Although strong research effort has been carried out to determine the η value of fluids with dispersed nanoparticles,^[201–203] currently, no theoretical model could predict it precisely. Einstein-Batchelor equation,^[204–206] $\eta = 1 + 2.5\phi + 6.2\phi^2$, describes the relationship between η and ϕ in the simple case of randomly dispersed spherical particles in the dilute dispersion regime ($\phi < 10$).

Another analytical approach to describe the effect of ϕ on the η of the dispersion has been formulated by Krieger and Dougherty^[207]

$$\frac{\eta_{nf}}{\eta_s} = \left(1 - \frac{\phi}{\phi_m}\right)^{-B\phi_m} \quad (2)$$

where η_{nf} is the particles fluid viscosity, η_s the viscosity of the pure solvent, ϕ_m the maximum particles packing fraction (varying in the 0.495–0.605 values range^[203]) and B the “Einstein coefficient” or “intrinsic viscosity”, which has the value of 2.5 for dispersion of monodispersed hard spheres, increasing its values for particles of high “aspect ratio,” L (lateral size vs thickness).^[208] In addition, the orientation of asymmetric particles in flowing dispersions will depend on the balance between hydrodynamic forces and the Brownian motions.^[198] The hydrodynamic forces oblige the particles to be aligned with the flow, while the Brownian motion tends to randomize their motion.^[198] The Peclét number, N_{Pe} :^[198]

$$N_{Pe} = \frac{6\pi\eta\lambda^3}{k_B T} \gamma \quad (3)$$

where λ is the characteristic particle size, determines what is the predominant contribution to the orientation of the particles in a fluid flow.

At low N_{Pe} value (<1) Brownian motion dominates the particles orientation, while, differently, for $N_{Pe} \geq 1$ the hydrodynamic forces prevail and, the fluids η varies between low-shear Newtonian and shear-thinning regimes, respectively.^[198]

In the case of 2D nanosheets, i.e., plate-like geometry, the η variation is strongly affected by the high aspect ratio (lateral size vs thickness).^[208–212] In fact, the increase in contact area and surface interaction between elongated and plate-like nanoparticles (e.g., 2D sheets represent an extreme case) results in an increase in the η of the dispersion, with respect to the one of spherical nanoparticles (at similar conditions of loadings and density).^[213]

The role of nanoparticle contents or ϕ on the η of the dispersion has also been largely investigated. For example, the η of an aqueous dispersion of Al_2O_3 nanoparticles increased with increasing nanoparticles ϕ .^[214] Similar results have also been demonstrated for aqueous dispersions of CNTs, where at a given shear rate, the dispersion η increases with the CNT concentration.^[215]

In the following sections, we will briefly introduce the main deposition/printing techniques that are currently more developed/used for the deposition/printing of 2D-crystal-based inks with a focus on the state of the art of the formulation of these functional inks.

3.1. Drop Casting and Spin Coating

3.1.1. Drop Casting

Drop casting is a simple and affordable approach (i.e., not requiring the structuring of the ink and the rheological parameters control) for the deposition of 2D crystals^[192,216] and other nanoparticle dispersions (e.g., organic polymer,^[217] fullerene,^[218] nanowires,^[219] CNTs,^[220] etc.). The process consists of casting the (nano)materials onto rigid or flexible substrates (e.g., poly(ethylene terephthalate) (PET)^[78,192,219,221] and poly(ethylene naphthalate) (PEN)^[222]) followed by solvent evaporation resulting in the formation of a thin film (Figure 6a). A final annealing step is often needed to remove residual solvent,^[223] even though the chemical composition of the substrate may limit this process step. The simplicity of the technique, i.e., no need of a complex ink formulation, is however balanced by the limited quality (i.e., homogeneity, thickness) of the final deposition/coating. In fact, although in principle it is possible to obtain films of good quality by simply varying the deposited dispersion/ink volume and/or the dispersed nanomaterial content (i.e., concentration), differential evaporation rates across the droplet can lead to a lack of control over the film thickness with the formation of a “picture framing effect” near the edges of the film.

In fact, in the cases of fast evaporation rates at the droplet edge, a flow of solvent and solute particles moves from the inner part to the edges to replenish the evaporated solvent (coffee ring effect^[224]) preventing uniform material deposition (Figure 6b).

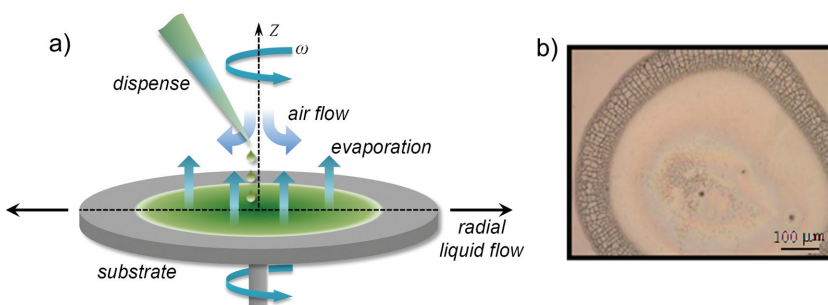


Figure 6. a,b) Illustration of the drop-casting technique (actually a spin-coating process is shown which is equivalent to drop casting if the substrate is not rotating) (a), together with representative images demonstrating the “coffee ring effect” (b).

A variety of strategies such as azeotropic mixture,^[225] inert gas purging,^[226] saturated solvent environment,^[227] or ultrasonic “substrate vibration-assisted drop casting” (SVADC),^[228,229] where the drop-cast dispersion is exposed to unidirectional sound waves (≈ 100 Hz), have been developed to improve the quality of the deposited film by controlling the solvent evaporation. Moreover, the chemical nature of the dispersed nanomaterial also influences the evaporation rate. It was demonstrated that GO sheets, for example, tend to block the solvent (i.e., water) evaporation path, leading to extended evaporation times.^[230] In addition, the properties of the surface functional groups determine the uniformity of the deposited films onto the substrates. For example, the catechol group favors the uniform deposition of RGO films on PET substrates.^[78]

The drop-casting approach is widely used in the deposition of 2D crystals in application areas where the control of the film quality (i.e., thickness, homogeneity) is not a stringent requirement, as for the case of electrodes for energy applications.^[36,231–233] Indeed, 2D-crystal-based electrodes fabricated by drop casting have been used in batteries,^[36] supercapacitors,^[231] and fuel cells.^[233]

Furthermore, drop-casting deposition of 2D crystals has been used for the realization of flexible, semitransparent, and free-standing GO membranes.^[77,234] The mechanical and optical properties (i.e., transparency) makes such membranes promising as electron transparent, but molecularly impenetrable electrodes for environmental electron microscopy in different environment (i.e., both in liquids and dense gases).^[77] Drop casting has also been proposed for using RGO on PET substrates as transparent conductive (TC) films. However, while these films show good transmittance (82%), they have high sheet resistance (R_S) value of $21.75 \text{ k}\Omega/\square$.

Drop casting has also shown to be a feasible approach for high-end applications. Indeed, BN and WS₂ sheets dispersed in water (with the aid of 1-pyrenesulfonic acid sodium salt as surfactant) and a mixture of ethanol/water, respectively, have been drop-cast on a preheated Si/SiO₂ substrate at 90 °C for BN and 60 °C for WS₂ to fabricate vertical heterostructures^[192] (see Section 5). However, although the obtained films were reported to be uniform and free of pinholes with no difference compared to other films produced by inkjet printing or vacuum filtration and transferring,^[192] this approach does not seem to be the most promising, reliable, and affordable for the realization of heterostructures from LPE 2D-crystal sheets when it comes to

large-scale reproducibility and micrometer control on the deposited features.

3.1.2. Spin Coating

Spin coating is a technique widely used in the production of microelectronic components.^[235–237] Therefore, significant efforts in recent years were devoted to applying this technique as a direct deposition tool of novel nanomaterial-based inks such as, quantum-dots,^[238–240] MNPs,^[241,242] CNTs,^[243,244] as well as 2D crystals such as RGO,^[56,57,245] graphene sheets,^[24] TMDs^[58,246] onto rigid or flexible

substrate. Typically, the ink is dropped onto the substrate, which is accelerated to a high angular velocity ω (rpm or Hz) to simultaneously spread the liquid across the entire surface and evaporate the solvent, to reach the targeted thickness (see Figure 6a). Depending on the ink and substrate properties, typical ω values vary in the range of 1500–6000 rpm (25–100 Hz).^[247] The balance between the centrifugal and the viscous (at the liquid/substrate interface) force governs the flow of the solvent in the radial direction.^[248] During the spin-coating process, a convective outflow of the liquid phase together with a solvent evaporation leads simultaneously to a decrease of the solvent diffusivity and to an increase of the solid-phase concentration.^[248] This determines an increase in the η of the dispersion.^[248] The final surface morphology and film thickness depend on several parameters such as, ω , η , ρ , γ and solute concentration.^[237] In particular, barring any unusual boundary jetting conditions, the ω value strongly influences the film thickness (from few nanometers to several micrometers).^[249]

Spin coating of 2D-crystal-based dispersions^[56–58,245,246] has been developed for the realization of electrodes for photovoltaic,^[57,58,246] micro-supercapacitors,^[245] or field emitters,^[56] where the thickness and homogeneity control of the electrode itself play a crucial role. For example, Kymakis et al.^[57] demonstrated the preparation of RGO films by spin coating with a thickness of 20 nm having a R_S of $2 \text{ k}\Omega/\square$ and a transparency higher than 70%. The as-produced film was then used as TC electrode in organic solar cells (OSCs).^[57] MoS₂ sheet-based films prepared by spin coating were instead used as hole transport layers in OSCs.^[58]

Spin coating has also been used for the realization of all solid-state RGO-based in-plane interdigital micro-supercapacitors on both rigid and flexible substrates through micro-patterning of spin-coated RGO films, having a thickness in the 6–100 nm range.^[245] Due to the high electrical conductivity (σ), i.e., 345 S cm^{-1} , of the fabricated RGO films and the in-plane geometry of the microdevices, the as-prepared micro-supercapacitors deliver a remarkable power density of 495 W cm^{-3} and an energy density of 2.5 mW h cm^{-3} , which is comparable to that of lithium thin-film batteries.^[245]

3.2. Inkjet Printing

Inkjet printing is a direct-write technique originally developed to transfer computer information data onto paper, polymeric,

metallic, and ceramic substrates,^[250,251] which subsequently evolved in other emerging technology areas such as biotechnology^[251–255] and electronics.^[76,256–258] Nowadays, inkjet printing is used to print a wide range of optoelectronic devices (i.e., organic field-effect transistor (OFETs),^[1,259,260] organic light-emitting diodes (OLEDs),^[261,262] sensors^[189] and solar cells,^[263,264] just to cite a few).

Inkjet printing is a non-contact (i.e., there is no contact between the print-head and the substrate) technique based on the digitally controlled deposition of small droplets (typical diameter 50–80 µm) of liquid inks, ejected (under pressure) from the print-head nozzle (a , µm) directly onto a specific position of a desired substrate.^[265,266] Continuous inkjet (CIJ)^[267,268] (see Figure 7a) and drop-on-demand (DOD)^[269] (Figure 7b) are the two most common inkjet printing modes. Today, the majority of inkjet printers are based on DOD technology.

In an inkjet process, a regular jetting from the print-head nozzle, a , where the reported unit in µm represents its diameter, is needed to prevent printing instabilities, such as satellite drops and jetting deflection (see Figure 7c).^[41,266,270] Indeed, each pressure pulse generates a single droplet composed by a leading drop and a tail that could break-up into satellite drops causing printing instability with decreasing printing resolution.^[271] In addition, depending on the ink wettability behavior at the nozzle orifice, undesirable spray formation rather than regular jetting may occur.^[251] Moreover, the final resolution of the printed feature is influenced by the impact velocity of the drop (i.e., 5–10 m s⁻¹) onto the substrate.^[271]

The realization of printable inks made of nanomaterials is thus a very challenging task, since the various liquid properties such as ρ , γ , and η have a strong effect on the printing process.^[272] These properties need to be carefully evaluated and tuned on-demand for the proper formation and ejection of droplets from the nozzles.^[250] All these ink physical properties can be summarized in dimensionless figures of merit (FoM) such as: the Reynolds (N_{Re}) and Weber (N_{We}) numbers representing the ratio of inertial to viscous forces and the balance

between inertial and capillary forces, respectively,^[273,274] and the inverse of the Ohnesorge number, Z ($1/N_{Oh}$).^[273] The Z number is independent of the drop velocity v (m s⁻¹) and it is defined as the ratio between the N_{Re} and the square root of the N_{We} . These three FoM are defined as follows:

$$N_{Re} = \frac{vap}{\nu}; \quad N_{We} = \frac{v^2 a \rho}{\gamma}; \quad Z = \frac{(a \rho \gamma)^{1/2}}{\nu} = \frac{N_{Re}}{(N_{We})^{1/2}} \quad (4)$$

In 1994, Fromm^[275] predicted $Z > 2$ for stable drop formation in drop-on-demand printing on the basis of numerical analysis. Later, Jang et al.^[276] redefined the printable range as $4 \leq Z \leq 14$ by considering single drop formation, printed drop position accuracy and jetting frequency. Z values lower than 4 result in droplet formation with long thin tails and long times to single droplet creation, negatively affecting accuracy in both position and resolution.^[276] In turn, Z values above 14 give rise to satellite drop formation,^[276] (Figure 7c). However, there are many other reports that have demonstrated stable inkjet printing with Z values of the printing ink outside this $4 \leq Z \leq 14$ range.^[41,277–280] For example, refs. [279,280] have demonstrated stable printing with Z of 1 and 2.7 for photoresist^[279] and water/glycerol^[280] inks, respectively. Stable inkjet printing with inks having Z values higher than 14 were reported for water/ethylene glycol (EG) ($Z = 35.5$)^[277] and water/glycerol ($Z = 68.5$)^[281] inks. Nanomaterial-based inks have also been inkjet printed with Z values higher than 14. Indeed, polystyrene nanoparticle-based inks with different Z values (from 21 to 91)^[278] and graphene-based inks in NMP-EG mixtures ($Z = 24$)^[41] have been successfully printed. It is important to note that NMP-based dispersions have shown $Z = 17$,^[43] which is in the required standard range for optimal inkjet conditions.^[276] The morphological properties (the lateral size in particular for 2D crystals) of the nanoparticles/nanotubes/sheets dispersed in the ink as well as the formation of aggregates in the ink and their accumulation on the print-head can also contribute to printing instabilities. It has been

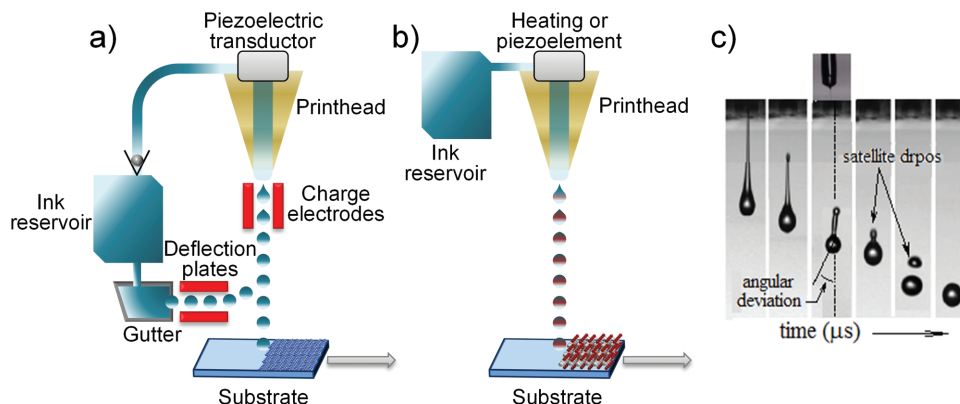


Figure 7. Schematic description of the inkjet-printing modes used for the deposition of 2D-crystal-based inks, such as graphene and WS₂. a) In the CIJ method, the ejected droplets are electrically charged by a charging electrode placed at the drop break-off point and then directed toward the substrate by a high-voltage deflection plate. The unused droplets are directed to a gutter and then to the ink reservoir. Typically, CIJ works with drop generation varying in the 50–175 kHz frequency range and drops in velocity at the nozzle > 10 m s⁻¹.^[267,268] b) In the DOD method, the ink droplets are jetted in a specific position onto the substrate only when required. In addition, DOD printers operate at acoustic frequency (1–20 kHz) and the pressure pulse for droplet ejection is generated by thermal heating (350–400 °C)^[269] or piezoelectric elements.^[268] c) Representative image sequence of DOD inkjet drop formation and jetting. Adapted with permission.^[280] Copyright 2012, Royal Society of Chemistry.

demonstrated^[282,283] that dispersed nanomaterials with lateral sizes smaller than $\approx 1/50$ of the nozzle diameter (typically $\geq 100 \mu\text{m}$ ^[179,284]) can largely reduce these detrimental effects.

In addition, the correct distance of the nozzle to the substrate (typically 1–3 mm)^[285] as well as wetting and adhesion^[266,270] to the substrate are further requirements for both ink optimization and its reliable and precise printing/deposition. The behavior of a droplet which spreads on the substrate under the action of the inertia and surface forces is characterized by the dynamic contact angle θ_c ,^[145,286] a parameter correlated with the substrate wettability.

Several inkjet printable conductive inks based on nanomaterials have been formulated, ranging from MNPs^[287] to organic semiconductors^[288] and CNTs.^[289–292] However, these nanomaterials suffer several limitations. For example, silver and copper MNPs,^[293,294] exploited for the formulation of conductive inks, are expensive and not stable in most common solvents (e.g., water, acetone, IPA, ethanol), thus requiring stabilizers for their dispersion in such solvents.^[187,272] Furthermore, MNPs-based inks show a tendency toward oxidation,^[187,272] and high-temperature sintering post-processing is often required.^[295] Organic semiconductor,^[296] used mainly for the realization of OFETs, have low mobilities (μ) of charge carriers ($\approx 1 \text{ cm}^2 \text{ V}^{-1} \text{ s}^{-1}$),^[297] while CNTs suffer electrical heterogeneity (being a combination of metallic and semiconducting),^[298] thus usually requiring separation prior to using them as conductive inks.^[155,164,165,299]

Hence, alternatives are being investigated. Graphene and other 2D crystals are emerging as promising functional materials for ink formulation.^[41–46] The first attempts in formulating 2D-crystal-based inks for inkjet printing were based on GO.^[185,187,188,300–311] Luechinger et al.^[187] produced a RGO-stabilized Cu nanoparticle ink to replace costly MNP-based inks.^[295] Refs. [189,300,307] reported inkjet-printed RGO films for sensor applications, with μ up to $90 \text{ cm}^2 \text{ V}^{-1} \text{ s}^{-1}$ having been achieved for inkjet-printed RGO films, with an ON/OFF current ratio up to 10.^[188]

The formulation of functional inks based on pristine LPE graphene sheets is mostly driven by the requirements set by the choice of solvents able to disperse the sheets in addition to the aforementioned constraints related to the ink printability,^[266–273] thus limiting the selection/choice of suitable solvents, as discussed in Section 2.1.2. The initial attempts^[41,42] exploited graphene inks prepared in NMP^[41] and DMF and subsequent solvent exchange with terpineol,^[42] respectively, to print conductive stripes reaching $R_S \approx 30 \text{ k}\Omega/\square$ on glass substrates. In refs.,[45,312] the authors printed graphene ink on rigid substrates (glass^[45] and SiO_2 ^[312]) previously treated with hexamethyldisilazane (HDMs), to prevent undesired coffee-ring effects of the printed features. In both cases, the as-printed graphene stripes were thermally post-annealed at temperatures higher than 250°C , achieving R_S in the 1–3 $\text{k}\Omega/\square$ range.^[45,312] Alternatively, coffee ring effects can be minimized by using low-boiling-point solvents, with higher enthalpy of vaporization (ΔH_{vap} ; kJ mol^{-1}) than water, as well as substrates that promote adhesion.^[313] However, in the case of 2D crystals, the use of low-boiling-point solvents during the exfoliation (see Section

2.1.2) could not be the right strategy due to the mismatch between γ of the solvent and the surface energy of the sheets. This issue could be overcome by the exploitation of co-solvents.^[46,148,149,153] Bonaccorso and co-workers^[46] demonstrated a strategy to tune the fluidic properties of water/ethanol mixtures for the LPE of graphite and the subsequent formulation of graphene-based inks with $Z = 10.3$. This allowed for the direct inkjet printing of conductive stripes from low-boiling-point solvents on PET ($R_S \approx 13 \text{ k}\Omega/\square$). There are other reports of graphene-based ink deposited on flexible substrates. Arapov et al.^[44] used graphene ink in ethylene glycol mixed with a copolymer of *N*-vinyl-2-pyrrolidone and vinyl acetate to print on “FS3” papers (a glossy, polymer-coated paper to increase the wettability), achieving $R_S \approx 1–2 \text{ k}\Omega/\square$. Finn et al.^[43] used a graphene ink in NMP to print conductive stripes on PET foils coated with aluminum oxide and poly(vinyl alcohol) to reduce substrate-related drying problems.

Recently, Li et al.^[191] and Östling et al.^[190] based on their previous experimental results,^[42,314] proposed a general route to efficiently integrate graphene inks as well as other 2D crystals (e.g., MoS₂, WS₂) with the inkjet printing technology, overcoming several still existing drawbacks for a reliable mass production of high-quality 2D-crystal-based films/patterns as described below. The process relies on a distillation-assisted solvent exchange in combination with polymer stabilization (ethyl cellulose (EC), $\eta = 4$ and 22 mPa s).^[190] This enabled them to formulate an environmentally friendly and printable MoS₂ ink consisting of MoS₂ few-layers (>6 layer by Raman investigation, 5–7 nm thick by cross-sectional profile analysis) in terpineol.^[190] The MoS₂/terpineol ink was tailored with ethanol-EtOH- ($\eta_{\text{EtOH}} \approx 1 \text{ mPa s}$ and MoS₂ concentration $\approx 1 \text{ mg mL}^{-1}$) and stabilized with EC polymer to allow for excellent jetting and printing resolution (droplet diameter or line width) of $\approx 80 \mu\text{m}$ on Si/SiO₂ substrate.^[190]

In 2014 Withers et al.^[192] reported on combining graphene, WS₂, MoS₂, and BN via drop-casting, inkjet printing, and vacuum filtration for the realization of heterostructures. However, the deposition methods used were not clear. No rheological characterization of the inks was reported and the concentration of the obtained dispersion appeared to be low for inkjet printing (WS₂ = 0.04 mg mL⁻¹, MoS₂ = 0.05 mg mL⁻¹ and BN = 0.1 mg mL⁻¹).

Despite this progress, several issues need to be still overcome for the optimization of 2D-crystal-based inkjet printing. The main problem is that the common solvents used in LPE (e.g., DMF and NMP) are toxic and have very low η (<2 mPa s), the latter strongly decreasing the jetting performance. In addition, the concentration of 2D crystals in these solvents is low (<1 g L⁻¹), thus requiring many print passes to obtain functional films. Another issue to be faced, especially with the use of high-boiling-point solvents is the required post-processing annealing for solvent removal,^[315] which poses severe limitations to the type of substrate to be used for the printing process. Similar issues are also faced in the case of 2D-crystal-based inks prepared in aqueous solution, where the surfactants/polymers removal requires thermal and/or chemical treatments,^[316] which are often not compatible with the substrate.

3.3. Spray Coating

Spray coating is a well-known deposition technique widely used in graphic art^[317] and industrial coating^[318,319] applications, allowing fast deposition of functional inks over both rigid and flexible large-area substrates (>several cm).^[320,321] The technique involves the spraying of the ink through a nozzle where a fine aerosol is formed, by applying pressure to a transporting gas or ultrasound automatism (ultrasonic spray deposition).^[320] The aerosol could also be formed by using electricity to disperse a liquid, through a technique called electrospray.^[322,323]

The aerosol formation as well as the drying process is not simple and several processing parameters such as solvent nature (e.g., polarity, solvent pressure),^[324] η ,^[325] flow rate,^[324] distance substrate/spray-nozzle (d),^[320,326] must be controlled in order to obtain a thin (from nm to μm range) uniform film.^[327] A critical parameter is the nature of the solvent, which determines its evaporation rate at the substrate surface. In fact, solvents with low vapor pressure such NMP (0.34 mm Hg @ 25 °C),^[328] promote long crystal formation time allowing for a reliable structural arrangement prior to the transition to the solid phase.^[324] On the contrary, high-vapor-pressure solvents such as IPA (33 mm Hg @ 25 °C) and toluene (24 mm Hg @ 25 °C) promote faster solvent evaporation. This substantially reducing the ability of the functional particles to organize themselves in a highly ordered fashion, which ultimately decreases the final device performance (e.g., μ in thin-film transistors (TFT)).^[324] In addition, small nozzle size and/or low pressure, which reduce the flow rate, produce scattered droplets on the substrate leading to a non-uniform coating.^[324] Differently, high deposition rates give rise to a continuous coating.^[324] The substrate/nozzle distance d is another key parameter determining the uniformity of the coating on the substrate underneath.^[320] For small d values, the ink on the substrate can be blown away by the incoming flow. On the contrary, for large d values, the solvent can evaporate before the droplets reach the substrate. Optimal d values have been reported to be comprised in the 10–15 cm range.^[321,324] To address this, Yu et al.^[329] reported a relationship between droplet size and spray height (Equation (5)):

$$D_{av} = \frac{\nu_d \Delta H_{vap}}{2\pi \kappa_d \Delta T} \quad (5)$$

where D_{av} is the average droplet diameter, ν_d is the average drying rate (mass/time) of the droplet, ΔH_{vap} is the latent heat of vaporization (J g^{-1}), κ_d is the thermal conductivity of the liquid droplet ($\text{W m}^{-1} \text{K}^{-1}$) and ΔT (K) is the mean temperature difference between the droplet surface and the surrounding air.^[330]

Significant advances of this technique using nanomaterials have been achieved,^[331–334] providing a platform for the realization of large-area devices ranging from flexible gas sensors^[331,335] to pharmaceutical applications^[332–334] and conductive patterns.^[336,337]

For example, in the context of conductive inks, a silver MNPs-based ink for OSCs was recently designed.^[338] However, despite the electrical performances achieved by the deposited silver-MNPs-based ink (R_S lower than $1 \Omega \square^{-1}$), these OSCs suffer several problems, such as high cost and oxidation.^[263] Graphene sheets, RGO, and graphene nanoplatelets (GNPs) are cheaper alternatives, showing most of the features essential to conducting inks (high σ ,^[16,31] mechanical robustness and flexibility,^[17,24,26,31] environmental stability,^[31] and cheap production strategies^[24]) providing a new prospective towards the use of new materials for large-area thin functional layer deposition.^[24,31]

Spray coating is very versatile, being the ideal deposition technique for large-area coatings (Figure 8a). An ultrasonic spray coating method has been reported by Lin et al.,^[339] to produce TC (transmittance $\geq 80\%$ and $R_S \leq 300 \Omega \square^{-1}$) films from a hybrid graphene/conductive nano-filaments (dimension < 200 nm, and filament/graphene weight ratio varying from 1/99 up to 99/1), for several applications ranging from solar cells, to light-emitting diodes to touch screens and displays. Spray coating of graphene sheets, synthesized by electrochemical exfoliation^[340] dispersed in DMF onto a $1.5 \times 1.5 \text{ cm}$ flexible polymer substrate (PET) was demonstrated for the realization of transparent electrodes.^[337] The obtained R_S was $1.35 \times 10^5 \Omega \square^{-1}$ at 70% transmittance.^[337]

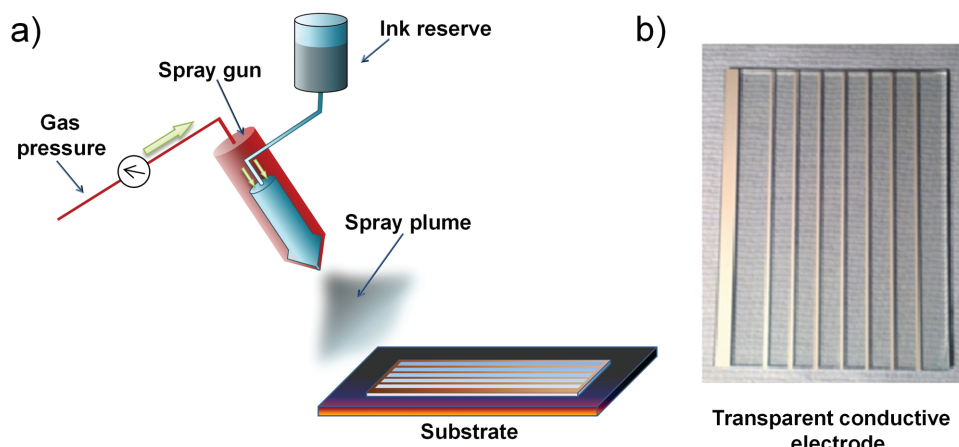


Figure 8. a) Schematic of the spray-coating process of a 2D-crystal-based ink, deposited through the air onto the substrate by a spray gun. b) Optical image of a large-area graphene-based transparent conductive electrode.

Recently, Casaluci et al.^[341] demonstrated the printability of graphene inks in DMF, on very large area transparent conductive oxide (TCO) ($>90\text{ cm}^2$) by spray coating using a low η ink ($\eta = 1.02\text{ mPa s}$, only $\approx 8\%$ higher than the solvent one $\eta = 0.93\text{ mPa s}$ ^[342]). The semitransparent (transmittance 44%) counter-electrode (CE) (Figure 8b) was successfully integrated in a large-area ($>43\text{ cm}^2$ active area) dye-sensitized solar cell (DSSC) module, with the graphene sheets used to replace platinum, the standard CE material,^[343] achieving a power conversion efficiency (η) of 3.5%.^[341]

Spray coating also allows for the deposition of more structured (multicomponent) inks. For example, a conductive ink made of thermoplastic starch-based polymer (Mater-Bi) and GNPs dispersed in chloroform was recently formulated and spray painted on pure cellulose sheets.^[60] After hot-pressing into their fiber network, the resultant nanostructured flexible composites have shown a very low R_S value of $\approx 10\text{ }\Omega/\square$.^[60]

3.4. Flexographic and Gravure Printing

Continuous roll-to-roll (R2R) (flexography or flexo^[344] and rotogravure or gravure^[345]) printing techniques are fast transfer printing pathways onto large-area target substrates (e.g., paper,^[346,347] plastic,^[348,349] polymer,^[350,351] and metal layers^[352]) for a large variety of end applications. For example, gravure (Figure 9a) and flexo (Figure 9b) are the main printing processes in the packaging industry,^[353] but they are also commonly used in other printing areas such as books and newspapers.^[346]

In flexography, the ink is transferred onto the sacrificial thin support-substrate placed on an engraved ink-metering “anilox” cylinder and then, after removal of the ink excess from non-image area surfaces (doctor blade), the relief passes to the

printing-plate (flexoplate) and is finally impressed onto the desired target substrate^[354] (Figure 9). Some stringent features must be guaranteed for a correct printing process.^[354] In this respect, the support substrate (also known as the web) must be flexible in order to wrap onto the anilox and must have sufficient high modulus and strength to imprint the dispersed active material.^[355] Differences between flexo and gravure mainly rely in the applied pressure and in the ink transfer pathway.^[263] In other words, flexography is a type of printing process that uses a plate with a raised surface and fast drying fluid inks to print directly onto the desired substrate.^[354] Alternatively, gravure is an intaglio printing process, which involves engraving the image onto an image carrier and then, printing on the target substrate under a given pressure (Figure 9a). Other differences between gravure and flexo rely in the printing speed (m min^{-1}), gravure being faster ($\approx 1000\text{ m min}^{-1}$) than flexo ($\approx 500\text{ m min}^{-1}$), as well as in the thickness of printed stripes ($<1\text{ }\mu\text{m}$ in flexo and $\approx 1\text{ }\mu\text{m}$ in gravure) and ink η .^[354] In particular, the ink η used in flexo printing (i.e., in the 50–500 mPa s range) is usually lower than that used in gravure (100–1000 mPa s) as well as in screen (500–5000 mPa s) and offset (100–10000 mPa s) printing techniques.^[354]

The inks have two main components: the active material, e.g., a colorant (pigment or dye)^[356] or nanoparticles (with silver, copper phthalocyanine blue, and carbon black being the most commonly used in the printing industry)^[357] and the vehicle, consisting of resins (binders), solvents and additives (i.e., plasticizers, waxes, and anti-foaming agents).^[359] The purpose of the vehicle is to carry the active material to the substrate, holding it there.^[358] Since the active material and binder are both solids, the main function of the solvent is to act as a carrier, which, however, must also be easily removed from the print after the transfer is completed.^[359]

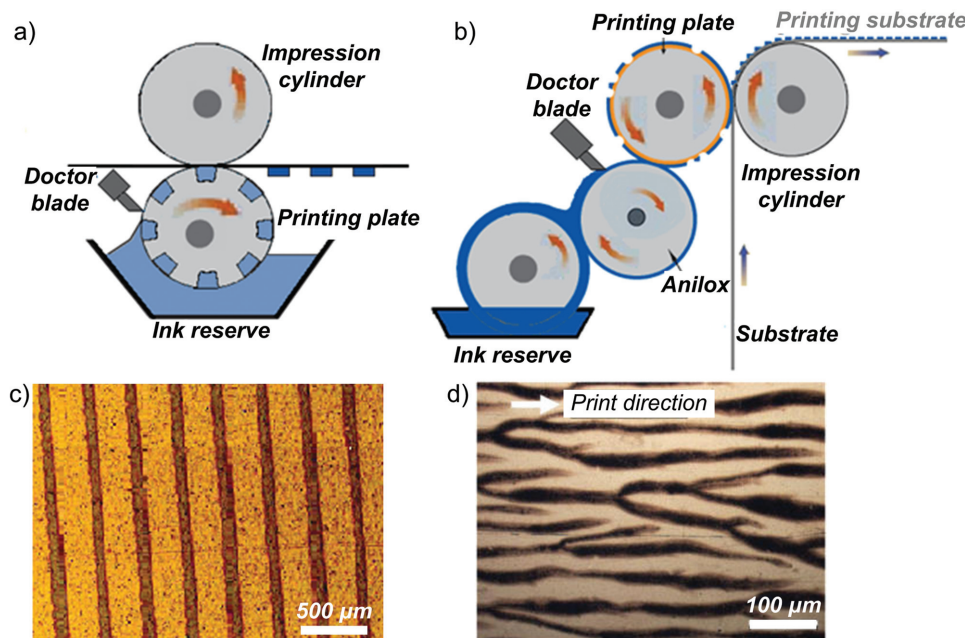


Figure 9. Schematic description of a) the gravure and b) the flexographic printing processes. Optical images showing c) the printed line formation for gravure printing. Adapted with permission.^[79] Copyright 2014, Wiley-VCH. d) GNP-based flexo-printed indium tin oxide (ITO) electrode. Adapted with permission.^[80] Copyright 2014, Taylor & Francis.

Successful gravure and flexo printing requires inks to be transferred to the substrate in a controlled and uniform way.^[360,361] Ink solvent, its η , or the applied pressure and transfer roll material significantly affect this critical step. For example, organic solvents (usually used in gravure printing) could cause swelling of the silicone that blanket the impression roll, distorting the printing quality i.e., the degree to which the appearance characteristics of the print fulfill those of the desired target,^[360,361] being the result of several interacting properties and factors.

Recently, R2R techniques have been used for the printing of nanomaterials.^[362–364] The flexographic printing technique was applied by Jo et al.^[362] to fabricate OFETs, based on bis(triisopropyl-silyl ethynyl) pentacene organic semiconductors, having field-effect mobility of $0.08 \text{ cm}^2 \text{ V}^{-1} \text{ s}^{-1}$ and on/off current ratio of $\approx 10^5$, on various plastic substrates. Schmidt et al.^[363] developed a combined flexographic and gravure to manufacture OFETs based on poly(3,4-ethylene dioxythiophene) doped with PEDOT:PSS with channel length down to $10 \mu\text{m}$.

Chang and Hong^[364] reported the fabrication of zinc oxide (ZnO)-based nanowire field-effect transistors (FETs) by a roll-transfer printing technique using a poly(dimethylsiloxane) (PDMS) as elastic transfer substrate material. The authors demonstrated excellent device characteristics (electron mobility $\approx 91 \text{ cm}^2 \text{ V}^{-1} \text{ s}^{-1}$; threshold voltage $\approx 0.25 \text{ V}$) suggesting how the technique is promising for high-speed production of nanowire-transistors for flexible devices and flat panel displays.

More recently, Secor et al.^[79] demonstrated a full gravure printing of large-area, high-resolution patterns of LPE graphene sheets on flexible substrate (Kapton) by using graphene-EC ink in combination with a printing parameter optimization.^[79] A stable graphene/terpineol polymeric ink with η varying in the range $0.2\text{--}3 \text{ Pa s}$ ($\epsilon = 10 \text{ s}^{-1}$) was obtained from homogeneous dispersion of graphene-EC powder (5–10 wt%) in low viscous ethanol/terpineol mixture (2.5:1 volume %) followed by ethanol removal.^[79] The authors pointed out that the use of small lateral size graphene sheets ($\approx 50 \text{ nm} \times 50 \text{ nm}$ with typical thickness of $\approx 2 \text{ nm}$), prepared using SBS, is critical for high-resolution gravure printing where sub-micrometer particles are needed.^[79] From the obtained result of continuous, electrically conductive printed stripes (see Figure 9c) the authors offered a novel strategy to integrate the gravure techniques with the 2D nature of graphene sheets in the manufacture of large-area printed electronics.

A GNP-based flexo ink was developed by Baker et al.^[80] by optimizing the GNP/binder (i.e., carboxymethylcellulose (CMC)) ratio in water/IPA solutions, reaching a η of $\approx 20 \text{ mPa s}$. The ink was R2R printed onto a flexible ITO substrate at a speed of 0.4 m s^{-1} , maximizing the optical transmission of the printed layer to replace platinum as CE catalyst in flexible DSSCs.^[80]

The formulation of 2D-crystal-based flexo and gravure inks is still at its infancy with just a few proof of concept inks developed.^[79,80] Both inks are based on volatile alcohols, e.g., ethanol^[79] and IPA,^[80] a fact that could not satisfy the current environmental regulations that require the minimization of volatile organic compounds (VOC) and thereby limiting the use of volatile alcohols.^[346,365]

The formulation of inks for printing on different substrate is another critical point to be addressed. For example, printing on non-absorbing substrates is sensitive to the surface chemistry of both the ink and the substrate, and it will be a challenge to combine good printability, adhesion and film properties. For example, viscous fingering, caused by surface instabilities at the nip between the plate cylinder and the substrate as the ink splits^[366] was observed by printing flexo inks onto ITO (Figure 9d).^[80] The viscous fingering effect is aligned in the printing direction. For future developments, it will be mandatory to correlate the ink and substrate properties with the printing performance in order to obtain a better understanding of different factors affecting both gravure and flexography printing.

4. Screen Printing

Screen printing or serigraphy is a mass-printing technology widely used for electronics^[367] and also in other technologically relevant areas such as photovoltaic,^[368] displays,^[369] and automotives.^[370] The key advantage of screen printing over other printing technologies relies on the compatibility with a wide variety of functional inks/pastes and substrates.^[371,372] In general, a squeegee is used to move a paste through a patterned screen to deposit onto the substrate (see Figure 10a). The squeegee provides shear stress to the paste to reduce η and allows it to flow through the screen. In the screen printing technology, the rheological behavior (thixotropism, viscoelasticity, see Figure 10b) of the paste plays a critical role for its printability.^[373] During the printing step, $\dot{\gamma}$ of the pastes changes from very low ($\approx 1 \text{ s}^{-1}$) to very high ($\approx 1000 \text{ s}^{-1}$)^[374] values while η gradually decreases.^[373] Then, after printing, $\dot{\gamma}$ returns to decrease while η approximates its initial value so the paste forms a pattern onto the substrate. The size of the mesh screens is determined by the final application. For example fine mesh screens allow the patterns of solar cell grid designs.^[375]

Despite the high σ ($\approx 10^6\text{--}10^7 \text{ S m}^{-1}$) of printable noble metal pastes (silver being amongst the most utilized^[376]), the high cost is a critical issue. In this respect many attempts are devoted to replace noble metal pastes with cheaper ones, such as copper^[377,378] or aluminum.^[379] However, oxidative effects^[380–383] as well as the need of post printing sintering processes (e.g., thermal,^[294,384,385] microwave,^[179,386] plasma,^[387,388] electrical,^[389] chemical,^[386,390] and photonic^[391–393]) to obtain continuous metallic lines remain critical drawbacks. In this context, graphene-based conductive-pastes appear as an effective alternative to overcome some of the aforementioned issues, with the added value of recyclability^[394] and low toxicity.^[31,130] However, despite the potential advantages with respect to the MNP-based pastes, the use of graphene,^[53] RGO,^[395–397] and GNPs^[398,399] as active material of screen printing pastes is not yet widely developed, with just a few works reported up to date.

Nonetheless, the range of applications where graphene-based pastes have been proposed is quite broad.^[53,395–398] Quian et al.^[395] used simple screen-printing technology to prepare large-scale RGO field emission cathodes. The printed RGO-based cathode exhibited stable field emission with low threshold field ($\approx 1.5 \mu\text{m}^{-1}$). Sensitive and antifouling devices selective for simultaneous determination of biologic specimen

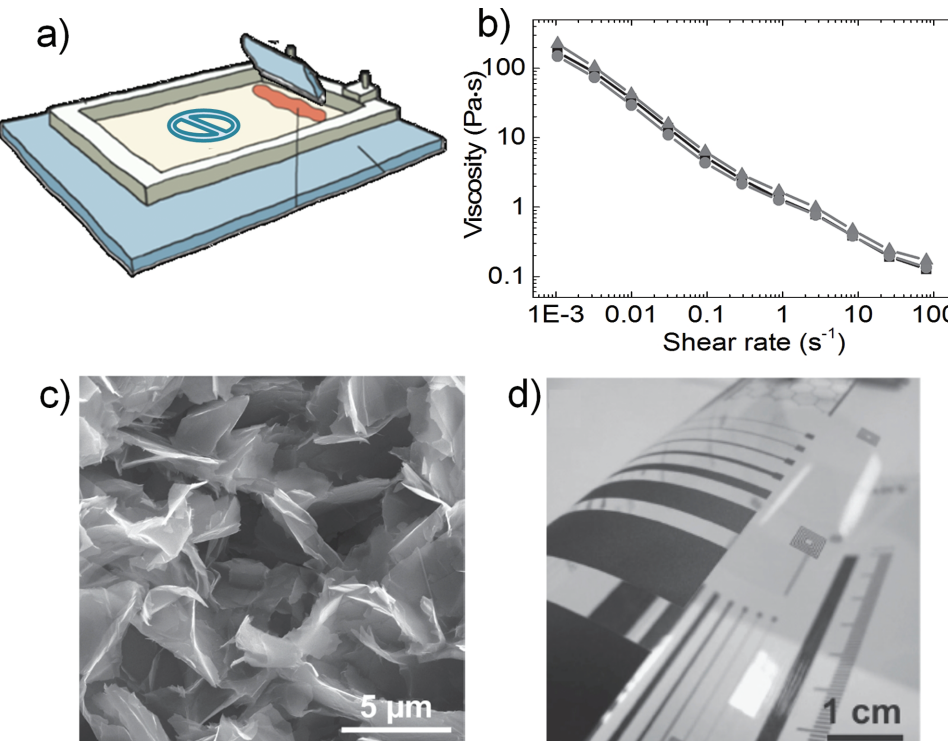


Figure 10. a) Schematic describing the screen printing process. b) Shear–viscosity curves for graphene paste. c) SEM image of a dried graphene gel. d) Graphene-based paste screen printed onto PET foil. b–d) Adapted with permission.^[54] Copyright 2014, Wiley-VCH.

(i.e., ascorbic acid (AA), dopamine (DA) and uric acid (UA)) in clinical and pharmaceutical applications were developed using screen printed RGO,^[397] proving its potential in the manufacture of alternative/novel pharmaceutical devices.

In 2014 Skrzetuska et al.^[400] prepared printing pastes for textronics applications,^[401] doping multiwall carbon nanotubes (MWNTs) with GNPs (1–3% wt%) and cross-linking additives (aliphatic urethane acrylate) promoted strong bonding with textile substrates. The obtained physicochemical properties of the printed paste were similar to those achieved by electronic printed elements on textile electro-conductive substrates.^[402] Wróblewski and Janczak^[398] fabricated transparent and flexible electrodes for electroluminescent displays, by screen printing GNPs-based paste in PET polymeric matrix onto different substrates (glass, Al₂O₃).

Very recently, Hyun et al.^[53] have demonstrated high-resolution screen printing of pristine graphene for printed electronics. They tackled one of the difficulties for graphene paste production, i.e., the realization of viscous and highly loaded dispersions of pristine graphene avoiding restacking and re-aggregation of the nanosheets. The paste was prepared from the graphene/EC powder in terpineol, with EC acting as a binder.^[53] The paste contained graphene sheets at a concentration of $\approx 80 \text{ mg mL}^{-1}$, with a η up to $\approx 10 \text{ Pa s}$ at a shear rate of 10 s^{-1} .^[53] The quality of the graphene paste was testified by the excellent σ ($\approx 1.9 \times 10^4 \text{ S m}^{-1}$) of screen printed stripes, which has allowed their use as source and drain printed electrode in an all-printed OFET,^[53] with poly(3-hexylthiophene) (P3HT), ion-gel, and PEDOT:PSS used as the semiconductor, gate dielectric, and gate electrode, respectively. The OFET has shown a μ of

$\approx 0.21 \text{ cm}^2 \text{ V}^{-1} \text{ s}^{-1}$ with a threshold voltage of $\approx 0.42 \text{ V}$.^[53] However, such performances are achieved after a thermal treatment at a temperature of $300 \text{ }^\circ\text{C}$ for 30 min to remove the polymer, i.e., EC, which was used to stabilize the nanomaterials in the ink.^[51]

Arapov et al.^[54] demonstrated a gelation approach starting from the dispersion of exfoliated expanded graphite in methyl ether dipropylene glycol in the presence of a binder (i.e., poly(vinyl acetate) and poly(vinylpyrrolidone)), which was developed to obtain a colloidally stable graphene paste for screen printing applications. The graphene paste has shown shear thinning behavior with structure restoration after mild shear, i.e., $< 10 \text{ s}^{-1}$, and structure breakdown at high shear rates, i.e., 100 s^{-1} (see Figure 10b).^[54] The paste is composed of defect-free graphene sheets (see Figure 10c) having excellent screen printability (<40 μm line width), with printed patterns showing $R_s = 30 \Omega/\square$ onto PET substrates (Figure 10d).^[54]

However, the development of 2D-crystal-based inks/pastes for screen printing requires huge effort is needed to understand the prospective of other 2D crystals (e.g., TMDs) in addition to the graphene-based materials (graphene, RGO, and GNP sheets). Paste chemistry and rheology must be carefully developed to take into account the processing conditions for the full-exploitation of 2D-crystal-based pastes.

5. Heterostructures

The availability of 2D-crystal-based inks with a large variety of optoelectronic properties could lead to the realization of heterostructures,^[403,404] i.e., isostructural system of 2D crystals

assembled by stacking different atomic planes in sandwiched structures. Heterostructures have already been demonstrated to play a key role in the development of current technology. Indeed, high mobility FETs,^[405] semiconductor lasers,^[406,407] and diodes^[408] are just a few examples of devices based on heterostructures. 2D-crystal-based heterostructures offer the prospect of extending existing technologies to their ultimate limit by using monolayer-thick tunnel barriers and quantum wells. First proof of principle 2D-crystal heterostructures e.g., p–n diodes based on a p-type BP/n-type monolayer MoS₂,^[409] vertical tunneling transistors based on graphene with a tunnel barrier made of atomically thin BN,^[410] or photovoltaic cells based on TMDs/graphene stacks,^[411] have already been demonstrated.

These first devices have raised interest in such heterostructures, where, in principle, it is easy to foresee many possible combinations of 2D crystals, to obtain stacks of many different layers with atomic precision. However, the practical realization of such vision is much more complicated. At present, three methods have been used for the realization of 2D-crystal-based heterostructures: I) layer by layer stacking via mechanical transfer;^[412–414] II) direct growth, both by CVD^[415–421] and molecular beam epitaxy (MBE);^[422] and III) layer by layer deposition of solution processed 2D crystals.^[190] Any industrial application will require a scalable approach. To this aim, “layer-by-layer deposition” from 2D-crystal-based inks could be, in the near future, the right strategy for the scalable production of 2D heterostructures. Progress on the large-scale placement of 2D-crystal-based inks by means of Langmuir–Blodgett,^[423] and drop casting and inkjet printing^[190,424] allows the deposition of layers of different 2D-crystal-based heterostructures on a large scale (see Figure 11).

Some proof of concept devices have already been demonstrated^[190] such as tunneling and in plane transistors, photodetectors, and photovoltaic devices. The simplest structure is an all-inkjet printed in-plane photodetector based on interdigitated graphene electrodes with a MoS₂ channel.^[43] Another example is a tunneling transistor, where the tunneling between the top and bottom graphene layer through a TMD layer, i.e., the barrier, is controlled by the back gate.^[425] A similar structure could also be exploited as a photovoltaic device, where light absorbed in the TMD is converted into photocurrent through the top and bottom conductive layers (e.g., graphene).

However, apart from the uniformity of large-area film stacks, the assembly of such heterostructures suffers from discontinuity of the individual crystals, thus resulting in structures with

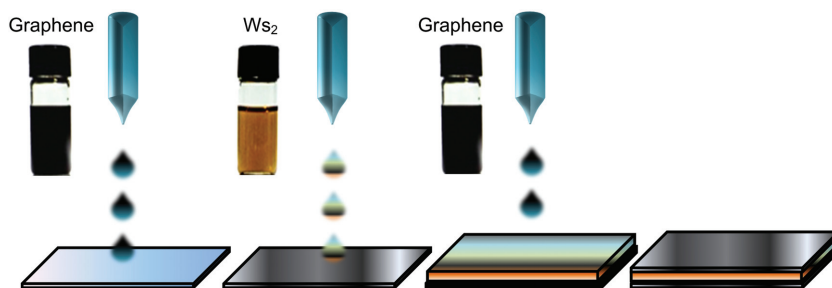


Figure 11. Scheme of a 2D-crystal-based heterostructure device-fabrication process.

optoelectronic properties of lower performance with respect to the one obtained by dry transfer methods such as layer by layer stacking via mechanical transfer^[412] and direct growth.^[415,422] Thus, before the layer-by-layer deposition of 2D-crystal-based dispersions and inks can be exploited for the realization of vertical 2D heterostructures with optoelectronic properties comparable with the ones achieved with the other approaches, a strong experimental effort is needed to fully evaluate the feasibility of this method and overcome the aforementioned issues.

6. Applications

In this section, we will briefly discuss some current key applications of 2D-crystal-based inks for the fabrication of printed optoelectronic devices, as well as sensors, solar cells, lithium ion-battery, and supercapacitors (Table 3).

6.1. Printed Optoelectronics

A number of applications require the development of large-area printed and flexible optoelectronics, with a market exceeding \$70B forecast by 2023.^[426] For “high end” electronic applications, such as tri-gate, ultrathin channel and planar ultrathin body transistors,^[32] it is very unlikely that these solution-processed 2D crystals will ever be used. However, there are many other applications that can exploit the optoelectronic properties of such nanomaterials. For example, in the field of TC films/electrodes, there are a number of every-day applications, such as smart windows (i.e., electrically switchable optical shutters),^[20,76] electromagnetic shielding,^[427] electrochromic windows,^[427] static dissipation,^[427] defrosting and oven windows,^[427] that could make use of, for example, graphene-based TC films. Considering that the majority of these low-tech applications do not require very low R_S (a few hundreds of Ω/\square are feasible values^[20]), LPE graphene could be the right candidate to replace conventional costly and brittle materials such as ITO^[427] for many of these applications, in particular due to the ease of fabrication and low cost. However, TC films produced by inkjet,^[41,42,45,46] gravure,^[51] and screen^[53] printing have not yet demonstrated acceptable values of R_S and transmittance, where for example the key requirements for TC windows in photovoltaic devices are $R_S < 10 \Omega/\square$ ^[428] and transmittance $>90\%$.^[428] Thus, future research will be necessary to reveal whether the achievement of such performances will be possible. Importantly, the use of spray and/or rod coating is likely the best strategy for TC film production, not having issues linked to the limited lateral size of the graphene sheets (clogging of the nozzle, see Section 3.2) affecting inkjet printing, and to the thickness of the printed feature (>15 nm), typical of gravure and screen printing.^[429]

Several inkjet-printed TFTs have been demonstrated with RGO as printable ink.^[188,189,300] The first inkjet-printed graphene-based TFT was presented by Torrisi et al.^[41] on Si/SiO₂ substrates. The

Table 3. Overview of printed components/devices based on 2D crystals. The target applications and the relative performances as well as the substrate type and the post-deposition treatments are summarized for graphene, GO, RGO, and TMD sheets. Please note that for the R_S value, the thickness is an essential parameter, but often not reported in literature. The extrapolation to 1 mil (25.4 μm), requiring a linear dependence of electrical conductivity with thickness, should always be reported for a correct and fair comparison of data.

Year	Process	Ink	Substrate	Posttreatment	Applications and performances	References
Graphene						
2012	Inkjet	LPE graphene in NMP	Si/SiO ₂ and glass with HMDS and O ₂ treatment	170 °C for 5'	TFT • $\mu \approx 95 \text{ cm}^2 \text{ V}^{-1} \text{ s}^{-1}$ • $R_S = 30 \text{ k}\Omega/\square$ • Tr = 80%	[41]
2012	Inkjet	Electrochemically exfoliated graphene in PEDOT/PSS	Carbon electrode	None	Electrodes for electrochemical detection of H ₂ O ₂ , NAD ⁺ /NADH and (Fe(CN) ₆ redox couple	[47]
2013	Inkjet	LPE graphene in EtOH and EC mixed in cyclohexanone/terpineol	HMDS-treated SiO ₂	250 °C for 730'	Flexible electrode • (electronic applications) • $R_S \approx 3 \text{ k}\Omega/\square$ • Thickness ≈ 140 nm	[312]
2013	Inkjet	LPE graphene in DMF, exchanged to terpineol	Glass slide	375–400 °C for 30'–60'	TFT and supercapacitor • Specific capacitances: • ≈ 0.59 mF cm ⁻² • $R_S = 30 \text{ k}\Omega/\square$ • Tr = 80%	[42]
2013	Rod coating	LPE graphene pre-exfoliated in NMP and redispersed in H ₂ O/EtOH	PET or Glass	None	Flexible TC film • $R_S = 45 \text{ k}\Omega/\square$ • Tr = 40%	[455]
2013	Screen printing	NGP/PANI hybrid inks ($\eta \approx 125 \text{ mPa s}$)	PET or carbon fabric substrates (NGP)	None	Supercapacitor • Specific capacitances: 26–269 F g ⁻¹ • Power density: 454 kW kg ⁻¹ • Energy density: 9.3 W h kg ⁻¹	[399]
2014	Inkjet	Ethylene glycol + Plasdome S-630 (copolymer of N-vinyl-2-pyrrolidone and vinyl acetate) ink	FS3 paper (glossy, polymer-coated paper) and LumiForte paper (rough paper without coating)	None	Mass production of conductive films for devices on paper • $R_S = 1\text{--}2 \text{ k}\Omega/\square$ • Thickness ≈ 800 nm	[44]
2014	Inkjet	LPE graphene mixed with EC and cyclohexanone	HMDS-treated glass slides	300 °C for 30 min	TC flexible electrodes • $R_S \approx 1 \text{ k}\Omega/\square$ • Tr = 60%	[45]
2014	Gravure printing	LPE in EtOH with EC	LPE in EtOH with EC	250 °C	Flexible and TC film • $R_S \approx 100 \text{ k}\Omega/\square$	[79]
2014	Inkjet	LPE in SDSB, addition of polyaniline	Carbon	80 °C for 2 h	Supercapacitors electrodes • Specific capacitance ≈ 82 F g ⁻¹ • Power density ≈ 124 kW kg ⁻¹ • Energy density ≈ 2.4 W h kg ⁻¹	[48]
2015	Inkjet	LPE graphene in H ₂ O/EtOH	PET	None	Conductive stripes • $R_S \approx 13 \text{ k}\Omega/\square$ • Tr = 22%	[46]
2015	Screen printing	LPE graphene in EC/Terpineol	PI	300 °C for 30'	Electrolyte-gated transistors (EGTs) • $R_S \approx 54 \text{ k}\Omega/\square$ • Thickness = 100–500 nm	[53]
2015	Screen printing	LPE graphene in EC/Terpineol (in presence of EtOH for dispersion)	Glassine paper	Photonic annealing with broad spectrum Xe lamp	Paper-based organic TFTs • Ink $\eta \approx 70 \text{ Pa s}$ • $R_S \approx 425 \text{ k}\Omega/\square$ • Thickness ≈ 1.1 μm	[81]
2015	Inkjet	$\gamma \approx 28.0 \text{ mN m}^{-1}$, $\eta \approx 2.34 \text{ mPa s}$, $\rho \approx 0.8 \text{ g cm}^{-3}$	LPE in IPA/PVA		CMOS devices as resistive humidity sensors	[456]

Table 3. Continued.

Year	Process	Ink	Substrate	Posttreatment	Applications and performances	References
2015	Inkjet	Graphene/EC in cyclohexanone/terpineol mixture (85:15) $\eta = 10\text{--}15 \text{ mPa s}$	PET, PEN, PI and glass	Annealing	TC film for flexible electronics	[51]
2015	Inkjet	Graphene–Ag/organic complex ink: graphene/EC in cyclohexanone–terpineol mixture graphene + TEC-CO-001	Si/SiO ₂ wafers (sonicated in EtOH for 30' and dried under argon flow)	>400 °C to remove the polymer stabilizer and reduce the Ag complex	Conductive flexible films for inkjet printed electronic devices • $R_S \approx 17.4 \text{ k}\Omega/\square$	[52]
GO and RGO						
2008	Inkjet	C/Cu nanopowder + copolymeric additive; ink $\eta = 1\text{--}2 \text{ mPa s}$	Laser/copier transparencies, Type C, Xerox	120 °C for 2 h	Metal nanocolloids in consumer goods	[187]
2009	Spin coating		Si/SiO ₂	Thermal annealing at 1000 °C	FET for CMOS technology $\mu > 50 \text{ cm}^2 \text{ V}^{-1} \text{ s}^{-1}$	[188]
2010	Inkjet	GO in H ₂ O/poly(ethylene glycol). RGO after ascorbic acid reduction redispersed in Tx-100	PET	Dried at 60 °C under vacuum for 12 h	Chemiresistor to detect NO ₂ and Cl ₂ vapors	[189]
2011	Inkjet	GO in H ₂ O	PET and PI coated with PSS and PEI	400 °C, for 3 h in 95% Ar + 5% H ₂	Flexible electronic circuit as H ₂ O ₂ sensor • $R_S \approx 1100 \text{ k}\Omega/\square$	[300]
2011	Inkjet	GO in H ₂ O	Ti foils	200 °C for 12 h in N ₂ flow	Specific capacitance of IPGE ranged from 48 to 132 F g ⁻¹	[302]
2011	Inkjet	GO in H ₂ O	Oxygen-plasma-treated PET	Hydrazine and ammonia vapor deposition, 90 °C [1 h]	Thin film as electrodes for a WB antenna (460.4–524.8 MHz) • $R_S \approx 65 \text{ k}\Omega/\square$ • Thickness ≈ 450 nm	[303]
2011	Inkjet	GO in H ₂ O	Oxygen-plasma-treated PVDF	Hydrazine and ammonia vapor deposition 90 °C [1 h]	Electrode as transparent flat-panel speaker • $R_S \approx 1.5 \text{ k}\Omega/\square$ • Tr = 67 %	[304]
2012	Inkjet	GO in H ₂ O	Oxygen-plasma-treated PET	IR heat 12' at 200 °C	Polymeric flexible NTC electrode: • Response time ≈ 0.5 s, • Recovery time ≈ 10 s • $R_S \approx 300 \text{ k}\Omega/\square$ • Tr = 86%	[305]
2012	Inkjet	Thermally reduced GO followed by high pressure homogenization in H ₂ O, acetone, or IPA	Inkjet printer foil	None	Flexible films for complex multilayer systems • $R_S \approx 980 \text{ k}\Omega/\square$ • Thickness = 5 μm	[306]
2012	Rod coating	GO/Pd in EtOH	PET	6 h H ₂ reduction in autoclave removal of Pd by immersion in HCl/H ₂ O	FETs for flexible electronic devices • $R_S \approx 1.7 \text{ k}\Omega/\square$ • Tr = 65%	[457]
2012	Inkjet	GO in H ₂ O with 1% ethylene glycol polyoxometalate	Mica, quartz, Si, ITO-coated glass	Irradiation of GO/phosphotungstic acid with 100 W mercury lamp for a few hours	Sensitive electrode for electrocatalytic activity of dopamine	[307]
2013	Air-brush	Electrochemically exfoliated graphene in DMF	PET	None	TE for flexible displays and electronic devices • $R_S \approx 10 \text{ k}\Omega/\square$ • Tr = 60%	[337]
2013	Inkjet	RGO (hydrazine) in SDS at pH 10	PI film	400 °C for 3 h, air flow	Conductive flexible PI film for high-density electronic devices • $R_S \approx 8200 \text{ k}\Omega/\square$	[185]
2013	Inkjet	GO with 20% ethylene glycol and 0.5 g L ⁻¹ SDBS	PET (pattern resolution ≈100 μm)	100 °C, HI vapor for 3' and rinsed with EtOH and H ₂ O to remove iodide	FET • On/off ratio ≈ 10 ⁴ • $\mu \approx 8 \text{ cm}^2 \text{ V}^{-1} \text{ s}^{-1}$ • $R_S \approx 25 \text{ k}\Omega/\square$ • Thickness = 1 μm	[308]

Table 3. Continued.

Year	Process	Ink	Substrate	Posttreatment	Applications and performances	References
2014	Inkjet	GO in H ₂ O, then reducing agent (ascorbic acid + FeCl ₂) at 60 °C	Glass	80 °C overnight in vacuum oven	TE for photovoltaic applications • $R_S \approx 108 \text{ k}\Omega/\square$ • $\text{Tr} = 41\%$	[49]
2014	Inkjet	GO and Ag nanoparticles in H ₂ O	Glass	Hydrazine treatment and heating to 110 °C for 3 h at low pressure	Hybrid metal-graphene-based functional devices • $R_S \approx 170 \text{ k}\Omega/\square$ • Thickness ≈ 90.2 nm	[50]
2015	Electro spray printing	GO in H ₂ O (1–40 µg mL ⁻¹)	Si/SiO ₂		TF as conductometric reactive NH ₃ gas sensors (concentrations < 500 ppm)	[335]
2015	Inkjet and rolling compression	Binder-free graphene ink		None	RFID • $R_S \approx 3.8 \text{ }\Omega/\square$	[431]
2015	Inkjet	GO suspension (ascorbic acid VC)	PET	100 °C for 5' and blow dried with N ₂ gas	Transistors and biosensors to detect dopamine molecules $R_S \approx 0.6 \text{ k}\Omega/\square$	[309]
2016	Inkjet	Ag/RGO composite dispersed into DI H ₂ O/EtOH/ ethylene glycol	Paper PET etched by ultrasonication for 10' in a H ₂ O/NH ₃ /H ₂ O ₂ mixture	Curing at 100 °C	Printable flexible electronics and graphene-based RFID antenna • $R_S \approx 0.5 \text{ k}\Omega/\square$	[311]
Other 2D crystals						
2014	Inkjet	LPE (MoS ₂ and graphene) in DMF, addition of EC, transfer to terpineol by distillation, addition of EtOH to tailor rheological properties	Glass slides Kapton Si/SiO ₂ wafers	Baking process at 400 °C for 1 h Annealing under N ₂ (max 450 °C)	TCs/ Supercapacitors/ Photoelectrodes, based on graphene or MoS ₂ • $R_S \approx 30 \text{ k}\Omega/\square$ • $\text{Tr} = 80\%$	[191]
2014	Inkjet	MoS ₂ in DMF stabilized by EC and final transfer to terpineol by distillation and EtOH addition to tailor rheological properties	Si/SiO ₂ wafers (thick SiO ₂ layer = 300 nm)	Annealing under N ₂ (max 450 °C)	TFTs based on MoS ₂ semiconductor	[190]
2015	Inkjet	MoS ₂ in NMP	PET coated with aluminum oxide and poly(vinyl alcohol)	Annealing for 2 h under vacuum at 200 °C	Printed photodetectors with MoS ₂ channel and graphene electrodes	[43]

graphene-based TFT has shown an I_{on}/I_{off} (≈ 10) comparable to those reported for RGO-TFT inkjet-printed^[188] and a μ of $\approx 95 \text{ cm}^2 \text{ V}^{-1} \text{ s}^{-1}$. The same authors also demonstrated the combination graphene/organic polymer {poly[5,50-bis(3-dodecyl-2-thienyl)-2,20-bithiophene]} (PQT-12)^[430], obtaining TFTs with $\mu \approx 0.1 \text{ cm}^2 \text{ V}^{-1} \text{ s}^{-1}$ and $I_{on}/I_{off} \approx 4 \times 10^5$,^[41] showing the potentiality of hybrid inks for high-performance printed electronics.

Recently, Huang et al.^[431] have demonstrated printable radio frequency identification (RFID) antenna by low temperature processing of graphene ink, achieving very low R_S value of $3.8 \text{ }\Omega/\square$, by rolling compression of binder-free graphene laminate. The performance of the graphene laminate antenna shows return loss, gain, bandwidth, and radiation patterns compatible with the set requirements, making it ideal for low cost printed RF applications, such as wearable wireless sensor networks and RFID tags.^[431]

Ink-based multilayer MoS₂ sheets were recently inkjet-printed onto SiO₂ substrate showing low I_{on}/I_{off} ratio of 2, and

σ of $8.9 \times 10^{-5} \text{ S m}^{-1}$.^[190] The authors also demonstrated the feasibility of the device as a photodetector.^[190] A photoresponsivity of $\approx 36 \text{ }\mu\text{A W}^{-1}$ was demonstrated,^[190] and although the measured value of the ensemble film is lower with respect to that obtained from photodetectors based on individual MoS₂ nanosheets,^[432–434] it is comparable to those based on single CNTs^[435] or graphene.^[436,437] Finn et al.^[43] moved forward demonstrating an all inkjet-printed photodetector with interdigitated graphene electrodes and a MoS₂ channel, observing a tenfold increase of conductance compared to dark conditions, suggesting the viable use of such devices as low-end photodetectors.

6.2. Sensors

Biological^[438] and chemical^[439] sensors are among the most remarkable applications in flexible and printed electronics, where biocompatibility of the active material is an added value.

For sensors such as transistors for recording the electrical activity of nerve cells^[440] or ultrahigh-sensitive biosensors,^[441] where small signals are expected (below 100 μV), high-quality 2D crystals, e.g., CVD graphene or graphene grown on SiC substrate, are required. However, for less demanding applications, such as electrochemical detection of analytes for food and environmental monitoring,^[442] the use of GO and LPE graphene, etc. could be sufficient.

A few examples of printed devices based on graphene have already been demonstrated.^[24,64,66,67,189,438] For example, an antenna/transceiver of a wireless bacteria detection system on tooth enamel was proposed by Manoor et al.^[438] where graphene was printed onto bioresorbable silk. The resistance of the graphene film changes as the analyte of interest is adsorbed on its surface, demonstrating a detection limit down to a single bacterium.^[438] Dua et al.^[189] designed a flexible sensor for NO_2 and Cl_2 vapors detection, based on RGO flakes (prepared by GO reduction with ascorbic acid) ink-jet printed on flexible PET substrate. The resulting film has shown high sensitivity to vapors (order of part per billion), conductivity values of $\approx 15 \text{ S cm}^{-1}$ and fewer defects compared to the RGO films obtained by hydrazine reduction.^[24,64,66,67]

Inkjet-printed TFTs from single and few layer GO-based inks were also discussed by Huang et al.^[300] where electrochemical H_2O_2 (hydrogen peroxide) sensors have been fabricated using electrically conductive and flexible patterns electronic (GO printed on treated PET and polyimide plastic substrate) circuits.

6.3. Energy Devices

Applications that could benefit most from 2D-crystal-based inks (in addition to flexible electronics^[32,76]), are batteries,^[36,443–445] supercapacitors,^[446,447] solar^[57,80,448–451] and fuel^[452,453] cells. For example, very small 2D sheets are useful in fuel cells where, for example, the edges of MoS_2 SLs can catalyze fuel oxidation—such as hydrogen, methanol, and ethanol.^[452,453]

Many of the aforementioned applications do not require a careful control of the rheological properties of the inks or defined film thicknesses and structures and many electrodes are simply prepared by drop casting and/or doctor-blade approaches, see ref. [34] for a review on 2D-crystal-based energy devices. Nevertheless, several electrodes for energy devices are now being produced by more “sophisticated” printing processes such as inkjet and flexographic printing as we summarize below.

Stable dispersions of GO nanosheets inkjet-printed onto Ti foils and thermally reduced ($T = 200^\circ\text{C}$) were first reported by Le and co-workers^[302] as a promising supercapacitor electrode. Although the power density of the fabricate electrodes was considerably lower (2.19 kW kg^{-1}) than that of CNT-based electrodes ($70\text{--}100 \text{ kW kg}^{-1}$)^[454] the obtained results proposed inkjet printing as a novel and scalable route to precisely pattern supercapacitor electrodes with lateral spatial resolution in the order of $\sim 50 \text{ }\mu\text{m}$.^[302] In 2013 Li et al.^[42] fabricated an inkjet-printed micro-supercapacitor in a planar (interdigitated) structure on Kapton, characterized by specific capacitance of $\approx 0.6 \text{ mF cm}^{-2}$ and frequency response time of $\approx 13 \text{ ms}$. Silver MNPs were initially printed as current collectors and the graphene was printed on the fingers as the active electrode.^[42]

A semitransparent catalytically active GNPs-based NMP ink was flexographically printed onto flexible ITO/PET ($60 \Omega/\square$) or FTO ($15 \Omega/\square$) substrates for the realization of DSSC electrodes.^[80] Lower photovoltaic performance of the DSSC with respect to the ones reached with platinum catalyst was probably linked with the reduced light transmission and viscous fingering (Figure 9d) due to instabilities at the nip between the plate cylinder and the substrate.^[80]

Casaluci et al.^[341] have demonstrated how spray coating can be a viable deposition approach for the realization of large-area graphene-based DSSC module ($>43 \text{ cm}^2$ active area), with η of 3.5% when using graphene sheets as platinum replacement at the CE.^[341] This work could open the way for all-printed graphene-based photovoltaics. However, these are only the first attempts to use industrially relevant printing strategies, such as spray coating, inkjet printing, and flexography for the realization of energy devices, and further work is necessary to optimize both processes and performances.

7. Outlook

Tremendous research efforts have been devoted to the exfoliation of layered crystals and their exploration in a number of applications, with research activities that are still growing. As discussed in this review article, one possible and very promising strategy is based on the exfoliation of parent bulk crystals in suitable liquids to yield dispersions that can subsequently be used for the formulation of functional inks, processed by established techniques such as spin and drop casting, spray coating, as well as inkjet, flexographic, gravure and screen printing. The greatest strength of this strategy is probably its versatility, as numerous layered crystals can be exfoliated and processed in a similar way giving access to a broad palette of materials that can be tailored according to the desired application. The solution processing will also allow for some fine-tuning of electrochemical and optoelectronic properties by the addition of molecules or polymers that provide supplementary functions and/or the control on doping levels. In addition, when considering the fabrication of heterostructures, where synergistic effects of different materials can be exploited, almost infinite possibilities exist. Without doubt, exciting prospects lie ahead.

However, both liquid phase exfoliation and particularly printing processes are still at an early stage of development and although it is easy to envision integration of various layered crystals in functional devices based on solution processing, it is currently unclear whether this will in fact lead to industrially relevant processes or products in the end. Numerous challenges, from the first stage of the process chain toward devices produced from liquid-exfoliated 2D crystals (see Figure 1), remain and need to be overcome. While liquid phase exfoliation of layered crystals has been explored over almost a decade, the involved processes per se are still not well understood especially with regard to the emerging technologies such as shear exfoliation or ball milling. In particular, it is very challenging to obtain precise control over size and thickness during the exfoliation mainly because high throughput techniques to characterize length and thickness distributions have been lacking until very recently.

The inability to control lateral size and thickness during the exfoliation makes post-exfoliation size selection extremely important, simply because different applications will require different nanosheet sizes and thicknesses. Ideally, dispersions consisting of monodisperse 2D crystals will need to be made available. That means, nanosheets with the desired thickness are required having a well-defined length. Again, although significant progress has been made so far, still, the full achievement of this goal is far away from its practical realization. In particular, if on the one hand, it is relatively easy to produce thin nanosheets of small lateral size, on the other hand it is extremely challenging to select thin and large ones. If the size selection process needs to become an integral part of further processing steps, it is almost mandatory to avoid the use of additives. Furthermore, the production of large quantities of size selected samples, i.e., the increase in yield of both exfoliation and size selection, is a must.

When moving one step further in the process chain to the actual deposition and printing, another challenge becomes clear. For the most sophisticated deposition techniques such as printing, the rheological properties of the ink need to be tailored on demand. This means, it will be necessary to manufacture inks having dispersed nanosheets with well-defined sizes and thicknesses in large quantities at any concentration with tailored viscosities in both high- and low-boiling-point, non-toxic solvents. We are currently far from the full achievement of this long list of requirements. One major problem in this regard is the fact that solvents that are good for exfoliation and nanosheet stabilization are not compatible with many printing processes. Hence, efficient ways to transfer the nanomaterial to any desired/targeted solvent, i.e., solvent exchange, at tailored concentration (while preventing re-aggregation) need to be further developed.

Furthermore, the resolution of the printing process needs to be improved. Inkjet and screen printing are probably the most promising techniques to achieve this target. However, an advantage and, at the same time, a disadvantage relies on the compatibility of these processes only with rather small lateral size nanosheets. It can be regarded as an advantage, as it is fairly straight forward to produce small and thin nanosheets by liquid phase exfoliation. However, at the same time, it is a significant disadvantage because in many cases, the electronic properties of small nanosheets, e.g., graphene, are often degraded compared to larger ones due to edge effects. Surely, in other applications such as catalysis, edge sites may be desired for both graphene and transition metal dichalcogenides. The future will reveal, whether industrially competitive transparent conductors based on printed graphene can be produced, possibly connecting individual nanosheets by post-deposition chemical treatment.

Last but not least, the issue with the scalability needs to be faced. In particular, to exploit the potential of 2D crystals in printed optoelectronics as well as energy storage and conversion, large quantities, i.e., tons, of exfoliated 2D crystals are needed. In this regard, despite the first demonstrations that these dispersions can be produced in industrially relevant quantities by the implementation of scalable exfoliation processes such as shear exfoliation or ball milling, further development and optimization are needed to assert their true potential.

Acknowledgements

The authors thank Alberto Ansaldi, Matteo Bruna, Simone Casaluci, Antonio Esau Del Rio Castillo, and Aldo Di Carlo for useful discussion. The authors acknowledge funding from the European Union's Horizon 2020 research and innovation programme under grant agreement No. 696656 – GrapheneCore1 and a Newton International Fellowship.

Received: December 25, 2015

Revised: March 9, 2016

Published online: June 6, 2016

- [1] Y. Hernandez, V. Nicolosi, M. Lotya, F. M. Blighe, Z. Sun, S. De, I. T. McGovern, B. Holland, M. Byrne, Y. K. Gun'ko, J. J. Boland, P. Niraj, G. Duesberg, S. Krishnamurthy, R. Goodhue, J. Hutchison, V. Scardaci, A. C. Ferrari, J. N. Coleman, *Nat. Nanotechnol.* **2008**, *3*, 563.
- [2] K. S. Novoselov, A. K. Geim, S. V. Morozov, D. Jiang, Y. Zhang, S. V. Dubonos, I. V. Grigorieva, A. A. Firsov, *Science* **2004**, *306*, 666.
- [3] R. Zallen, M. Slade, *Phys. Rev. B* **1974**, *9*, 1627.
- [4] M. C. Schabel, J. L. Martins, *Phys. Rev. B* **1992**, *46*, 7185.
- [5] M. Xu, T. Liang, M. Shi, H. Chen, *Chem. Rev.* **2013**, *113*, 3766.
- [6] S. Z. Butler, S. M. Hollen, L. Cao, Y. Cui, J. A. Gupta, H. R. Gutierrez, T. F. Heinz, S. S. Hong, J. Huang, A. F. Ismach, E. Johnston-Halperin, M. Kuno, V. V. Plashnitsa, R. D. Robinson, R. S. Ruoff, S. Salahuddin, J. Shan, L. Shi, M. G. Spencer, M. Terrones, W. Windl, J. E. Goldberger, *ACS Nano* **2013**, *7*, 2898.
- [7] D. Jariwala, V. K. Sangwan, L. J. Lauhon, T. J. Marks, M. C. Hersam, *ACS Nano* **2014**, *8*, 1102.
- [8] V. Nicolosi, M. Chhowalla, M. G. Kanatzidis, M. S. Strano, J. N. Coleman, *Science* **2013**, *340*, 1420.
- [9] M. Osada, T. Sasaki, *Adv. Mater.* **2012**, *24*, 209.
- [10] M. Naguib, V. N. Mochalin, M. W. Barsoum, Y. Gogotsi, *Adv. Mater.* **2014**, *26*, 992.
- [11] J. Zhu, X. Liu, M. L. Geier, J. J. McMorrow, D. Jariwala, M. E. Beck, W. Huang, T. J. Marks, M. C. Hersam, *Adv. Mater.* **2016**, *28*, 63.
- [12] G. Abellán, C. Martí-Gastaldo, A. Ribera, E. Coronado, *Acc. Chem. Res.* **2015**, *48*, 1601.
- [13] R. F. Frindt, *J. Phys. Chem. Solids* **1963**, *24*, 1107.
- [14] R. F. Frindt, *Phys. Rev.* **1965**, *140*, A536.
- [15] R. F. Frindt, *Phys. Rev. Lett.* **1972**, *28*, 299.
- [16] A. K. Geim, K. S. Novoselov, *Nat. Mater.* **2007**, *6*, 183.
- [17] S. Stankovich, D. A. Dikin, G. H. B. Dommett, K. M. Kohlhaas, E. J. Zimney, E. A. Stach, R. D. Piner, S. T. Nguyen, R. S. Ruoff, *Nature* **2006**, *442*, 282.
- [18] T. Hasan, Z. Sun, F. Wang, F. Bonaccorso, P. H. Tan, A. G. Rozhin, A. C. Ferrari, *Adv. Mater.* **2009**, *21*, 3874.
- [19] F. Schwierz, *Nat. Nanotechnol.* **2010**, *5*, 487.
- [20] F. Bonaccorso, Z. Sun, T. Hasan, A. C. Ferrari, *Nat. Photonics* **2010**, *4*, 611.
- [21] K. S. Novoselov, D. Jiang, F. Schedin, T. J. Booth, V. V. Khotkevich, S. V. Morozov, A. K. Geim, *Proc. Natl. Acad. Sci. USA* **2005**, *102*, 10451.
- [22] M. Chhowalla, H. S. Shin, G. Eda, L.-J. Li, K. P. Loh, H. Zhang, *Nat. Chem.* **2013**, *5*, 263.
- [23] Q. H. Wang, K. Kalantar-Zadeh, A. Kis, J. N. Coleman, M. S. Strano, *Nat. Nanotechnol.* **2012**, *7*, 699.
- [24] F. Bonaccorso, A. Lombardo, T. Hasan, Z. Sun, L. Colombo, A. C. Ferrari, *Mater. Today* **2012**, *15*, 564.
- [25] X. Li, W. Cai, J. An, S. Kim, J. Nah, D. Yang, R. Piner, A. Velamakanni, I. Jung, E. Tutuc, S. K. Banerjee, L. Colombo, R. S. Ruoff, *Science* **2009**, *324*, 1312.
- [26] S. Bae, H. Kim, Y. Lee, X. Xu, J.-S. Park, Y. Zheng, J. Balakrishnan, T. Lei, H. R. Kim, Y. I. Song, Y.-J. Kim, K. S. Kim, B. Özyilmaz, J.-H. Ahn, B. H. Hong, S. Iijima, *Nat. Nanotechnol.* **2010**, *5*, 574.

- [27] Y. Hao, M. S. Bharathi, L. Wang, Y. Liu, H. Chen, S. Nie, X. Wang, H. Chou, C. Tan, B. Fallahazad, H. Ramanarayanan, C. W. Magnuson, E. Tutuc, B. I. Yakobson, K. F. McCarty, Y.-W. Zhang, P. Kim, J. Hone, L. Colombo, R. S. Ruoff, *Science* **2013**, *342*, 720.
- [28] E. G. Acheson, US Patent 615648, **1896**.
- [29] C. Berger, Z. Song, T. Li, X. Li, A. Y. Ogbazghi, R. Feng, Z. Dai, A. N. Marchenkov, E. H. Conrad, P. N. First, W. A. de Heer, *J. Phys. Chem. B* **2004**, *108*, 19912.
- [30] K. V. Emtsev, F. Speck, Th. Seyller, L. Ley, J. D. Riley, *Phys. Rev. B* **2008**, *77*, 155303.
- [31] A. C. Ferrari, F. Bonaccorso, V. Fal'ko, K. S. Novoselov, S. Roche, P. Boggild, S. Borini, F. H. L. Koppens, V. Palermo, N. Pugno, J. A. Garrido, R. Sordan, A. Bianco, L. Ballerini, M. Prato, E. Lidorikis, J. Kivioja, C. Marinelli, T. Ryhanen, A. Morpurgo, J. N. Coleman, V. Nicolosi, L. Colombo, A. Fert, M. Garcia-Hernandez, A. Bachtold, G. F. Schneider, F. Guinea, C. Dekker, M. Barbone, Z. Sun, C. Gallois, A. N. Grigorenko, G. Konstantatos, A. Kis, M. Katsnelson, L. Vanderven, A. Loiseau, V. Morandi, D. Neumaier, E. Treossi, V. Pellegrini, M. Polini, A. Tredicucci, G. M. Williams, B. H. Hong, J.-H. Ahn, J. M. Kim, H. Zirath, B. J. van Wees, H. van der Zant, L. Occhipinti, A. Di Matteo, I. A. Kinloch, T. Seyller, E. Quesnel, X. Feng, K. Teo, N. Rupesinghe, P. Hakonen, S. R. T. Neil, Q. Tannock, T. Lofwander, J. Kinaret, *Nanoscale* **2015**, *7*, 4598.
- [32] G. Fiori, F. Bonaccorso, G. Iannaccone, T. Palacios, D. Neumaier, A. Seabaugh, S. K. Banerjee, L. Colombo, *Nat. Nanotechnol.* **2014**, *9*, 768.
- [33] C. Zhi, Y. Bando, C. tang, H. Kuwahara, D. Golberg, *Adv. Mater.* **2009**, *21*, 2889.
- [34] F. Bonaccorso, L. Colombo, G. Yu, M. Stoller, V. Tozzini, A. C. Ferrari, R. S. Ruoff, V. Pellegrini, *Science* **2015**, *347*, 1246501.
- [35] C. Backes, R. J. Smith, N. McEvoy, N. C. Berner, D. McCloskey, H. C. Nerl, A. O'Neill, P. J. King, T. Higgins, D. Hanlon, N. Scheuschner, J. Maultzsch, L. Houben, G. S. Duesberg, J. F. Donegan, V. Nicolosi, J. N. Coleman, *Nat. Commun.* **2014**, *5*, 4576.
- [36] J. Hassoun, F. Bonaccorso, M. Agostini, M. Angelucci, M. G. Betti, R. Cingolani, M. Gemmi, C. Mariani, S. Panero, V. Pellegrini, B. Scrosati, *Nano Lett.* **2014**, *14*, 4901.
- [37] A. A. Green, M. C. Hersam, *Nano Lett.* **2009**, *9*, 4031.
- [38] J. Kang, J.-W. T. Seo, D. Alducin, A. Ponce, M. J. Yacaman, M. C. Hersam, *Nat. Commun.* **2014**, *5*, 5478.
- [39] J. Zhu, J. Kang, J. Kang, D. Jariwala, J. D. Wood, J.-W. T. Seo, K.-S. Chen, T. J. Marks, M. C. Hersam, *Nano Lett.* **2015**, *15*, 7029.
- [40] Z. Sun, T. Hasan, F. Torrisi, D. Popa, G. Privitera, F. Wang, F. Bonaccorso, A. Basko, A. C. Ferrari, *ACS Nano* **2010**, *4*, 803.
- [41] F. Torrisi, T. Hasan, W. Wu, Z. Sun, T. Kulmala, A. Lombardo, G. W. Hshieh, F. Bonaccorso, P. J. Paul, D. P. Chu, A. C. Ferrari, *ACS Nano* **2012**, *6*, 2992.
- [42] J. Li, F. Ye, S. Vaziri, M. Muhammed, M. C. Lemme, M. Östling, *Adv. Mater.* **2013**, *25*, 3985.
- [43] D. J. Finn, M. Lotya, G. Cunningham, R. J. Smith, D. McCloskey, J. F. Donegan, J. N. Coleman, *J. Mater. Chem. C* **2014**, *2*, 925.
- [44] K. Arapov, R. Abbel, G. De With, H. Friedrich, *Faraday Discuss.* **2014**, *173*, 323.
- [45] Y. Gao, W. Shi, W. Wang, Y. Leng, Y. Zhao, *Ind. Eng. Chem. Res.* **2014**, *53*, 16777.
- [46] A. Capasso, A. E. Del Rio Castillo, H. Sun, A. Ansaldi, V. Pellegrini, F. Bonaccorso, *Solid State Comm.* **2015**, *224*, 53.
- [47] C. Sriprachuabwong, C. Karuwan, A. Wisitsorrat, D. Phokharatkul, T. Lomas, P. Sritongkham, A. Tuantranont, *J. Mater. Chem.* **2012**, *22*, 5478.
- [48] Y. Xu, I. Henning, D. Freyberg, A. J. Strudwick, M. G. Schwab, T. Weitz, K. C.-P. Cha, *J. Power Sources* **2014**, *248*, 483.
- [49] K. Kim, S. I. Ahn, K. C. Choi, *Carbon* **2014**, *66*, 172.
- [50] L. Li, Y. Guo, X. Zhang, Y. Song, *J. Mater. Chem. A* **2014**, *2*, 19095.
- [51] E. B. Secor, B. Y. Ahn, T. Z. Gao, J. A. Lewis, M. S. Hersam, *Adv. Mater.* **2015**, *27*, 6683.
- [52] G. Wang, Z. Wang, Z. Liu, J. Xue, G. Xin, Q. Yu, J. Lian, M. Y. Chen, *Chem. Eng. J.* **2015**, *260*, 582.
- [53] W. J. Hyun, E. B. Secor, M. C. Hersam, C. D. Frisbie, L. F. Francis, *Adv. Mater.* **2015**, *27*, 109.
- [54] K. Arapov, E. Rubingh, R. Abbel, J. Laven, G. de With, H. Friedrich, *Adv. Funct. Mater.* **2016**, *26*, 586.
- [55] X. Wang, L. Zhi, K. Mullen, *Nano Lett.* **2007**, *8*, 323.
- [56] G. Eda, H. E. Unalan, N. Rupesinghe, G. A. J. Amaralunga, M. Chhowalla, *Appl. Phys. Lett.* **2008**, *93*, 233502.
- [57] E. Kymakis, E. Stratakis, M. M. Stylianakis, E. Koudoumas, C. Fotakis, *Thin Solid Films* **2011**, *520*, 1238.
- [58] X. Yang, W. Fu, W. Liu, J. Hong, Y. Cai, C. Jin, M. Xu, H. Wang, D. Yang, H. Chen, *J. Mater. Chem. A* **2014**, *2*, 7727.
- [59] P. Blake, P. D. Brimicombe, R. R. Nair, T. J. Booth, D. Jiang, F. Schedin, L. A. Ponomarenko, S. V. Morozov, H. Gleeson, E. W. Hill, A. K. Geim, K. S. Novoselov, *Nano Lett.* **2008**, *8*, 1704.
- [60] P. Cataldi, I. S. Bayer, F. Bonaccorso, V. Pellegrini, A. Athanassiou, R. Cingolani, *Adv. Electron. Mater.* **2015**, DOI: 10.1002/aelm.201500224.
- [61] A. Pénicaud, C. Drummond, *Acc. Chem. Res.* **2013**, *46*, 129.
- [62] P. Joensen, R. F. Frindt, S. R. Morrison, *Mater. Res. Bull.* **1986**, *21*, 457.
- [63] G. F. Walker, W. G. Garrett, *Science* **1967**, *156*, 385.
- [64] S. Eigler, A. Hirsch, *Angew. Chem., Int. Ed.* **2014**, *53*, 7720.
- [65] K. Parvez, Z.-S. Wu, R. Li, X. Liu, R. Graf, X. Feng, K. Müllen, *J. Am. Chem. Soc.* **2014**, *136*, 6083.
- [66] D. R. Dreyer, S. Park, C. W. Bielawski, R. S. Ruoff, *Chem. Soc. Rev.* **2010**, *39*, 228.
- [67] M. J. Allen, V. C. Tung, R. B. Kaner, *Chem. Rev.* **2010**, *110*, 132.
- [68] S. Park, R. S. Ruoff, *Nat. Nanotechnol.* **2009**, *4*, 217.
- [69] Y. Zhu, S. Murali, W. Cai, X. Li, J. W. Suk, J. R. Potts, R. S. Ruoff, *Adv. Mater.* **2010**, *22*, 3906.
- [70] G. Eda, M. Chhowalla, *Adv. Mater.* **2010**, *22*, 2392.
- [71] C. Mattevi, G. Eda, S. Agnoli, S. Miller, K. A. Mkhoyan, O. Celik, D. Mastrogiovanni, G. Granozzi, E. Garfunkel, M. Chhowalla, *Adv. Funct. Mater.* **2009**, *19*, 2577.
- [72] J. N. Coleman, *Acc. Chem. Res.* **2013**, *46*, 14.
- [73] J. N. Coleman, M. Lotya, A. O'Neill, S. D. Bergin, P. J. King, U. Khan, K. Young, A. Gaucher, S. De, R. J. Smith, I. V. Shvets, S. K. Arora, G. Stanton, H.-Y. Kim, K. Lee, G. T. Kim, G. S. Duesberg, T. Hallam, J. J. Boland, J. J. Wang, J. F. Donegan, J. C. Grunlan, G. Moriarty, A. Shmeliov, R. J. Nicholls, J. M. Perkins, E. M. Grieveson, K. Theuwissen, D. W. McComb, P. D. Nellist, V. Nicolosi, *Science* **2011**, *331*, 568.
- [74] K. R. Paton, E. Varrla, C. Backes, R. J. Smith, U. Khan, A. O'Neill, C. Boland, M. Lotya, O. M. Istrate, P. King, T. Higgins, S. Barwick, P. May, P. Puczarks, I. Ahmed, M. Moebius, H. Pettersson, E. Long, J. Coelho, S. E. O'Brien, E. K. McGuire, B. M. Sanchez, G. S. Duesberg, N. McEvoy, T. J. Pennycook, C. Downing, A. Crossley, V. Nicolosi, J. N. Coleman, *Nat. Mater.* **2014**, *13*, 624.
- [75] C.-H. Chang, T.-C. Huang, C.-W. Peng, T.-C. Yeh, H.-I. Lu, W.-I. Hung, C.-J. Weng, T.-I. Yang, J.-M. Yeh, *Carbon* **2012**, *50*, 5044.
- [76] A. Nathan, A. Ahnood, M. T. Cole, S. Lee, Y. Suzuki, P. Hirralal, F. Bonaccorso, T. Hasan, L. Garcia-Gancedo, A. Dyadyusha, S. Haque, P. Andrew, S. Hofmann, J. Moultrie, D. Chu, A. J. Flewitt, A. C. Ferrari, M. J. Kelly, J. Robertson, *Proc. IEEE* **2012**, *100*, 1486.
- [77] M. Krueger, S. Berg, D. Stone, E. Strelcov, D. A. Dilkin, J. Kim, L. J. Cote, J. Huang, A. Kolmakov, *ACS Nano* **2011**, *5*, 10047.
- [78] C. Zhao, L. Xing, J. Xiang, L. Cui, J. Jiao, H. Sai, Z. Li, F. Li, *Particulology* **2014**, *17*, 66.
- [79] E. B. Secor, S. Lim, H. Zhang, C. D. Frisbie, L. F. Francis, M. C. Hersam, *Adv. Mater.* **2014**, *26*, 4533.

- [80] J. Baker, D. Deganello, D. T. Gethin, T. M. Watson, *Energy Mater.* **2014**, *9*, 86.
- [81] W. J. Hyun, E. B. Secor, G. A. Rojas, M. C. Hersam, L. F. Francis, C. D. Frisbie, *Adv. Mater.* **2015**, *27*, 7058.
- [82] T. Hebner, C. Wu, D. Marcy, M. Lu, J. Sturm, *Appl. Phys. Lett.* **1998**, *72*, 519.
- [83] K. S. Kim, Y. Zhao, H. Jang, S. Y. Lee, J. M. Kim, K. S. Kim, J.-H. Ahn, P. Kim, J.-Y. Choi, B. H. Hong, *Nature* **2009**, *457*, 706.
- [84] A. Ciesielski, P. Samori, *Chem. Soc. Rev.* **2014**, *43*, 381.
- [85] M. Yi, Z. Shen, *J. Mater. Chem. A* **2015**, *3*, 11700.
- [86] F. Bonaccorso, Z. Sun, *Opt. Mater. Express* **2014**, *4*, 63.
- [87] U. Khan, A. O'Neill, M. Lotya, S. De, J. N. Coleman, *Small* **2010**, *6*, 864.
- [88] M. Lotya, P. J. King, U. Khan, S. De, J. N. Coleman, *ACS Nano* **2010**, *4*, 3155.
- [89] H. M. Santos, C. Lodeiro, J.-L. Capelo-Martínez, in *Ultrasound in Chemistry*, (Ed: J.-L. Capelo-Martínez), Wiley-VCH, Weinheim, Germany **2009**; DOI: 10.1002/9783527623501; 1–16.
- [90] W. Zhao, M. Fang, F. Wu, H. Wu, L. Wang, G. Chen, *J. Mater. Chem.* **2010**, *20*, 5817.
- [91] W. Zhao, F. Wu, H. Wu, G. Chen, *J. Nanomater.* **2010**, *2010*, 1.
- [92] C. Knieke, A. Berger, M. Voigt, R. N. K. Taylor, J. Röhrl, W. Peukert, *Carbon* **2010**, *48*, 3196.
- [93] C. Damm, T. J. Nacken, W. Peukert, *Carbon* **2015**, *81*, 284.
- [94] Y. Yao, Z. Lin, Z. Li, X. Song, K.-S. Moon, C.-P. Wong, *J. Mater. Chem.* **2012**, *22*, 13494.
- [95] M. A. Ibrahim, T.-W. Lan, J. K. Huang, Y.-Y. Chen, K.-H. Wei, L.-J. Li, C. W. Chu, *RSC Adv.* **2013**, *3*, 13193.
- [96] E. Varrla, K. R. Paton, C. Backes, A. Harvey, R. J. Smith, J. McCauley, J. N. Coleman, *Nanoscale* **2014**, *6*, 11810.
- [97] E. Varrla, C. Backes, K. R. Paton, A. Harvey, Z. Gholamvand, J. McCauley, J. N. Coleman, *Chem. Mater.* **2015**, *27*, 1129.
- [98] L. Liu, Z. Shen, M. Yi, X. Zhang, S. Ma, *RSC Adv.* **2014**, *4*, 36464.
- [99] M. Yi, Z. Shen, *Carbon* **2014**, *78*, 622.
- [100] A. Pattammattel, C. V. Kumar, *Adv. Funct. Mater.* **2015**, *25*, 7088.
- [101] N. D. Mansukhani, L. M. Guiney, P. J. Kim, Y. Zhao, D. Alducin, A. Ponce, E. Larios, M. J. Yacaman, M. C. Hersam, *Small* **2016**, *12*, 294.
- [102] J. M. Hughes, D. Aherne, J. N. Coleman, *J. Appl. Polym. Sci.* **2013**, *127*, 4483.
- [103] M. V. Bracamonte, G. I. Lacconi, S. E. Urreta, L. E. F. F. Torres, *J. Phys. Chem. C* **2014**, *118*, 15455.
- [104] J. R. Brent, N. Savjani, E. A. Lewis, S. J. Haigh, D. J. Lewis, P. O'Brien, *Chem. Commun.* **2014**, *50*, 13338.
- [105] J. T. Han, J. I. Jang, H. Kim, J. Y. Hwang, H. K. Yoo, J. S. Woo, S. Choi, H. Y. Kim, H. J. Jeong, S. Y. Jeong, K.-J. Baeg, K. Cho, G.-W. Lee, *Sci. Rep.* **2014**, *4*, 5133.
- [106] D. Hanlon, C. Backes, T. M. Higgins, M. Hughes, A. O'Neill, P. King, N. McEvoy, G. S. Duesberg, B. Mendoza Sanchez, H. Pettersson, V. Nicolosi, J. N. Coleman, *Chem. Mater.* **2014**, *26*, 1751.
- [107] D. Hanlon, C. Backes, E. Doherty, C. S. Cucinotta, N. C. Berner, C. Boland, K. Lee, P. Lynch, Z. Gholamvand, A. Harvey, S. Zhang, K. Wang, G. Moynihan, A. Pokle, Q. M. Ramasse, N. McEvoy, W. J. Blau, J. Wang, G. Abellán, F. Hauke, A. Hirsch, S. Sanvito, D. D. O'Regan, G. S. Duesberg, V. Nicolosi, J. N. Coleman, *Nat. Commun.* **2015**, *6*, 8563.
- [108] A. Harvey, C. Backes, Z. Gholamvand, D. Hanlon, D. McAtee, H. C. Nerl, E. McGuire, A. Seral-Ascaso, Q. M. Ramasse, N. McEvoy, S. Winters, N. C. Berner, D. McCloskey, J. Donegan, G. Duesberg, V. Nicolosi, J. N. Coleman, *Chem. Mater.* **2015**, *27*, 3483.
- [109] J. Shen, Y. He, J. Wu, C. Gao, K. Keyshar, X. Zhang, Y. Yang, M. Ye, R. Vajtai, J. Lou, P. M. Ajayan, *Nano Lett.* **2015**, *15*, 5449.
- [110] A. H. Woomer, T. W. Farnsworth, J. Hu, R. A. Wells, C. L. Donley, S. C. Warren, *ACS Nano* **2015**, *9*, 8869.
- [111] M. Lotya, Y. Hernandez, P. J. King, R. J. Smith, V. Nicolosi, L. S. Karlsson, F. M. Blighe, S. De, Z. Wang, I. T. McGovern, G. S. Duesberg, J. N. Coleman, *J. Am. Chem. Soc.* **2009**, *131*, 3611.
- [112] L. Guardia, M. J. Fernández-Merino, J. I. Paredes, P. Solís-Fernández, S. Villar-Rodil, A. Martínez-Alonso, J. M. D. Tascón, *Carbon* **2011**, *49*, 1653.
- [113] R. J. Smith, P. J. King, M. Lotya, C. Wirtz, U. Khan, S. De, A. O'Neill, G. S. Duesberg, J. C. Grunlan, G. Moriarty, J. Chen, J. Wang, A. I. Minett, V. Nicolosi, J. N. Coleman, *Adv. Mater.* **2011**, *23*, 3944.
- [114] T. Nacken, C. Damm, H. Xing, A. Rüger, W. Peukert, *Nano Res.* **2015**, *8*, 1865.
- [115] T. Hasan, F. Torrisi, Z. Sun, D. Popa, V. Nicolosi, G. Privitera, F. Bonaccorso, A. C. Ferrari, *Phys. Status Solidi B* **2010**, *247*, 2953.
- [116] O. M. Maragó, F. Bonaccorso, R. Saija, G. Privitera, P. G. Gucciardi, M. A. Iati, G. Calogero, P. H. Jones, F. Borghese, P. Denti, *ACS Nano* **2010**, *4*, 7515.
- [117] P. May, U. Khan, J. M. Hughes, J. N. Coleman, *J. Phys. Chem. C* **2012**, *116*, 11393.
- [118] G. Guan, S. Zhang, S. Liu, Y. Cai, M. Low, C. P. Teng, I. Y. Phang, Y. Cheng, K. L. Duei, B. M. Srinivasan, Y. Zheng, Y.-W. Zhang, M.-Y. Han, *J. Am. Chem. Soc.* **2015**, *137*, 6152.
- [119] V. Vega-Mayoral, C. Backes, D. Hanlon, U. Khan, Z. Gholamvand, M. O'Brien, G. S. Duesberg, C. Gadermaier, J. N. Coleman, *Adv. Funct. Mater.* **2016**, *26*, 1028.
- [120] K. F. Mak, C. Lee, J. Hone, J. Shan, T. F. Heinz, *Phys. Rev. Lett.* **2010**, *105*, 136805.
- [121] J. S. Bunch, Y. Yaish, M. Brink, K. Bolotin, P. L. McEuen, *Nano Lett.* **2005**, *5*, 287.
- [122] T. J. Mason, *Sonochemistry*, Oxford University Press, Oxford, UK **1999**.
- [123] F. Hennrich, R. Krupke, K. Arnold, J. A. R. Stütz, S. Lebedkin, T. Koch, T. Schimmel, M. M. Kappes, *J. Phys. Chem. B* **2007**, *111*, 1932.
- [124] J. Kang, J. D. Wood, S. A. Wells, J.-H. Lee, X. Liu, K.-S. Chen, M. C. Hersam, *ACS Nano* **2015**, *9*, 3596.
- [125] K. Kouroupis-Agalou, A. Liscio, E. Treossi, L. Ortolani, V. Morandi, N. M. Pugno, V. Palermo, *Nanoscale* **2014**, *6*, 5926.
- [126] E. Y. Polyakova, K. T. Rim, D. Eom, K. Douglass, R. L. Opila, T. F. Heinz, A. V. Teplyakov, G. W. Flynn, *ACS Nano* **2011**, *5*, 6102.
- [127] E. T. Skaltsas, X. Ke, C. Bittencourt, N. Tagmatarchis, *J. Phys. Chem. C* **2013**, *117*, 23272.
- [128] M. Yi, Z. Shen, S. Liang, L. Liu, X. Zhang, S. Ma, *Chem. Commun.* **2013**, *49*, 11059.
- [129] V. León, M. Quintana, M. A. Herrero, J. L. G. Fierro, A. de la Hoz, M. Prato, E. Vázquez, *Chem. Commun.* **2011**, *47*, 10936.
- [130] A. Fabbro, D. Scaini, V. León, E. Vázquez, G. Cellot, G. Privitera, L. Lombardi, F. Torrisi, F. Tomarchio, F. Bonaccorso, S. Bosi, A. C. Ferrari, L. Ballerini, M. Prato, *ACS Nano* **2016**, *10*, 615.
- [131] C. Backes, B. M. Szydłowska, A. Harvey, S. Yuan, V. Vega-Mayoral, B. R. Davies, P.-L. Zhao, D. Hanlon, E. J. G. Santos, M. I. Katsnelson, W. J. Blau, C. Gadermaier, J. N. Coleman, *ACS Nano* **2016**, *10*, 1589.
- [132] C. Backes, K. R. Paton, D. Hanlon, S. Yuan, M. I. Katsnelson, J. Houston, R. J. Smith, D. McCloskey, J. F. Donegan, J. N. Coleman, *Nanoscale* **2016**, *8*, 5737.
- [133] C. Y. Zhi, Y. Bando, C. C. Tang, H. Kuwahara, D. Golberg, *Adv. Mater.* **2009**, *21*, 2889.
- [134] A. Jawaid, D. Nepal, K. Park, M. Jespersen, A. Qualley, P. Mirau, L. F. Drummy, R. A. Vaia, *Chem. Mater.* **2016**, *28*, 337.
- [135] A. Favron, E. Gaufres, F. Fossard, A.-L. Phaneuf-Lheureux, N. Y. W. Tang, P. L. Levesque, A. Loiseau, R. Leonelli, S. Francoeur, R. Martel, *Nat. Mater.* **2015**, *14*, 826.
- [136] J. D. Wood, S. A. Wells, D. Jariwala, K.-S. Chen, E. Cho, V. K. Sangwan, X. Liu, L. J. Lauhon, T. J. Marks, M. C. Hersam, *Nano Lett.* **2014**, *14*, 6964.
- [137] H. C. Yau, M. K. Bayazit, J. H. G. Steinke, M. S. P. Shaffer, *Chem. Commun.* **2015**, *51*, 16621.

- [138] Candidate list of substances of very high concern for authorisation, <http://echa.europa.eu/it/candidate-list-table>; accessed: May 2016.
- [139] D. R. Lide, *CRC Handbook of Chemistry and Physics*, Taylor & Francis, Boca Raton, FL, USA 2014–2015.
- [140] List of Chemicals as Known to the State of California to Cause Cancer or Reproductive Toxicity, California OEHHA, http://www.oehha.ca.gov/prop65/prop65_list/Newlist.html; accessed: April 2012.
- [141] Hazardous substance fact sheet for dimethylformamide, <http://nj.gov/health/eoh/rtkweb/documents/fs/0759.pdf>; accessed: January 2011.
- [142] A. O'Neill, U. Khan, P. N. Nirmalraj, J. Boland, J. N. Coleman, *J. Phys. Chem. C* **2011**, *115*, 5422.
- [143] U. Khan, A. O'Neill, H. Porwal, P. May, K. Nawaz, J. N. Coleman, *Carbon* **2012**, *50*, 470.
- [144] H. C. Hamaker, *Physica* **1937**, *4*, 1058.
- [145] J. N. Israelachvili, *Intermolecular and Surface Forces*, Vol. 4, Academic Press, Waltham, MA, USA **1992**, p. 178.
- [146] J. Kim, S. Kwon, D.-H. Cho, B. Kang, H. Kwon, Y. Kim, S. O. Park, G. Y. Jung, E. Shin, W.-G. Kim, H. Lee, G. H. Ryu, M. Choi, T. H. Kim, J. Oh, S. Park, S. K. Kwak, S. W. Yoon, D. Byun, Z. Lee, C. Lee, *Nat. Commun.* **2015**, *6*, 8294.
- [147] N. B. Vargaftik, B. N. Volkov, L. D. Voljak, *J. Phys. Chem. Ref. Data* **1983**, *12*, 817.
- [148] K. G. Zhou, N. N. Mao, H. X. Wang, Y. Peng, H. L. Zhang, *Angew. Chem., Int. Ed.* **2011**, *50*, 10839.
- [149] U. Halim, C. R. Zheng, Y. Chen, Z. Lin, S. Jiang, R. Cheng, Y. Huang, X. Duan, *Nat. Commun.* **2013**, *4*, 2213.
- [150] D. Tasis, K. Papagelis, P. Spiliopoulos, C. Gallois, *Mater. Lett.* **2013**, *94*, 47.
- [151] S. Barwick, U. Khan, J. N. Coleman, *J. Phys. Chem. C* **2013**, *117*, 19212.
- [152] A. L. Tiano, L. Gibbons, M. Tsui, S. I. Applin, R. Silva, C. Park, C. C. Fay, *Nanoscale* **2016**, *8*, 4348.
- [153] I. S. Khatab, F. Bandarkar, M. A. A. Fakhree, A. Jouyban, *Korean J. Chem. Eng.* **2012**, *29*, 812.
- [154] W. Wenseleers, I. I. Vlasov, E. Goovaerts, E. D. Obraztsova, A. S. Lobach, A. Bouwen, *Adv. Funct. Mater.* **2004**, *14*, 1105.
- [155] F. Bonaccorso, T. Hasan, P. H. Tan, C. Sciascia, G. Privitera, G. Di Marco, P. G. Gucciardi, A. C. Ferrari, *J. Phys. Chem. C* **2010**, *114*, 17267.
- [156] S. Paria, K. C. Khilar, *Adv. Colloid Interface Sci.* **2004**, *110*, 75.
- [157] D. Nuvoli, L. Valentini, V. Alzari, S. Scognamillo, S. B. Bon, M. Piccinini, J. Illescas, A. Mariani, *J. Mater. Chem.* **2011**, *21*, 3428.
- [158] J.-W. T. Seo, A. A. Green, A. L. Antaris, M. C. Hersam, *J. Phys. Chem. Lett.* **2011**, *2*, 1004.
- [159] *Stabilization of Colloidal Dispersions by Polymer Adsorption*, (Eds: T. Sato, R. Ruch), Marcel Dekker Inc., New York, USA, **1980**.
- [160] J. O. Island, G. A. Steele, H. S. J. van der Zant, A. Castellanos-Gomez, *2D Mater.* **2015**, *2*, 011002.
- [161] X. Lu, M. Yu, H. Huang, R. S. Ruoff, *Nanotechnology* **1999**, *10*, 269.
- [162] T. Svedberg, K. O. Pedersen, *The Ultracentrifuge*, Oxford University Press, Oxford, UK **1940**.
- [163] F. Bonaccorso, M. Zerbetto, A. C. Ferrari, V. Amendola, *J. Phys. Chem. C* **2013**, *117*, 13217.
- [164] M. S. Arnold, S. I. Stupp, M. C. Hersam, *Nano Lett.* **2005**, *5*, 713.
- [165] M. S. Arnold, A. A. Green, J. F. Hulvat, S. I. Stupp, M. C. Hersam, *Nat. Nanotechnol.* **2006**, *1*, 60.
- [166] S. Li, F. Zhu, H. Li, Q. Yue, J. Liu, *J. Electroanal. Chem.* **2013**, *703*, 135.
- [167] A. O'Neill, U. Khan, J. N. Coleman, *Chem. Mater.* **2012**, *24*, 2414.
- [168] J. W. Williams, K. E. Van Holde, R. L. Baldwin, H. Fujita, *Chem. Rev.* **1958**, *58*, 715.
- [169] M. Behrens, *Hoppe-Seyler's Z. Physiol. Chem.* **1939**, *258*, 27.
- [170] J. B. Ifft, J. Vinograd, *J. Phys. Chem.* **1966**, *70*, 2814.
- [171] F. Bonaccorso, *Int. J. Photoenergy* **2010**, *2010*, 727134.
- [172] D. M. Small, S. A. Penkett, D. Chapman, *Biochem. Biophys. Acta* **1969**, *176*, 178.
- [173] N. A. Mazer, M. C. Carey, R. F. Kwasnick, G. B. Benedek, *Biochemistry* **1979**, *18*, 3064.
- [174] R. Duro, C. Souto, J. L. Gomez-Amoza, R. Martinez-Pacheco, A. Concheiro, *Drug Dev. Ind. Pharm.* **1999**, *25*, 817.
- [175] M. K. Brakke, *Arch. Biochem.* **1953**, *45*, 275.
- [176] X. Sun, D. Luo, J. Liu, D. G. Evans, *ACS Nano* **2010**, *4*, 3381.
- [177] Y. Y. Noh, X. Cheng, H. Sirringhaus, J. I. Sohn, M. E. Welland, D. J. Kang, *Appl. Phys. Lett.* **2007**, *91*, 043109.
- [178] J. C. Ramos, D. L. Kabir, I. Mejia, M. Mireles, C. A. Martinez, M. A. Quevedo-Lopez, *ECS Solid State Lett.* **2013**, *2*, 67.
- [179] J. Perelaer, B.-J. de Gans, U. S. Schuber, *Adv. Mater.* **2006**, *18*, 2101.
- [180] T. Shimoda, Y. Matsuki, M. Furusawa, T. Aoki, I. Yudasaka, H. Tanaka, H. Iwasawa, D. Wang, M. Miyasaka, Y. Takeuchi, *Nature* **2006**, *440*, 783.
- [181] Y. Yoshioka, G. E. Jabbour, *Synth. Metals* **2006**, *156*, 779.
- [182] G. W. Hsieh, F. M. Li, P. Beecher, A. Nathan, Y. L. Wu, B. S. Ong, *J. Appl. Phys.* **2009**, *106*, 123706.
- [183] H. Okimoto, T. Takenobu, K. Yanagi, Y. Miyata, H. Shimotani, H. Kataura, Y. Iwasa, *Adv. Mater.* **2010**, *22*, 3981.
- [184] M. Ha, Y. Xia, A. A. Green, W. Zhang, M. J. Renn, C. H. Kim, M. C. Hersam, C. D. Frisbie, *ACS Nano* **2010**, *4*, 4388.
- [185] C.-L. Lee, C.-H. Chen, C.-W. Chen, *Chem. Eng. J.* **2013**, *230*, 296.
- [186] Y. Yoon, K. Samanta, H. Lee, K. Lee, A. P. Tiwari, J. Lee, J. Yang, H. Lee, *Sci. Rep.* **2015**, *5*, 14177.
- [187] N. Luechinger, A. E. K. Athanassiou, W. J. Stark, *Nanotechnology* **2008**, *19*, 445201.
- [188] S. Wang, P. K. Ang, Z. Wang, A. L. L. Tang, J. T. L. Thong, K. P. Loh, *Nano Lett.* **2009**, *10*, 92.
- [189] V. Dua, S. Surwade, S. Ammu, S. Agnihotra, S. Jain, K. Roberts, S. Park, R. S. Ruoff, S. Manohar, *Angew. Chem., Int. Ed.* **2010**, *49*, 2154.
- [190] J. Li, M. M. Naiini, S. Vaziri, M. C. Lemme, M. Östling, *Adv. Funct. Mater.* **2014**, *24*, 6524.
- [191] J. Li, M. C. Lemme, M. Östling, *Chem. Phys. Chem.* **2014**, *15*, 3427.
- [192] F. Withers, H. Yang, L. Britnell, A. P. Rooney, E. Lewis, A. Felten, C. R. Woods, T. Georgiou, A. Eckmann, Y. J. Kim, S. G. Yeates, S. J. Haigh, A. K. Geim, K. S. Novoselov, C. Casiraghi, *Nano Lett.* **2014**, *14*, 3987.
- [193] A. Y. Malkin, A. I. Isayev, *Rheology: Concepts, Methods & Applications*, ChemTec. Publ., Toronto **2006**.
- [194] J. Park, J. Moon, *Langmuir* **2006**, *22*, 3506.
- [195] A. Pekarovicova, V. Husovska, in *Printing on Polymers: Fundamentals and Applications*, (Eds: J. Izdebska, S. Thomas), Elsevier Inc., Oxford, UK **2016**.
- [196] F. Evans, H. Wennerström, *The Colloidal Domain: Where Physics, Chemistry, Biology, and Technology Meet*, 2nd ed., Wiley-VCH, Weinheim, Germany **1999**.
- [197] S. Viswanath, T. K. Ghosh, D. H. L. Prasad, N. V. K. Dutt, K. Y. Rani, *Viscosity of Liquids: Theory, Estimation, Experiment, and Data*, Springer, New York **2007**.
- [198] N. Willenbacher, K. Georgieva, in *Product Design and Engineering: Formulation of Gels and Pastes*, (Eds: U. Brockel, W. Meier, G. Wagner), Wiley-VCH, Weinheim, Germany **2013**.
- [199] P. C. Hiemenz, R. Rajagopalan, *Principles of Colloid and Surface Chemistry*, CRC Press, Boca Raton, FL, USA **1997**.
- [200] H. C. Burstyn, J. V. Sengers, P. Esfandiari, *Phys. Rev. A* **1980**, *22*, 282.
- [201] J. Garg, B. Poudel, M. Chiesa, J. B. Gordon, J. J. Ma, J. B. Wang, Z. F. Ren, Y. T. Kang, H. Ohtani, J. Nanda, G. H. McKinley, G. Chen, *J. Appl. Phys.* **2008**, *103*, 074301.

- [202] I. M. Mahbubul, R. Saidur, M. A. Amalina, *Int. J. Heat Mass Transfer* **2012**, *55*, 874.
- [203] P. C. Mishra, S. Mukherjee, S. K. Nayak, A. Panda, *Int. Nano Lett.* **2014**, *4*, 109.
- [204] A. Einstein, *Ann. Phys.* **1906**, *324*, 289.
- [205] A. Einstein, *Ann. Phys.* **1911**, *34*, 591.
- [206] G. K Batchelor, *J. Fluid Mech.* **1977**, *83*, 97.
- [207] I. M. Krieger, T. J. Dougherty, *Trans. Soc. Rheol.* **1959**, *3*, 137.
- [208] S. Mueller, E. W. Llewellyn, H. M. Mader, *Proc. R. Soc. A* **2010**, *466*, 1201.
- [209] D. Quemada, *Rheol. Acta* **1977**, *16*, 82.
- [210] S. R. Williams, A. P. Philipse, *Phys. Rev. E* **2003**, *67*, 051301.
- [211] M. Gan, N. Gopinathan, X. Jia, R. A. Williams, *KONA* **2004**, *22*, 82.
- [212] A. Donev, I. Cisse, D. Sachs, E. A. Variano, F. H. Stillinger, R. Connelly, S. Torquato, P. M. Chaikin, *Science* **2004**, *303*, 990.
- [213] E. V. Timofeeva, J. L. Routbort, D. Singh, *J. Appl. Phys.* **2009**, *106*, 014304.
- [214] N. Putra, R. Wilfried, K. Sarit, *Heat Mass Transf.* **2003**, *39*, 775.
- [215] Y. Ding, H. Alias, D. Wen, R. A. Williams, *Int. J. Heat Mass Transfer* **2006**, *49*, 240.
- [216] K. Tremel, S. Ludwigs, *Adv. Polym. Sci.* **2014**, *265*, 39.
- [217] J. Park, S. Lee, H. H. Lee, *Org. Electron.* **2006**, *7*, 256.
- [218] R. Dattani, J. T. Cabra, *Soft Matter* **2015**, *11*, 3125.
- [219] Y. Liu, X. Zhao, B. Cai, T. Pei, Y. Tong, Q. Tang, Y. Liu, *Nanoscale* **2014**, *6*, 1323.
- [220] P. R. Somani, S. P. Somani, S. P. Lau, E. Flahaut, M. Tanemura, M. Umeno, *Solid State Electron.* **2007**, *51*, 788.
- [221] A. Carlson, A. M. Bowen, Y. Huang, R. G. Nuzzo, J. A. Rogers, *Adv. Mater.* **2012**, *24*, 5284.
- [222] S. Logothetidis, *Rev. Adv. Mater. Sci.* **2005**, *10*, 387.
- [223] F. Bensebaa, *Nanoparticles Technology: from Lab to Market*, Academic Press, Cambridge, MA, USA **2013**.
- [224] R. D. Degane, O. Bakajin, T. F. dupont, G. Huber, S. R. Nagel, T. A. Witte, *Nature* **1997**, *389*, 827.
- [225] S. S. Le, C. S. Kim, E. D. Gomez, B. Purushothaman, M. F. Toney, C. Wang, A. Hexemer, J. A. Anthony, Y. L. Loo, *Adv. Mater.* **2009**, *21*, 3605.
- [226] J. Chen, C. K. Tee, M. Shtain, D. C. Martin, J. Anthony, *Org. Electron.* **2009**, *10*, 696.
- [227] S. Wang, M. Kappl, I. Liebwirth, M. Muller, K. Kirchhoff, W. Pisula, K. Mullen, *Adv. Mater.* **2012**, *24*, 417.
- [228] P. J. Diemer, C. R. Lyle, Y. Mei, C. Sutton, M. M. Payne, J. E. Anthony, V. Coropceanu, J.-L. Brédas, O. D. Jurchescu, *Adv. Mater.* **2013**, *25*, 6956.
- [229] M. Eslamian, F. Zabihi, *Nanoscale Res. Lett.* **2015**, *10*, 462.
- [230] F. Kim, L. J. Cote, J. Huang, *Adv. Mater.* **2010**, *22*, 1954.
- [231] M. A. Pope, S. Korkut, C. Punckt, I. A. Aksay, *J. Electrochem. Soc.* **2013**, *160*, A1653.
- [232] D. Chakravarty, D. J. Late, *Eur. J. Inorg. Chem.* **2015**, *2015*, 1973.
- [233] J. Mahmood, E. K. Lee, M. Jung, D. Shin, I.-Y. Jeon, S.-M. Jung, H.-J. Choi, J.-M. Seo, S.-Y. Bae, S.-D. Sohm, N. Park, J. H. Oh, H.-J. Shin, J.-B. Baek, *Nat. Commun.* **2015**, *6*, 6486.
- [234] C. Chen, Q.-H. Yang, Y. Yang, W. Lv, Y. Wen, P.-X. Hou, M. Wang, H.-M. Cheng, *Adv. Mater.* **2009**, *21*, 3007.
- [235] H. Sirringhaus, P. J. Brown, R. H. Friend, M. M. Nielsen, K. Bechgaard, B. M. W. Langeveld-Voss, A. J. H. Spiering, R. A. J. Janssen, E. W. Meijer, *Synth. Met.* **2000**, *111/112*, 129.
- [236] J.-F. Chang, B. Sun, D. W. Breiby, M. M. Nielsen, T. I. Sølling, M. Giles, I. McCulloch, H. Sirringhaus, *Chem. Mater.* **2004**, *16*, 4772.
- [237] K. Norrman, A. Ghanbari-Siahkali, N. B. Larsen, K. Norrman, *Annu. Rep. Prog. Chem., Sect. C* **2005**, *101*, 174.
- [238] X. Pi, Q. Li, D. Li, D. Yan, *Sol. Energy Mater. Sol. Cells* **2011**, *95*, 2941.
- [239] R. Plass, S. Pelet, J. A. Krueger, M. Grätzel, *J. Phys. Chem. B* **2002**, *106*, 7578.
- [240] a) Q. Sun, Y. A. Wang, L. S. Li, D. Wang, T. Zhu, J. Xu, C. Yang, Y. Li, *Nat. Photonics* **2007**, *1*, 717; b) Q. Sun, Y. A. Wang, L. S. Li, D. Wang, T. Zhu, J. Xu, C. Yang, Y. Li, *Nat. Photonics* **2007**, *1*, 717.
- [241] C. Yeo, J. H. Choi, J. B. Kim, J. C. Lee, Y. T. Lee, *Opt. Mater. Express* **2014**, *4*, 346.
- [242] J. He, T. Kunitake, A. Nakao, *Chem. Mater.* **2003**, *15*, 4401.
- [243] H. Z. Geng, K. K. Kim, K. P. So, Y. S. Lee, Y. Chang, Y. H. Lee, *J. Am. Chem. Soc.* **2007**, *129*, 7758.
- [244] E. Artukovic, M. Kaempgen, D. S. Hecht, S. Roth, G. Gruner, *Nano Lett.* **2005**, *5*, 757.
- [245] Z.-S. Wu, K. Parvez, X. Feng, K. Mullen, *Nat Commun.* **2013**, *4*, 2487.
- [246] M. A. Ibrahim, T.-W. Lan, J. K. Huang, Y.-Y. Chen, K.-H. Wei, L.-J. Li, C. W. Chu, *RSC Adv.* **2013**, *3*, 13193.
- [247] Z. Zhu, J. Lowes, J. Berron, B. Smith, D. Sullivan, *ECS Trans.* **2014**, *60*, 293.
- [248] Y. Chang, W. C. Wu, W. C. Chen, *J. Electrochem. Soc.* **2001**, *148*, F77.
- [249] *Modern Coating and Drying Technology*, (Eds: E. Cohen, E. Gutoff), Wiley-VCH, Weinheim, Germany **1992**.
- [250] B. Derby, N. Reis, *MRS Bull.* **2003**, *28*, 815.
- [251] B.-J de Gans, P. C. Duineveld, U. S. Schubert, *Adv. Mater.* **2004**, *16*, 203.
- [252] S. V. Murphy, A. Atala, *Nat. Biotechnol.* **2014**, *32*, 773.
- [253] E. Sachlos, D. A. Wahl, J. T. Triffitt, J. T. Czernuszka, *Acta Biomater.* **2008**, *4*, 1322.
- [254] R.-H. Kim, D.-H. Kim, J. Xiao, B. H. Kim, S.-I. Park, B. Panilaitis, R. Ghaffari, J. Yao, M. Li, Z. Liu, V. Malyarchuk, D. G. Kim, A.-P. Le, R. G. Nuzzo, D. L. Kaplan, F. G. Omenetto, Y. Huang, Z. Kang, J. A. Rogers, *Nat. Mater.* **2010**, *9*, 929.
- [255] G. Lukacs, N. Maloney, M. Hegner, *J. Sensors* **2012**, *2012*, 561256.
- [256] D. Lupo, W. Clemens, S. Breitung, K. Hecker, in *Applications of Organic and Printed Electronics*, (Ed: E. Cantatore), Springer, Boston, MA, USA **2013**, 1.
- [257] A. Teichler, J. Perelaer, U. S. Schubert, *J. Mater. Chem. C* **2013**, *1*, 1910.
- [258] A. Kamyshny, S. Magdassi, *Small* **2014**, *10*, 3515.
- [259] B. Kang, W. H. Lee, K. Cho, *Appl. Mater. Interfaces* **2013**, *5*, 2302.
- [260] D. Kwak, J. A. Lim, B. Kang, W. H. Lee, K. Cho, *Adv. Funct. Mater.* **2013**, *23*, 5224.
- [261] H. Gorter, M. J. J. Coeren, M. W. L. Slaats, M. Ren, W. Lu, C. J. Kuijpers, W. A. Groen, *Thin Solid Films* **2013**, *532*, 11.
- [262] T. M. Eggenhuizen, M. J. J. Coeren, M. W. L. Slaats, W. A. Groen, *J. Imaging Sci. Technol.* **2014**, *58*, 40402.
- [263] F. C. Krebs, *Sol. Energy Mater. Sol. Cells* **2009**, *93*, 394.
- [264] S. H. Eom, H. Park, S. H. Mujawar, S. C. Yoon, S.-S. Kim, S.-I. Na, S.-J. Kang, D. Khim, D.-Y. Kim, S.-H. Lee, *Org. Electron.* **2010**, *11*, 1516.
- [265] G. Cummins, M. P. Y. Desmulliez, *Circuit World* **2012**, *38*, 193.
- [266] A. Kamyshny, S. Magdassi, in *Inkjet-Based Micromanufacturing*, (Eds: J. P. Korvink, P. J. Smith, D.-Y. Shin), Wiley-VCH, Weinheim, Germany **2012**, p. 173.
- [267] A. Hudd, in *The Chemistry of Inkjet Inks*, (Ed: S. Magdassi), World Scientific, Singapore **2010**, p. 3.
- [268] B. Derby, *Ann. Rev. Mater.* **2010**, *40*, 395.
- [269] P. Calvert, *Chem. Mater.* **2001**, *13*, 3299.
- [270] S. Magdassi, in *The Chemistry of Inkjet Inks*, (Ed: S. Magdassi), World Scientific, Singapore **2010**, p. 19.
- [271] G. D. Martin, S. D. Hoath, I. M. Hutchings, *J. Phys. Conf. Ser.* **2008**, *105*, 012001.
- [272] M. Singh, H. M. Haverinen, P. Dhagat, G. E. Jabbour, *Adv. Mater.* **2010**, *22*, 673.
- [273] G. K. Batchelor, *An Introduction to Fluid Dynamics*, Cambridge University Press, Cambridge, UK **1967**.
- [274] V. Bergeron, D. Bonn, J. Y. Martin, L. Vovelle, *Nature* **2000**, *405*, 772.
- [275] J. E. Fromm, *IBM J. Res. Dev.* **1984**, *28*, 322.
- [276] D. Jang, D. Kim, J. Moon, *Langmuir* **2009**, *25*, 2629.
- [277] P. Shin, J. Sung, M. H. Lee, *Microelectron. Reliab.* **2011**, *51*, 797.

- [278] B. de Gans, E. Kazancioglu, W. Meyer, U. S. Schubert, *Macromol. Rapid Commun.* **2004**, *25*, 292.
- [279] W. K. Hsiao, S. D. Hoath, G. D. Martin, I. M. Hutchings, *J. Imaging Sci. Technol.* **2009**, *53*, 050304.
- [280] S. Jung, I. M. Hutchings, *Soft Matter* **2012**, *8*, 2686.
- [281] H. M. Dong, W. W. Carr, J. F. Morris, *Phys. Fluids* **2006**, *18*, 072102.
- [282] Fluid Properties Effects on Ink-Jet Device Performance; <http://www.microfab.com/images/pdfs/technote99-02.pdf>; accessed: May 2016.
- [283] T. H. J. van Osch, J. Perelaer, A. W. M. de Laat, U. S. Schubert, *Adv. Mater.* **2008**, *20*, 343.
- [284] D. Kim, S. Jeong, J. Moon, K. Kang, *Mol. Cryst. Liq. Cryst.* **2006**, *459*, 45.
- [285] R. E. Saunders, B. Derby, *Int. Mater. Rev.* **2014**, *59*, 430.
- [286] P. G. De Gennes, *Rev. Mod. Phys.* **1985**, *57*, 827.
- [287] A. C. Arias, J. D. MacKenzie, I. McCulloch, J. Rivnay, A. Salleo, *Chem. Rev.* **2010**, *110*, 3.
- [288] C. Ruiz, E. M. García-Frutos, G. Hennrich, B. Gómez-Lor, *J. Phys. Chem. Lett.* **2012**, *3*, 1428.
- [289] C. Wang, K. Takei, T. Takahashi, A. Javey, *Chem. Soc. Rev.* **2013**, *42*, 2592.
- [290] K. Kordás, T. Mustonen, G. Tóth, H. Jantunen, M. Lajunen, C. Soldano, S. Talapatra, S. Kar, R. Vajtai, P. M. Ajayan, *Small* **2006**, *2*, 1021.
- [291] H. Okimoto, T. Takenobu, K. Yanagi, Y. Miyata, H. Shimotani, H. Kataura, Y. Iwasa, *Adv. Mater.* **2010**, *22*, 3981.
- [292] T. Takenobu, N. Miura, S.-Y. Lu, H. Okimoto, T. Asano, M. Shiraishi, Y. Iwasa, *Appl. Phys. Express* **2009**, *2*, 025005.
- [293] A. L. Dearden, P. J. Smith, D.-Y. Shin, N. Reis, B. Derby, P. O'Brien, *Macromol. Rapid Commun.* **2005**, *26*, 315.
- [294] S. Gamerith, A. Klug, H. Scheiber, U. Scherf, E. Moderegger, E. J. W. List, *Adv. Funct. Mater.* **2007**, *17*, 3111.
- [295] B. K. Park, D. Kim, S. Jeong, J. Moon, J. S. Kim, *Thin Solid Films* **2007**, *515*, 7706.
- [296] K. E. Paul, W. S. Wong, S. E. Ready, R. A. Street, *Appl. Phys. Lett.* **2003**, *83*, 2070.
- [297] T. Sekitani, T. Yokota, U. Zschieschang, H. Klauk, S. Bauer, K. Takeuchi, M. Takamiya, T. Sakurai, T. Someya, *Science* **2009**, *326*, 1516.
- [298] A. Jorio, G. Dresselhaus, M. S. Dresselhaus, *Carbon Nanotubes: Advanced Topics in the Synthesis, Structure, Properties and Applications*, Springer Science & Business Media, Berlin/Heidelberg, Germany **2007**.
- [299] I. Yahya, F. Bonaccorso, S. Clowes, A. C. Ferrari, S. R. P. Silva, *Carbon* **2015**, *93*, 574.
- [300] L. Huang, Y. Huang, J. Liang, X. Wan, Y. Chen, *Nano Res.* **2011**, *4*, 675.
- [301] Y. M. Jo, S. Yoon, J.-H. Lee, S.-J. Park, S. R. Kim, I. In, *Chem. Lett.* **2011**, *40*, 54.
- [302] L. T. Le, M. H. Ervin, H. Qiu, B. E. Fuchs, W. Y. Lee, *Electrochem. Commun.* **2011**, *13*, 355.
- [303] K. Y. Shin, J.-Y. Hong, J. Jang, *Adv. Mater.* **2011**, *23*, 2113.
- [304] K. Y. Shin, J.-Y. Hong, J. Jang, *Chem. Commun.* **2011**, *47*, 8527.
- [305] D. Kong, L. T. Le, Y. Li, J. L. Zunino, W. Lee, *Langmuir* **2012**, *28*, 13467.
- [306] F. J. Tölle, M. Fabritious, R. Mülhaupt, *Adv. Funct. Mater.* **2012**, *22*, 1136.
- [307] H. Zhang, A. Xie, Y. Shen, L. Qiu, X. Tian, *Phys. Chem. Chem. Phys.* **2012**, *14*, 12757.
- [308] Y. Su, J. Du, D. Sun, C. Liu, H. Cheng, *Nano Res.* **2013**, *6*, 842.
- [309] Y. Su, S. Jia, J. Du, J. Yuan, C. Liu, W. Ren, H. Cheng, *Nano Res.* **2015**, *8*, 3954.
- [310] Y. Yoon, K. Samanta, H. Lee, K. Lee, A. P. Tiwari, J. Lee, J. Yang, H. Lee, *Sci. Rep.* **2015**, *5*, 14177.
- [311] W. Zhang, E. Bi, M. Li, L. Gao, *Colloids Surf. A* **2016**, *490*, 232.
- [312] E. B. Secor, P. L. Prabhumirashi, K. Puntambekar, M. L. Geier, M. C. Hersam, *J. Phys. Chem. Lett.* **2013**, *4*, 1347.
- [313] R. C. Osthoff, S. W. Kantor, *Organosilazane Compounds*, John Wiley & Sons, Inc., New York **1997**.
- [314] J. Li, F. Ye, S. Vaziri, M. Muhammed, M. C. Lemme, M. Östling, *Carbon* **2012**, *50*, 3092.
- [315] Y.-H. Kim, B. Yoo, J. E. Anthony, S. K. Park, *Adv. Mater.* **2012**, *24*, 497.
- [316] S. Brimaud, C. Coutanceau, E. Garnier, J.-M. Léger, F. Gérard, S. Pronier, M. Leoni, *J. Electroanal. Chem.* **2007**, *602*, 226.
- [317] VTT Technical Research Centre, *Research, Development and Commercialisation Highlights in Printed Intelligence 2011–2012*, (Eds: H. Rupprecht, R. Rikkola, I. Hernberg), VTT, Espoo, Finland **2012**.
- [318] A. Moridi, S. M. Hassani-Gangaraj, M. Guagliano, M. Dao, *Surf. Eng.* **2014**, *36*, 369.
- [319] P. L. Fauchais, J. V. R. Heberlein, M. Boulus, *Thermal Spray Fundamentals: From Powder to Part*, Springer Science+Business Media, Berlin/Heidelberg, Germany **2014**, Ch. 2, pp. 17–72, DOI: 10.1007/978-0-387-68991-3_2.
- [320] K. X. Steirer, M. O. Reese, B. L. Rupert, N. Kopidakis, D. C. Olson, R. T. Collins, D. S. Ginle, K. X. Steirera, M. O. Reeseb, B. L. Rupertb, N. Kopidakis, D. C. Olson, R. T. Collins, D. S. Ginle, *Sol. Energy Mater. Sol. Cells* **2009**, *93*, 447.
- [321] Y. Zheng, S. Li, W. Shi, J. Yu, *Nanoscale Res. Lett.* **2014**, *9*, 145.
- [322] G. Taylor, *Proc. R. Soc. A* **1964**, *280*, 383.
- [323] O. V. Salata, *Curr. Nanosci.* **2005**, *1*, 25.
- [324] J. W. Owen, N. A. Azarova, M. A. Loth, M. Paradinas, M. Coll, C. Ocal, J. E. Anthony, O. D. Jurchescu, *J. Nanotechnol.* **2011**, *2011*, 914510.
- [325] L.-L. Xing, J. E. Glass, R. H. Fernando, in *Technology for Waterborne Coatings, ACS Symposium Series*, Vol. 663, (Ed: J. E. Glass), ACS, Washington DC, USA **2009**, Ch. 15, pp. 265–295.
- [326] G. Perfetti, T. Alphazan, P. van Hee, W. J. Wildeboer, G. M. H. Meesters, *Eur. J. Pharm. Sci.* **2011**, *42*, 262.
- [327] S. Bose, S. S. Keller, T. S. Alstrøm, A. Boisen, K. Almda, *Langmuir* **2013**, *29*, 6911.
- [328] D. G. Baldwin, P. C. Manz, M. E. Williams, *Semiconductor Industrial Hygiene Handbook: Monitoring, Ventilation, Equipment and Ergonomics*, Noyes Publications, Saddle River NJ, USA, 1995.
- [329] B. K. Yu, D. Vak, J. Jo, S. I. Na, S. S. Kim, M. K. Kim, D. Y. Kim, *IEEE J. Sel. Top. Quantum Electron.* **2010**, *1838*, 16.
- [330] K. Masters, *Spray Drying Handbook*, 5th ed., Wiley, New York **1991**.
- [331] X. Yu, N. Zhou, S. Han, H. Lin, D. B. Buchholz, J. Yu, R. P. H. Chang, T. J. Marks, A. Facchetti, *J. Mater. Chem. C* **2013**, *1*, 6532.
- [332] S. W. Morton, K. P. Herlihy, K. E. Shopsowitz, Z. J. Deng, K. S. Chu, C. J. Bowerman, J. M. DeSimone, P. T. Hammond, *Adv. Mater.* **2013**, *25*, 4707.
- [333] R. Gaspar, R. Duncan, *Adv. Drug Delivery Rev.* **2009**, *61*, 1220.
- [334] R. Duncan, R. Gaspar, *Mol. Pharmaceutics* **2011**, *8*, 2101.
- [335] P. T. Anthony, F. V.-G. Luis, *Nanotechnology* **2015**, *26*, 505301.
- [336] Y. Zheng, S. Li, W. Shi, J. Yu, *Nanoscale Res. Lett.* **2014**, *145*, 9.
- [337] C.-M. Gee, C.-C. Tseng, F.-Y. Wu, H.-P. Chang, L.-J. Li, Y.-P. Hsieh, C.-T. Lin, J.-C. Chen, *Displays* **2013**, *34*, 315.
- [338] W. J. Hyun, O. O. Park, B. D. Chin, *Adv. Mater.* **2013**, *25*, 4729.
- [339] Y.-J. Lee, A. Zhamu, B. Z. Jang, S. Y. Lee, J. C. Lin, WO2014159656 A1 **2014**.
- [340] C. Y. Su, A. Y. Lu, Y. P. Xu, F. R. Chen, A. N. Khlobystov, L. J. Li, *ACS Nano* **2011**, *5*, 2332.
- [341] S. Casaluci, M. Gemmi, V. Pellegrini, A. Di Carlo, F. Bonaccorso, *Nanoscale* **2016**, *8*, 5368.
- [342] E. J. Wensink, A. C. Hoffmann, P. J. van Maaren, D. van der Spoel, *J. Chem. Phys.* **2003**, *119*, 7308.
- [343] G. Calogero, A. Bartolotta, G. Di Marco, A. Di Carlo, F. Bonaccorso, *Chem. Soc. Rev.* **2015**, *44*, 3244.
- [344] *Printing: Papermaking Science and Technology*, (Eds: P. Oittinen, H. Saarelma) Fapet Oy, Helsinki, Finland **1998**.
- [345] O. M. Lilien, *History of Industrial Gravure Printing up to 1920*, Lund Humphries Publishers Ltd., London, UK **1972**.

- [346] D. Argent, in *Flexography: Principles & Practices*, Vol. 5, 5th ed., (Ed: G. Cusdin), Foundation of Flexographic Technical Association, Bohemia, NY, USA **1999**.
- [347] *Encyclopedia of Journalism*, (Ed: C. H. Sterling), SAGE Publishing, Thousand Oaks, CA, USA **2009**.
- [348] S. H. Ahm, L. J. Guo, *Adv. Mater.* **2008**, *20*, 2044.
- [349] A. Schleunitz, C. Spreu, T. Mäkelä, T. Haatainen, A. Klukowska, H. Schift, *Microelectron. Eng.* **2011**, *88*, 2113.
- [350] T. Mäkelä, T. Haatainen, P. Majander, J. Ahopelto, *Microelectron. Eng.* **2007**, *84*, 877.
- [351] J. John, Y. Y. Tang, J. P. Rothstein, J. J. Watkins, K. R. Carte, *Nanotechnology* **2013**, *24*, 505307.
- [352] N. Kooy, K. Mohamed, L. T. Pim, O. S. Guan, *Nanoscale Res. Lett.* **2014**, *9*, 320.
- [353] A. White, *High Quality Flexography*, Pira International, Leatherhead, UK **1992**.
- [354] K. Suganuma, *Introduction to Printed Electronics*, Springer Briefs in Electrical and Computer Engineering, Springer, New York, **2014**, DOI: 10.1007/978-1-4614-9625-0.
- [355] S. Garner, G. Merz, J. Tosch, C. Chang, D. Marshall, X. Li, J. Matusick, J. Lin, C. Kuo, S. Lewis, C. Kang, *Flexible Glass Substrates for Roll-to-Roll Manufacturing*, <http://dnn.convertingquarterly.com/Portals/1/files/matteucci-awards/2011-Flexible-Glass-Substrates-for-R2R-Manufacturing.pdf>, Accessed: May 2016.
- [356] Ink Technology Rules, <http://www.epson.com.au/downloads/pdf/epsonhdrinktech-54final.pdf>; accessed: May 2016.
- [357] D. E. Bisset, *The Printing Ink Manual*, 3rd ed., Northwood Books, London, UK, **1979**.
- [358] *Flexography: Principles & Practices*, Vol. 1, 5th ed., (Ed: G. Cusdin), Foundation of Flexographic Technical Association, Bohemia, NY, USA **1999**.
- [359] R. E. Todd, *Printing Inks: Formulation Principles, Manufacture and Quality Control Testing Procedures*, Pira International, Leatherhead, UK **1994**.
- [360] B. Thompson, *Printing Materials: Science and Technology*, Pira International, Leatherhead, UK **1998**.
- [361] R. C. Thompson, *Surf. Coat. Int., Part A* **2001**, *1*, 24.
- [362] J. Jo, J. S. Yu, T. M. Lee, D. S. Kim, *Jpn. J. Appl. Phys.* **2009**, *48*, 04C181.
- [363] G. C. Schmidt, M. Bellmann, B. Meier, M. Hambach, K. Reuter, H. Kempa, A. C. Hübner, *Org. Electron.* **2010**, *11*, 1683.
- [364] Y.-K. Chang, F. C.-N. Hong, *Nanotechnology* **2009**, *20*, 195302.
- [365] M. J. Maust, *TAPPJ* **1993**, *76*, 95.
- [366] H. M. Sauer, N. Bornemann, E. Dorsam, *LOPEC Conf. Proc.* **2011**, *2011*, *1*.
- [367] Z. Bao, Y. Feng, A. Dodabalapur, V. R. Raju, A. J. Lovinger, *Chem. Mater.* **1997**, *9*, 1299.
- [368] D. Erath, A. Filipovic, M. Retzlaff, A. Goetz, F. Clement, D. Biro, R. Preu, *Solar Energy Mater. Sol. Cells* **2010**, *94*, 57.
- [369] D. A. Pardo, G. E. Jabbour, N. Peyghambarian, *Adv. Mater.* **2000**, *12*, 1249.
- [370] M. Sauer, S. Meilchen, A. Kallede, M. Mennig, H. Schmidt, in *Sol-Gel Technologies for Glass Producers and Users*, (Eds: M. A. Aegeerter, M. Mennig), Springer Science+Business Media, New York **2004**.
- [371] T.-M. Lee, Y.-J. Choi, S.-Y. Nam, C.-W. You, D.-Y. Na, H.-C. Choi, D.-Y. Shin, K.-Y. Kim, K.-I. Jung, *Thin Solid Films* **2008**, *516*, 7875.
- [372] M. Zirkl, A. Sawatdee, U. Helbig, M. Krause, G. Scheipl, E. Kraker, P. A. Ersman, D. Nilsson, D. Platt, P. Bodö, S. Bauer, G. Domann, B. Stadlober, *Adv. Mater.* **2011**, *23*, 2069.
- [373] R. F. Rosu, R. A. Shanks, S. N. Bhattacharya, *Polymer* **1999**, *40*, 5891.
- [374] L. Dybowska-Sarapuk, D. Janczak, G. Wróblewski, M. Sloma, M. Jakubowska, *Proc. SPIE* **2015**, *9662*, 966242.
- [375] C. N. Hoth, P. Schilinsky, S. A. Choulis, S. Balasubramanian, C. J. Brabec, in *Applications of Organic and Printed Electronics*, (Ed: E. Cantatore), Springer Science+Business Media, New York **2013**, Ch. 2, pp. 27.
- [376] K. Park, D. Seo, J. Lee, *Colloids Surf. A* **2008**, *313–314*, 351.
- [377] D. Deng, T. Qi, Y. Chen, Y. Jin, F. Xiao, *13th Int. Conf. on Electronic Packaging Technology & High Density Packaging (ICEPT-HDE)*, **2012**, p. 250.
- [378] K. Kuroda, H. Nakado, M. inada, T. Nouada, Y. Kumashiro, *Trans. Jpn. Inst. Electron. Packag.* **2012**, *5*, 20.
- [379] H. M. Lee, S.-Y. Choi, K. T. Kim, J.-Y. Yun, D. S. Jung, S. B. Park, J. Park, *Adv. Mater.* **2011**, *23*, 5524.
- [380] X. P. Xia, C. S. Xie, S. Z. Cai, Z. H. Yang, X. L. Yang, *Corros. Sci.* **2006**, *48*, 3924.
- [381] A. Yanase, H. Komiyama, *Surf. Sci.* **1991**, *248*, 11.
- [382] H. Wieder, A. W. Czanderna, *J. Phys. Chem.* **1962**, *66*, 816.
- [383] A. Yanase, H. Komiyama, *Surf. Sci.* **1991**, *248*, 20.
- [384] S. B. Fuller, E. J. Wilhelm, J. M. Jacobson, *J. Microelectromech. Syst.* **2002**, *11*, 54.
- [385] J.-T. Wu, L.-C. Hsu, M.-H. Tsai, W.-S. Hwang, *Thin Solid Films* **2009**, *517*, 5913.
- [386] S. Magdassi, M. Grouchko, A. Kamysny, *Proc. Non-Impact Printing* **2009**, *25*, 611.
- [387] I. Reinhold, C. E. Hendriks, R. Eckardt, J. M. Kranenburg, J. Perelaer, R. R. Baumann, U. S. Schubert, *J. Mater. Chem.* **2009**, *19*, 3384.
- [388] H. Ko, J. Jhin, D. Byun, J. Lee, D. Park, *IEEE Trans. Compon. Packag. Technol.* **2005**, *28*, 781.
- [389] M. L. Allen, M. Aronniemi, T. Mattila, A. Alastalo, K. Ojanper, M. Suhonen, H. Sepp, *Nanotechnology* **2008**, *19*, 175201.
- [390] S. Magdassi, M. Grouchko, O. Berezin, A. Kamysny, *ACS Nano* **2010**, *4*, 1943.
- [391] J. Perelaer, M. Klokkenburg, C. E. Hendriks, U. S. Schubert, *Adv. Mater.* **2009**, *21*, 4830.
- [392] H.-S. Kim, S. R. Dhage, D.-E. Shim, H. T. Hahn, *Appl. Phys. A* **2009**, *97*, 791.
- [393] N. R. Bieri, J. Chung, D. Poulikakos, C. P. Grigoropoulos, *Superlattices Microstruct.* **2004**, *35*, 437.
- [394] H. Bi, X. Xie, K. Yin, Y. Zhou, S. Wan, L. He, F. Xu, F. Banhart, L. Sun, R. S. Ruoff, *Adv. Funct. Mater.* **2012**, *22*, 4421.
- [395] M. Qian, T. Feng, H. Ding, L. Lin, H. Li, Y. Chen, Z. Sun, *Nanotechnology* **2009**, *20*, 425702.
- [396] D. W. Zhang, X. D. Li, H. B. Li, S. Chen, Z. Sun, X. J. Yin, S. M. Huang, *Carbon* **2011**, *49*, 5382.
- [397] J. Ping, J. Wu, Y. Wang, Y. Ying, *Biosens. Bioelectron.* **2012**, *34*, 70.
- [398] G. Wróblewski, D. Janczak, *Proc. SPIE* **2012**, *8454*, 84541E.
- [399] Y. Xu, M. G. Schwab, A. J. Strudwick, I. Hennig, X. Feng, Z. Wu, K. Müllen, *Adv. Energy Mater.* **2013**, *3*, 1035.
- [400] E. Skrzetuska, M. Puchalski, I. Krucińska, *Sensors* **2014**, *14*, 16816.
- [401] K. Gniotek, I. Krucińska, *Fibres Text. East. Eur.* **2004**, *12*, 13.
- [402] I. Krucińska, E. Skrzetuska, W. Urbaniak-Domagała, *J. Appl. Polym. Sci.* **2011**, *121*, 483.
- [403] K. S. Novoselov, *Rev. Mod. Phys.* **2011**, *83*, 838.
- [404] A. K. Geim, I. V. Grigorieva, *Nature* **2013**, *499*, 419.
- [405] T. Mimura, *IEEE Trans. Microwave Theory Tech.* **2002**, *50*, 780.
- [406] Z. I. Alferov, R. F. Kazarinov, “Semiconductor laser with electric pumping,” Inventor’s Certificate 181737 [in Russian], Appl. 950840, priority as of March 30, **1963**.
- [407] H. Kroemer, US Patent 3 309 553, **1967**.
- [408] Z. I. Alferov, V. M. Andreev, V. I. Korol’kov, E. L. Portnoi, A. A. Yakovenko, *Fiz. Tekh. Poluprovodn.* **1969**, *3*, 930.
- [409] Y. Deng, Z. Luo, N. J. Conrad, H. Liu, Y. Gong, S. Najmaei, P. M. Ajayan, J. Lou, X. Xu, P. D. Ye, *ACS Nano* **2014**, *8*, 8292.

- [410] L. Britnell, R. V. Gorbachev, R. Jalil, B. D. Belle, F. Schedin, A. Mishchenko, T. Georgiou, M. I. Katsnelson, L. Eaves, S. V. Morozov, N. M. R. Peres, J. Leist, A. K. Geim, K. S. Novoselov, L. A. Ponomarenko, *Science* **2012**, *335*, 947.
- [411] L. Britnell, R. M. Ribeiro, A. Eckmann, R. Jalil, B. D. Belle, A. Mishchenko, Y.-J. Kim, R. V. Gorbachev, T. Georgiou, S. V. Morozov, A. N. Grigorenko, A. K. Geim, C. Casiraghi, A. H. Castro Neto, K. S. Novoselov, *Science* **2012**, *340*, 1311.
- [412] A. S. Mayorov, R. V. Gorbachev, S. V. Morozov, L. Britnell, R. Jalil, L. A. Ponomarenko, P. Blake, K. S. Novoselov, K. Watanabe, T. Taniguchi, A. K. Geim, *Nano Lett.* **2011**, *11*, 2396.
- [413] C. R. Dean, A. F. Young, I. Meric, C. Lee, L. Wang, S. Sorgenfrei, K. Watanabe, T. Taniguchi, P. Kim, K. L. Shepard, J. Hone, *Nat. Nanotechnol.* **2010**, *5*, 722.
- [414] S. J. Haigh, A. Gholinia, R. Jalil, S. Romani, L. Britnell, D. C. Elias, K. S. Novoselov, L. A. Ponomarenko, A. K. Geim, R. Gorbachev, *Nat. Mater.* **2012**, *11*, 764.
- [415] T. Tanaka, A. Ito, A. Tajima, E. Rokuta, C. Oshima, *Surf. Rev. Lett.* **2003**, *10*, 721.
- [416] Z. Liu, L. Song, S. Zhao, J. Huang, L. Ma, J. Zhang, J. Lou, P. M. Ajayan, *Nano Lett.* **2011**, *11*, 2032.
- [417] W. J. Yu, Z. Li, H. Zhou, Y. Chen, Y. Wang, Y. Huang, X. Duan, *Nat. Mater.* **2012**, *12*, 246.
- [418] Y.-C. Lin, C.-Y. S. Chang, R. K. Ghosh, J. Li, H. Zhu, R. Addou, B. Diaconescu, T. Ohta, X. Peng, N. Lu, M. J. Kim, J. T. Robinson, R. M. Wallace, T. S. Mayer, S. Datta, L.-J. Li, J. A. Robinson, *Nano Lett.* **2014**, *14*, 6936.
- [419] M.-Y. Li, Y. Shi, C.-C. Cheng, L.-S. Lu, Y.-C. Lin, H.-L. Tang, M.-L. Tsai, C.-W. Chu, K.-H. Wei, J.-H. He, W.-H. Chang, K. Suenaga, L.-J. Li, *Science* **2015**, *349*, 524.
- [420] X. Duan, C. Wang, J. C. Shaw, R. Cheng, Y. Chen, H. Li, X. Wu, Y. Tang, Q. Zhang, A. Pan, J. Jiang, R. Yu, Y. Huang, X. Duan, *Nat. Nanotechnol.* **2014**, *9*, 1024.
- [421] X. Zhang, F. Meng, J. R. Christianson, C. Arroyo-Torres, M. A. Lukowski, D. Liang, J. R. Schmidt, S. Jin, *Nano Lett.* **2014**, *14*, 3047.
- [422] X. Yuan, L. Tang, S. Liu, P. Wang, Z. Chen, C. Zhang, Y. Liu, W. Wang, Y. Zou, C. Liu, N. Guo, J. Zou, P. Zhou, W. Hu, F. Xiu, *Nano Lett.* **2015**, *15*, 3571.
- [423] M. Osada, T. Sasaki, *Adv. Mater.* **2012**, *24*, 210.
- [424] D. J. Finn, M. Lotya, G. Cunningham, R. J. Smith, D. McCloskey, J. F. Donegan, J. N. Coleman, *J. Mater. Chem. C* **2014**, *2*, 925.
- [425] T. Georgiou, R. Jalil, B. D. Belle, L. Britnell, R. V. Gorbachev, S. V. Morozov, Y.-J. Kim, A. Gholinia, S. J. Haigh, O. Makarovsky, L. Eaves, L. A. Ponomarenko, A. K. Geim, K. S. Novoselov, A. Mishchenko, *Nat. Nanotechnol.* **2013**, *8*, 100.
- [426] Printed, organic & flexible electronics forecasts, players & opportunities 2016–2026. <http://www.idtechex.com>; accessed: 2015.
- [427] R. G. Gordon, *MRS Bull.* **2000**, *52*.
- [428] M. W. Rowell, M. D. McGehee, *Energy Environ. Sci.* **2011**, *4*, 131.
- [429] G. E. Jabbour, R. Radspinner, N. Peyghambarian, *IEEE J. Sel. Top. Quantum Electron.* **2001**, *7*, 769.
- [430] Y. Wu, P. Liu, B. S. Ong, T. Sri Kumar, N. Zhao, G. Botton, S. Zhu, *Appl. Phys. Lett.* **2005**, *86*, 142102.
- [431] X. Huang, T. Leng, X. Zhang, J. C. Chen, K. H. Chang, A. K. Geim, K. S. Novoselov, Z. Hu, *Appl. Phys. Lett.* **2015**, *106*, 203105.
- [432] Z. Yin, H. Li, H. Li, L. Jiang, Y. Shi, Y. Sun, G. Lu, Q. Zhang, X. Chen, H. Zhang, *ACS Nano* **2012**, *6*, 74.
- [433] D.-S. Tsai, K.-K. Liu, D.-H. Lien, M.-L. Tsai, C.-F. Kang, C.-A. Lin, L.-J. Li, J.-H. He, *ACS Nano* **2013**, *7*, 3905.
- [434] O. Lopez-Sanchez, D. Lembke, M. Kayci, A. Radenovic, A. Kis, *Nat. Nanotechnol.* **2013**, *8*, 497.
- [435] M. Freitag, J. C. Tsang, A. Bol, D. Yuan, J. Liu, P. Avouris, *Nano Lett.* **2007**, *7*, 2037.
- [436] F. Xia, T. Mueller, Y.-M. Lin, A. Valdes-Garcia, P. Avouris, *Nat. Nanotechnol.* **2009**, *4*, 839.
- [437] M. C. Lemme, F. H. L. Koppens, A. L. Falk, M. S. Rudner, H. Park, L. S. Levitov, C. M. Marcus, *Nano Lett.* **2011**, *11*, 4134.
- [438] M. S. Mannoor, H. Tao, J. D. Clayton, A. Sengupta, D. L. Kaplan, R. R. Naik, N. Verma, F. Omenetto, M. McAlpine, *Nat. Commun.* **2012**, *3*, 763.
- [439] B. Mailly-Giacchetti, A. Hsu, H. Wang, V. Vinciguerra, F. Pappalardo, L. Occhipinti, E. Guidetti, S. Coffa, J. Kong, T. Palacios, *J. Appl. Phys.* **2013**, *114*, 084545.
- [440] P. Fromherz, *Nanoelectronics and Information Technology*, Wiley, Berlin, Germany **2003**, pp. 781–810.
- [441] S. Garaj, W. Hubbard, A. Reina, J. Kong, D. Branton, J. A. Golovchenko, *Nature* **2010**, *467*, 190.
- [442] G. Alarcon Angeles, G. A. Á. Romero, A. Merkoçi, *Advanced Carbon Materials and Technology*, Wiley, Berlin, Germany **2013**, pp. 87–128.
- [443] G. Wang, X. Shen, J. Yao, J. Park, *Carbon* **2009**, *47*, 2049.
- [444] B. Lung-Hao Hu, F. Y. Wu, C. T. Lin, A. N. Khlobystov, L. J. Li, *Nat. Commun.* **2013**, *4*, 1687.
- [445] H. Sun, A. E. Del Rio Castillo, S. Monaco, A. Capasso, D. A. Dinh, A. Ansaldi, M. Prato, V. Pellegrini, B. Scrosati, L. Manna, F. Bonaccorso, *J. Mater. Chem. A* **2016**, *4*, 6886.
- [446] Y. Zhu, S. Murali, M. D. Stoller, K. J. Ganesh, W. Cai, P. J. Ferreira, A. Pirkle, R. M. Wallace, K. A. Cychosz, M. Tommes, D. Su, E. A. Stach, R. S. Ruoff, *Science* **2011**, *332*, 1537.
- [447] L. Zhang, F. Zhang, X. Yang, G. long, Y. Wu, T. Zhang, K. Leng, Y. Huang, Y. Ma, A. Yu, Y. Chen, *Sci. Rep.* **2013**, *3*, 1408.
- [448] X. Wang, L. Zhi, K. Müllen, *Nano Lett.* **2008**, *8*, 323.
- [449] P. Robaeyns, F. Bonaccorso, E. Bourgeois, J. D'Haen, W. Dierckx, W. Dexters, D. Spoltore, J. Drijkonigen, J. Liesenborgs, A. Lombardo, A. C. Ferrari, F. Van Reeth, K. Haenen, J. V. Manca, M. Nesladek, *Appl. Phys. Lett.* **2014**, *105*, 083306.
- [450] F. Bonaccorso, N. Balis, M. M. Stylianakis, M. Savarese, C. Adamo, M. Gemmi, V. Pellegrini, E. Stratakis, E. Kymakis, *Adv. Funct. Mater.* **2015**, *25*, 3870.
- [451] A. L. Palma, L. Cinà, S. Pescetelli, A. Agresti, M. Raggio, F. Paolese, F. Bonaccorso, A. Di Carlo, *Nano Energy* **2016**, *22*, 349.
- [452] S. Hu, M. Lozada-Hidalgo, F. C. Wang, A. Mischchenko, F. Schedin, R. R. Nair, E. W. Hill, D. W. Boukhvalov, M. I. Katnelson, R. A. W. Dryfe, I. V. Grigorieva, H. A. Wu, A. K. Geim, *Nature* **2014**, *516*, 227.
- [453] L. Dong, R. R. S. Gari, Z. Li, M. M. Craig, S. Hou, *Carbon* **2010**, *48*, 781.
- [454] M. Kaempgen, C. K. Chan, J. Ma, Y. Cui, G. Gruner, *Nano Lett.* **2009**, *9*, 1872.
- [455] X. Han, Y. Chen, H. Zhu, C. Preston, J. Wan, Z. Fang, L. Hu, *Nanotechnology* **2013**, *24*, 205304.
- [456] S. Santra, G. Hu, R. C. T. Howe, A. De Luca, S. Z. Ali, F. Udrea, J. W. Gardner, S. K. Raj, P. K. Guha, T. Hasan, *Sci. Rep.* **2015**, *5*, 17374.
- [457] J. Wang, L. Liang, Y. Fang, T. Qiu, J. Zhang, L. Zhi, *Adv. Mater.* **2012**, *24*, 2874.